POSSIBLE EFFECTS OF THE LOOP CURRENT ON INTENSITY AND RAPID INTENSIFICATION OF HURRICANES IN THE GULF OF MEXICO

by

Sherry L. Young

A Thesis
Submitted to the
Graduate Faculty
of
George Mason University
in Partial Fulfillment of
The Requirements for the Degree
of
Master of Science
Earth Systems Science

Committee:

_____	Dr. Randy McBride, Thesis Director
_____	Dr. Barry A. Klinger, Committee Member
_____	Dr. Celso Ferreira, Committee Member
_____	Dr. Dieter Pfoser, Department Chairperson
_____	Dr. Donna M. Fox, Associate Dean, Office of Student Affairs & Special Programs, College of Science
_____	Dr. Peggy Agouris, Dean, College of Science
Date: _____	Spring Semester 2019 George Mason University Fairfax, VA

Possible Effects of the Loop Current on Intensity and Rapid Intensification of Hurricanes in the Gulf of Mexico

A Thesis submitted in partial fulfillment of the requirements for the degree of Master of Science at George Mason University

by

Sherry L. Young
Bachelor of Science
University of Mary Washington, 2015

Director: Dr. Randy McBride, Associate Professor
Department of Atmospheric, Oceanic, and Earth Sciences

Spring Semester 2019
George Mason University
Fairfax, VA

DEDICATION

This is dedicated to my wonderful and much appreciated husband Keith, my adored son Joshua, and my beloved cats and dogs; all of whom have been accommodating, patient, and supportive during my many years of academic endeavors, and to my mother Karen, who has always been my biggest cheerleader.

ACKNOWLEDGEMENTS

I would like to thank the numerous professors and academic advisors who have offered me guidance and support and taught me the knowledge that made this possible. I would specifically like to thank Dr. Klinger, who patiently, kindly, and thoroughly answered my endless questions, Dr. McBride who allowed me this opportunity and offered his guidance throughout my graduate career, and Dr. Ferreira who volunteered his valuable time and knowledge and agreed to be part of this committee.

TABLE OF CONTENTS

LIST OF TABLES

LIST OF FIGURES

LIST OF EQUATIONS

LIST OF ABBREVIATIONS

Convective Condensation Level CCL
Cold Core Eddy ..... CCE
Gulf Common Water ..... GCW
Gulf of Mexico ..... GOM
Hurricane Category ..... Cat
Loop Current LC
Maximum Potential Intensity ..... MPI
Maximum Sustained Wind Speed ..... MSWS
Ocean Heat Content ..... OHC
National Hurricane Center ..... NHC
National Oceanic and Atmospheric Administration ..... NOAA
National Weather Service ..... NWS
Rapid De-Intensification ..... RDI
Rapid Intensification ..... RI
Radius of Maximum Wind ..... Rmax
Sea Surface Height ..... SSH
Sea Surface Height Anomaly ..... SSHA
Sea Surface Temperature ..... SST
Sverdrup ..... Sv
Tropical Cyclone Heat Potential ..... TCHP
Warm Core Eddy ..... WCE

ABSTRACT

POSSIBLE EFFECTS OF THE LOOP CURRENT ON INTENSITY AND RAPID INTENSIFICATION OF HURRICANES IN THE GULF OF MEXICO

Sherry L. Young, M.S.

George Mason University, 2019

Thesis Director: Dr. Randy McBride

Increasing population in coastal communities is putting more lives and property at risk from hurricanes. A great need exists for a better understanding of hurricane intensity and rapid intensification; especially if frequency and intensity could increase because of warming oceans. Eleven Gulf of Mexico hurricanes and their fluctuations in intensity relative to proximity to the Loop Current, ocean heat content, depth to the 26°C isotherm, and SST were investigated. ESRI ArcMap was utilized to map and relate hurricane and ocean surface layer data obtained by satellite, reanalysis products, and National Hurricane Center observations. 164 data points were binned to sort by proximity to the Loop Current and to isolate other factors such as eyewall replacement cycles and wind shear. Linear regression was used to calculate correlations between variables and intensity, percent of maximum potential intensity, and to calculate probability of rapid intensification. Katrina had the best correlation between sustained wind speed and ocean heat content at 91% during rapid intensification episodes. During favorable conditions, data points with the highest sustained wind speeds of 250 km/hr or more and that reached 100% of maximum potential intensity occurred where sea surface temperature was

29.75°C or greater, depth to the 26°C isotherm was 50 m or more, and tropical cyclone heat potential was 90 kJ/cm² or more. Hurricanes over the Loop Current had a greater probability of intensifying at 39% and undergoing rapid intensification at 26.5%, compared to those over Gulf common water where ~25% intensified and ~17% rapidly intensified, and had less of a probability of de-intensifying during both favorable and unfavorable conditions. During favorable conditions, hurricanes over the Loop Current intensified ~62% and rapidly intensified ~57% of the time while those over Gulf common water intensified ~48% and rapidly intensified ~40% of the time. Results suggest that increased ocean heat content and depth to the 26°C isotherm in the Loop Current limits surface cooling due to mixing permitting additional intensification during favorable conditions.

1. INTRODUCTION

Between 1960 and 2008 population along the Gulf Coast increased by approximately 150%; an amount that is more than double the national average (Wilson and Fischetti, 2008). According to the 2016 U.S. Census, ~15.5 million people live within the 55 counties that border the Gulf coastline (U.S. Census Bureau, Population Division). Another ~43 million live in the 128 counties along the Atlantic coast for a total ~58.5 million people that live in counties potentially adversely affected by hurricanes, and this number is expected to continue to rise. Increasing population density and development in coastal communities is putting more lives and property at risk from tropical cyclones yearly (Meehl et al., 2007; Walsh et al., 2015; Balaguru et al. 2016).

Even though forecasting tropical cyclone trajectory has greatly improved within the last decade, the skill level of forecasting intensity still needs improvement; especially in predicting episodes of rapid intensification (RI), so much so that it is a top forecast priority of the National Hurricane Center (NHC) and the Tropical Prediction Center (Shay et al. 2000; Kaplan and DeMaria, 2003; Walker et al., 2009; Rapport et al. 2010; Wu et al., 2012). Rapid intensification is defined by the NHC as an increase in the maximum sustained wind speed of a tropical cyclone by 30 kts (56.5 km/hr) or more within 24 hours (Rapport et al. 2010). Processes involved in rapid intensification are still poorly understood and predicting it is still relatively difficult and often unsuccessful (Rapport et al. 2010, Kaplan et al., 2010). This puts life and property at great risk because

hurricanes in the Gulf of Mexico have rapidly intensified before; greatly increasing their intensity and destructiveness, sometimes within just hours of landfall (Lin et al., 2013 (b); Shay et al., 2000).

Hurricane Camille (1969) rapidly intensified from a category 3 hurricane to a category 5 hurricane 34 hours before making landfall (Kieper et al., 2016). Camille de-intensified slightly 16 hours before landfall during an eyewall replacement cycle (Kieper et al., 2016). Within the last 6 hours, Camille intensified and made landfall near Waveland, Mississippi as a category 5 hurricane with ~277 km/hr sustained winds (Kieper et al., 2016). Damages from Camille totaled 1.4 billion in 1969 U.S. dollars (9.2 billion adjusted for inflation to 2011) and left 256 dead (Blake et al., 2011).

Hurricane Opal (1995) rapidly intensified to a category 4 hurricane within 48 hours of landfall; luckily, Opal just as rapidly de-intensified to a category 3 storm within 12 hours of landfall (Kaplan and DeMaria, 2003). Hurricane Katrina (2005) explosively intensified to a category 5 hurricane within 24 hours of landfall; then rapidly de-intensified 6 hours before making landfall as a category 3 hurricane (Rapport et al., 2010). Even though Katrina's intensity decreased considerably before landfall, the resulting damages totaled 125 billion in 2005 U.S. dollars (160 billion adjusted for inflation to 2017) and caused 1200 documented deaths making it one of the costliest and deadliest hurricanes to make landfall in the U.S. (Blake et al., 2011).

The most lethal historic hurricane that made landfall in the continental United States was the category 4 Galveston Hurricane of 1900 with ~8000 deaths (Emanuel, 2003). Today, just one bridge on I-45 connects Galveston Island to the mainland; Galveston currently has a population of ~50,000 people. Because of increased population density within coastal communities, there could be inadequate time for successful evacuations resulting in a large number of casualties if the forecast for a high intensity storm at landfall comes too late. Furthermore, evacuations are costly and sometimes carried out when unnecessary because of uncertainty in the forecast for intensification and landfall location (Emanuel, 1999).

With population and development increasing along coasts yearly, a great need exists for a better understanding of hurricane intensity and rapid intensification; especially if tropical cyclone frequency and intensity could increase because of warming oceans in the coming decades (Lin, et al., 2013; Walsh et al., 2015; Balaguru et al. 2016). Current research suggests that climate change could increase tropical cyclone intensity, frequency, and duration, especially of the most intense storms (Emanuel, 2008 & 2013; Knutson et al., 2015; Oouchi et al., 2006; Walsh et al., 2015; Balaguru et al., 2016, Sobel et al., 2016). Knutson et al. (2015) proposed an average increase from 2.7 to 4.3 category 4 and 5 tropical cyclones per year and a 35% increase in the number of days with a category 4 or 5 storm. Warming of the ocean's mixed layer was the mechanism proposed to be responsible for increases in intensity and frequency of strong hurricanes (Emanuel et al., 2013; Knutson et al., 2015).

It's been hypothesized that high sea surface temperatures (SST) under the path of a hurricane affects the storm's capability to undergo rapid intensification (Emanuel, 1986; Kaplan and DeMaria, 2003; Knutson et al., 2010). Other studies have proposed that regions of high ocean heat content (OHC) affect maximum intensity and can trigger episodes of RI (Shay et al. 2000, Shay and Uhlhorn, 2008; Uhlhorn and Shay, 2011; Lin et al. 2013 (a & b); Jaimes et al., 2016). The Loop Current (LC), which enters the Gulf of Mexico (GOM) from the Caribbean Sea through the Yucatán Straits, has been hypothesized to be responsible for rapid intensification of Gulf hurricanes because of the deep warm water it transports (Shay et al. 2000, Shay and Uhlhorn, 2008; Keim and Muller, 2009; Uhlhorn and Shay, 2011; Lin et al. 2013 (a), Jaimes et al., 2016). Do areas of high OHC, such as in the Loop Current and its warm core eddies (WCE), trigger episodes of rapid intensification? If they do, does a statistical relationship exist that can be used to improve forecasting of RI and the maximum intensity hurricanes will achieve just before landfall? This study investigated 11 historic GOM hurricanes and their fluctuations in intensity relative to proximity to the Loop Current, ocean heat content, and sea surface temperature, in an effort to increase our understanding of rapid intensification and hurricane maximum intensity.

1.1. Scope

The scope of this study is a subset of 11 hurricanes that occurred between the years of 2002 and 2012 that made landfall on the Gulf Coast (Figure 2-1). Tracks of the

focus hurricanes passed over the east-central region of the Gulf of Mexico where the Loop Current is generally located and where the associated eddies originate. Five of the hurricanes completed cycles of RI. The six other hurricanes had numerous episodes of increase or decrease in sustained wind speed; however, these episodes did not qualify as full RI cycles. All of the focus storms achieved at least category 1 hurricane status while in the GOM; four had periods in which they were classified as tropical storms with sustained winds of less than 119 km/hr. Analysis of each hurricane's track in relation to the Loop Current and its eddies and intensity fluctuations were completed in order to detect if relationships between OHC, SST, depth to the 26° C isotherm and intensity exist.

1.2. Goal and Objectives

The goal of this study was to evaluate what effects, if any, the Loop Current and its associated eddies have on rapid intensification and the maximum intensity of hurricanes in the GOM, and to detect any mathematical or statistical relationships that may exist between ocean heat content, sea surface temperature, depth to the 26°C isotherm and intensity. One additional goal of this study was to analyze if OHC or SST affected the percentage of maximum potential intensity (MPI) the hurricanes ultimately achieved. The overall objective of this research was to further our understanding of the process of rapid intensification and to determine if the amount of OHC available in the Loop Current and its eddies affects the maximum intensity achieved in order to increase our skill level of forecasting intensity and rapid intensification.

The following process was conducted in order to achieve these goals and objectives. First, tracklines of the 11 hurricanes were mapped in ESRI ArcMap over a raster containing sea surface height (SSH) altimeter data that provided the location of the Loop Current and its associated eddies. Next, National Hurricane Center (NHC) observational and HURDAT2 data was collected and attached to data points based on location and time in ArcMap. SST, tropical cyclone heat potential (TCHP), and depth to the 26°C isotherm data were collected and entered into ArcMap as layers. Then, the theoretical maximum potential intensity (MPI) for each data point was calculated and compared to the actual intensity. Maximum sustained wind speeds were assessed for changes and compared to the ocean surface data layers. Finally, all of the recorded data was analyzed to formulate statistics and probabilities of changes in intensification and RI compared to oceanic and atmospheric conditions.

1.3. Significance

Significance of this research is that it will contribute to a better understanding of hurricane intensity and episodes of RI, and how OHC and SST may affect hurricane intensity. Increasing our understanding could increase our skill level in forecasting hurricane intensity and assist in predicting the possible effects of ocean warming on future hurricane intensity. Additionally, with increased understanding, more accurate and timely predictions of risk may be made allowing for faster implementation of evacuation plans and mitigation strategies; thus, reducing risk to lives and property. This study varies

from known previous studies in that it takes a geographic approach in relating historical hurricane intensity to areas of elevated OHC and in that it also statistically analyzes relationships between intensity, other factors that affect intensity, and spatial location for multiple hurricanes over several seasons.

1.4. Overview of Study

This study is organized into the following eight sections; Introduction, Study Area, Background, Datasets and Methods, Results and Discussion, Discussion, Conclusions, and the Appendix. In the "Introduction" the importance of this research and its scope, goals, and objectives are defined. In section two; "Study Area", the Gulf of Mexico's geography and general climatology is provided. Section three contains all of the "Background" information that was utilized in this study. Here you will find the literature review, explanations of the equations and theories, details about the Loop Current, basics of hurricane thermodynamics, research questions and working hypotheses. Section four "Datasets and Methods" provides detailed information about the methods and data formats that were used. In the "Results and Discussion" section, detailed results about each hurricane and the summary results of the statistical analysis are given. "Discussion" elaborates on the statistical results and any problems encountered. The last written section is "Conclusions", this is where the research results are summarized. The very last section, the "Appendix", is where you will find detailed tables of all of the data collected and analyzed.

2. STUDY AREA

Study area includes the Gulf of Mexico and coastal communities of eastern Texas, Louisiana, Mississippi, Alabama, and Florida where the focus hurricanes made landfall (Figure 2-1). This region is located in the subtropics between 20°N and 30°N latitude and 23°W and 27°W longitude. Atmospheric circulation at the surface is dominated by the Easterly Trade Winds. Köppen climate classification is humid subtropical; average high temperatures are relatively warm between ~25°C and 27°C, and precipitation is abundant year-round with tropical cyclones frequent during the summer and early fall (Table 2-1).

The Gulf of Mexico is characterized by low elevation coastal plains, estuaries, wetlands, and sandy beaches (Pendleton et al., 2010). Abundant sediment is transported by the vast Mississippi River drainage system which creates a large delta and numerous wave dominated barrier islands (Pendleton et al., 2010). Wave energy and tidal range are low because of the shallow water depth on the wide gently sloping continental shelf, as well as the blocking of the astronomical tidal bulge by the Florida Peninsula and Caribbean Islands; however, storm surge and storm induced waves increase in height due to friction and can become large in magnitude (Needham, 2013; Irish et al., 2008).

Figure 2-1 Study area: Gulf of Mexico

Table 2-1 Average climatic conditions

Average climatic conditions of coastal cities in the Gulf of Mexico (U.S. Climate Data, 2018)

City, State	Average Annual High Temperature	Average Annual Low Temperature	Average Annual Precipitation Rain/Snow
Clearwater, Florida	27.7°C	18.6°C	138.9 cm/0.0 cm
Mobile, Alabama	25.3°C	13.9°C	168.1 cm/0.5 cm
Gulfport, Mississippi	25.1°C	15.2°C	165.6 cm/0.0 cm
New Orleans, Louisiana	25.1°C	16.8°C	161.3 cm/0.0 cm

3. BACKGROUND

3.1. The Gulf of Mexico and the Loop Current

The Gulf of Mexico's primary features are its wide shallow continental shelves, the Mississippi Fan and associated canyons, continental slopes and rises, basins and plains, salt domes, escarpments, and the Loop Current and its associated eddies. Width of the continental shelves vary from 40 km to 200 km offshore; with the widest being the West Florida Shelf and the Yucatán Shelf (Figure 2-1). Bathymetry varies from less than 120 meters on the shelves to more than 3500 meters at the bottom of the Sigsbee Abyssal Plain (Figure 3-1) (NOAA Gulf of Mexico Data Atlas).

The Loop Current (LC) is a geostrophic current that connects the Yucatán Current to the Florida Current that transports warm tropical water and heat from the Caribbean Sea poleward (Figures 3-1, 3-2, & 3-3) (Shay and Uhlhorn, 2008; Uhlhorn and Shay, 2011; LeHénaff et al., 2012). The anticyclonic current is approximately 200-300 km wide and 800-1000 meters deep (Masters, 2014; National Academies of Sciences, 2018) with a mixed layer of approximately 50 meters during the summer and fall (Shay and Uhlhorn, 2008) (Figures 3-3). Because of Ekman transport, water pools in the center of the Loop Current and its WCE raising the surface by ~1 meter, thus deepening the thermocline due to downwelling (Figure 3-2 & 3-3). This creates adjacent cyclonic cold core eddies (CCE) (Shay and Uhlhorn, 2008) which have a raised thermocline due to upwelling. Recent estimates approximate the Loop Current's mean transport at ~24 Sv. with a near

surface velocity of up to ~1.0-2.0 m/s (Sheinbaum et al., 2002; Shay and Uhlhorn, 2008; Masters, 2014) (Figure 3-3).

The Loop Current has two states; the retracted state and the extended state (Figure 3-2) (LeHénaff et al., 2012; National Academies of Sciences, 2018). During the retracted state, the Loop Current stays close to the northern shore of Cuba and flows to the east directly into the Florida Current. During the extended state, the current forms a large loop with clockwise flow that can extend as far north as 28° N latitude, or ~500 km northward, before heading south and then east into the Florida Current (Shay et al., 2000; LeHénaff et al., 2012). Once the current extends to its farthest extent, anticyclonic rings pinch off the Loop Current and travel westward across the Gulf basin as warm core eddies at a speed of approximately 2.1 km a day (Elliott, 1982; LeHénaff et al., 2012).

These WCEs transport 7 x 10^6 kJ/m^2 of heat and 17 g/cm^2 of salt which mixes convectively into the Gulf common water (GCW) over a time period of approximately a year (Elliott, 1982). The WCEs can be as large as 300 km wide and 500-1000 meters deep with a current velocity of ~1-2 m/s (Figure 3-3) (National Academies of Sciences, 2018). WCEs form on average once every 8 to 9 months; however, they can form within a few weeks to as long as 19 months; multiple WCEs may exist at one time (Shay and Uhlhorn, 2008). Even though the Loop Current's exact geographic location and extent varies, satellite altimetry data can identify the location of the Loop Current and its eddies because of the sea surface anomalies they create (LeHénaff et al., 2012).

During the most active summer months of hurricane season, climatological mean SST in the GOM varies less than 1 degree; from 28.5°C to 29.5°C, with the warmest temperatures occurring on the continental shelves (Figure 3-5) (Boyer et al., 2011). The highest average mean SSTs occur during the months of July, August, and September with average highs between 29°C-29.5°C (Figure 3-6). August has the most homogenous mean SST across the entire Gulf basin varying between 28.5°C-29.5°C, with the majority of the basin having a mean SST greater than 29°C (Boyer et al., 2011). Kaplan et al. (2010) found that 68.7% of the hurricanes that rapidly intensified in the Atlantic basin including the GOM from 1989 to 2006, occurred in the months of August and September.

During the rest of the year, the variance in mean SST is greater with the warmest temperatures occurring in the Loop Current, Florida Current, and off the coast of Veracruz, Mexico (Figures 3-5 & 3-6) (Boyer et al., 2011). SST variance is greatest, up to 10°C, in the winter months of January through March. Spring months, April through June, show less variance in mean SST of ~3°C, while the fall months of October through December show slightly more variation up to ~6°C. Climatological mean SST remains above 26.5°C in the Loop Current from April to December with the highest temperatures occurring from July to September (Boyer et al., 2011).

Temperatures at depth in the Loop Current and WCEs is greater than the temperature in the surrounding GCW and CCEs (Figures 3-7 & 3-8). Climatological mean temperature remains above 26.5°C in August, September, and October in the LC

down to a depth of at least ~60 meters; whereas, in the surrounding GCW it is up to ~10°C cooler at the same depth (Figures 3-7 & 3-8) (Boyer et al., 2011). Temperatures in October are higher at depth in the LC than in August and September even though the SST is starting to cool. During November the temperatures at depth in the LC start to cool slightly (Figure 3-8); however, temperatures at depth in the LC remain warmer than those in the GCW year-round. The coolest mean temperatures at 60 m depth in the LC: 23°C-25.5°C, occur in February and March.

Ocean heat content is higher in the LC and its WCEs than the GCW and CCEs, even in the summer months, because of the increased temperatures at depth (Uhlhorn and Shay, 2011). In the LC and WCEs the 20°C isotherm is ~270 m deep and the 26°C isotherm is ~60-125 m deep (Figures 3-3 & 3-4) (Shay et al., 2000; Uhlhorn and Shay, 2011; Jaimes et al., 2016). This is much deeper than it is in the GCW where the 20°C isotherm is ~100 m deep and the 26°C isotherm is ~50 m deep or less (Figure 3-4) (Boyer et al., 2011, Uhlhorn and Shay, 2011). In the CCEs the 26°C isotherm can be as shallow as ~30 m or less; cooler water this close to the sea surface greatly reduces the ocean heat content (Shay et al., 2000; Uhlhorn and Shay, 2011; Jaimes et al., 2016). The exact depths of the thermoclines vary by season and month. Because OHC is integrated from the surface starting with the SST, sometimes even CCEs can have relatively higher than mean OHC if the SST is higher than normal.

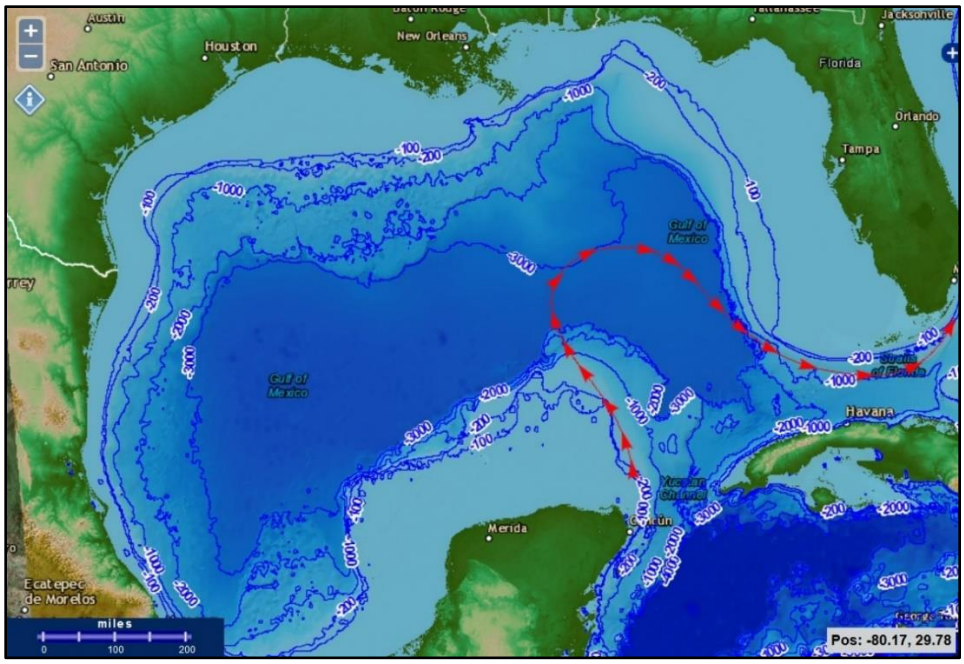

Figure 3-1 Bathymetry of the Gulf of Mexico

Seafloor depth in the Gulf of Mexico in meters. The expansive continental shelves are shown in pale blue and the LC and its direction of flow are shown by the red line with arrows. From the NOAA Gulf of Mexico Data Atlas website.

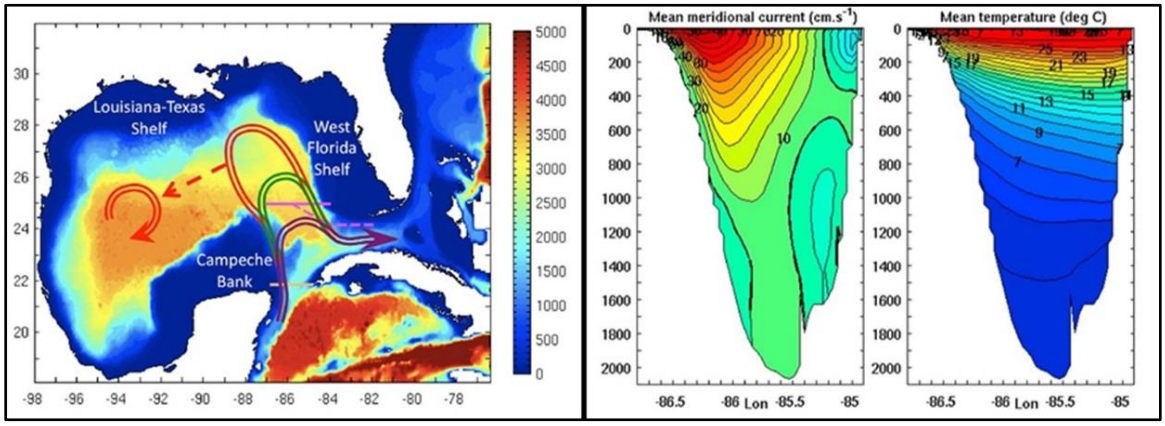

Figure 3-2 Loop Current states

Left: background coloration shows bathymetry depth in meters, the purple state is retracted, green is average, and red is the extended state showing a detached eddy. Right: Cross sections of the Loop Current at 21.85°N Latitude at the opening of the Gulf in the Yucatán Strait showing velocity in cm/s (left) and temperature at depth (right) in °C from the model used in LeHénaff et al., 2012

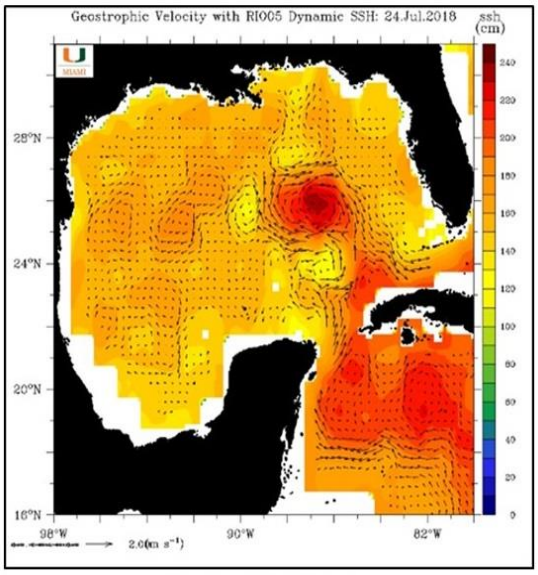

Geostrophic Velocity

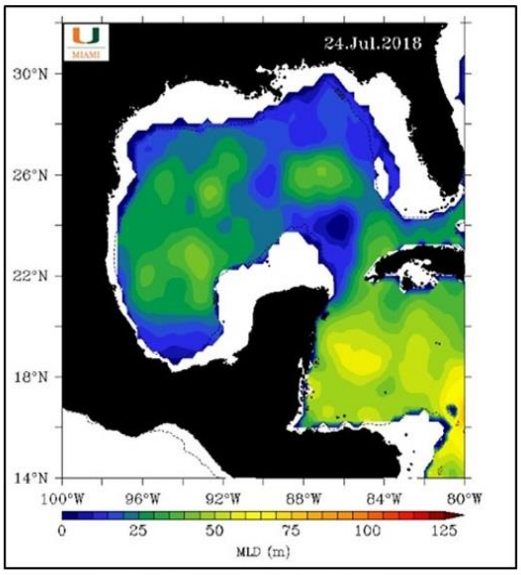

Mixed Layer Depth in Meters

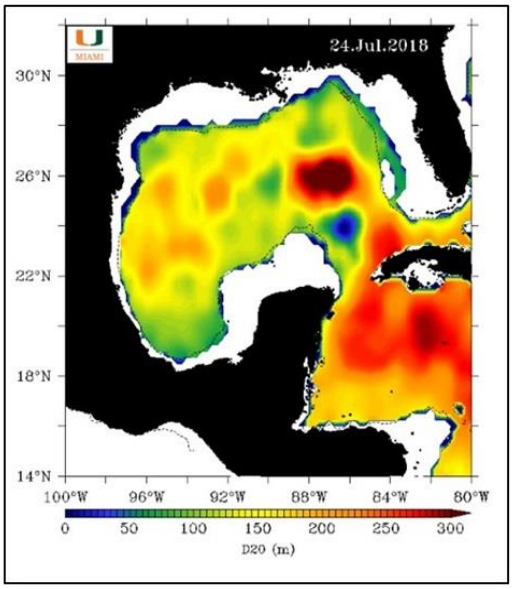

Depth to the 20°C Isotherm

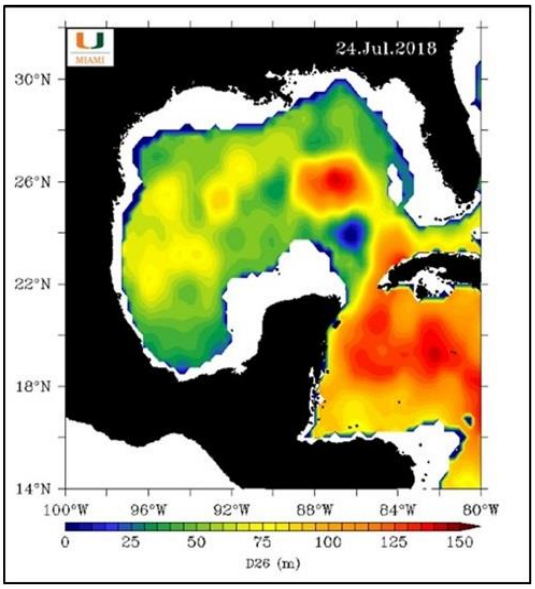

Depth to the 26°C Isotherm

Figure 3-3 Loop Current velocity diagram & depths

Top left: velocity of flow by length of arrows, and dynamic SSH in cm by background color. Top right: the mixed layer depth in meters. Bottom left: depth to the 20°C isotherm and bottom right: depth to the 26°C isotherm in meters for 07/24/2018 (Diagrams: Rosenstiel School of Marine and Atmospheric Science, Shay, 2019)

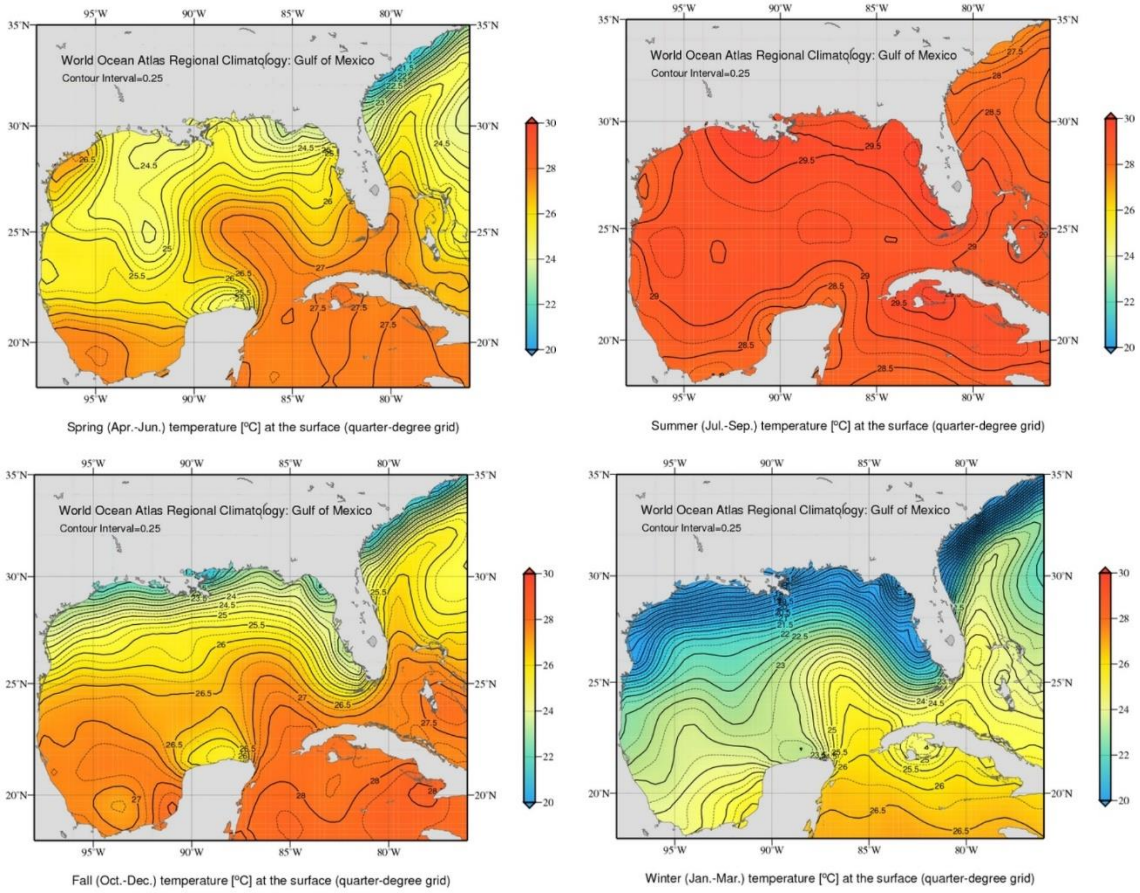

Figure 3-4 Climatological mean SST by season.
(Diagrams: NOAA National Centers for Environmental Information Gulf of Mexico Data Atlas, Boyer et al. 2011)

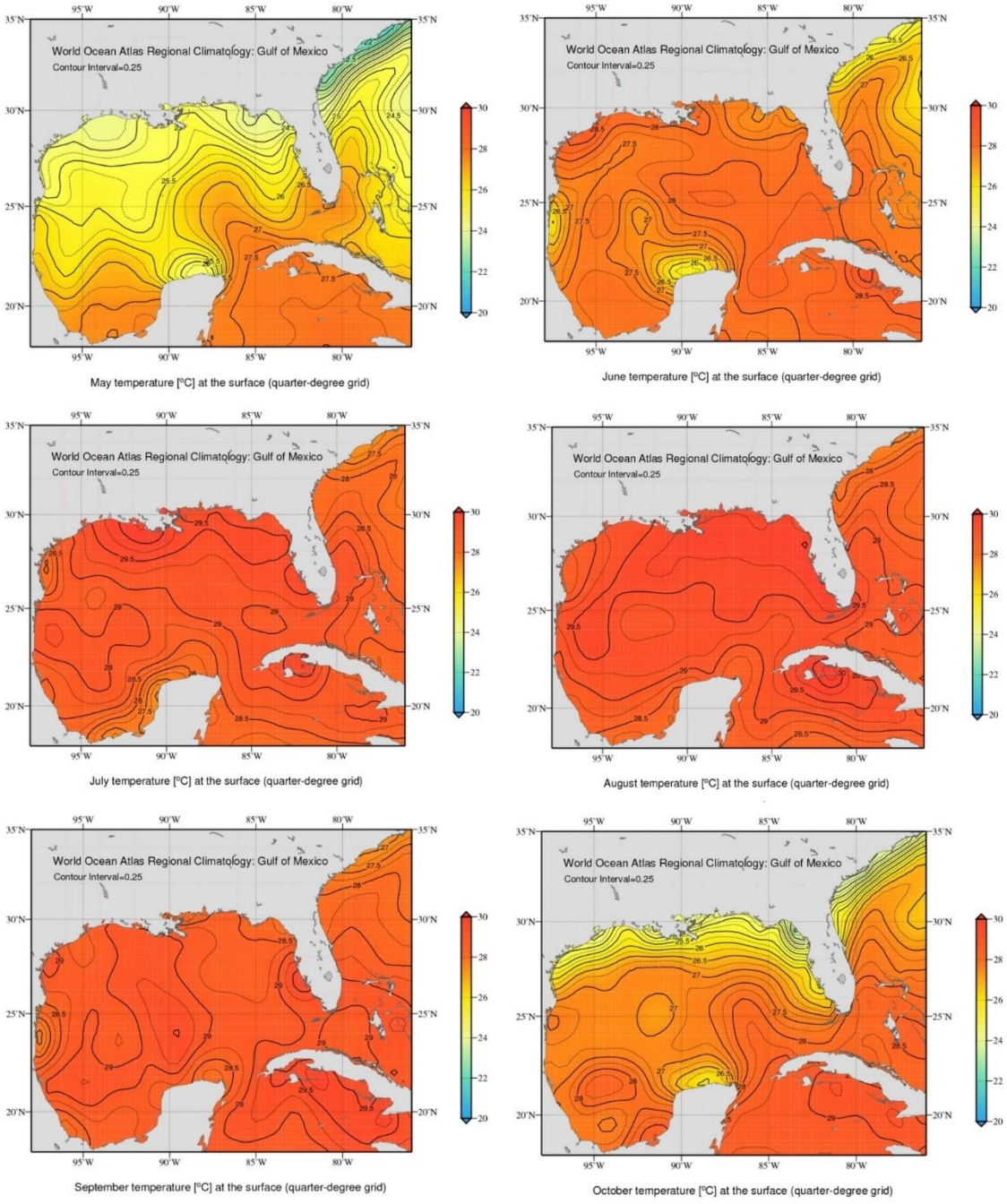

Figure 3-5 Climatological mean SST by month
(Diagrams: NOAA National Centers for Environmental Information Gulf of Mexico Data Atlas, Boyer et al. 2011)

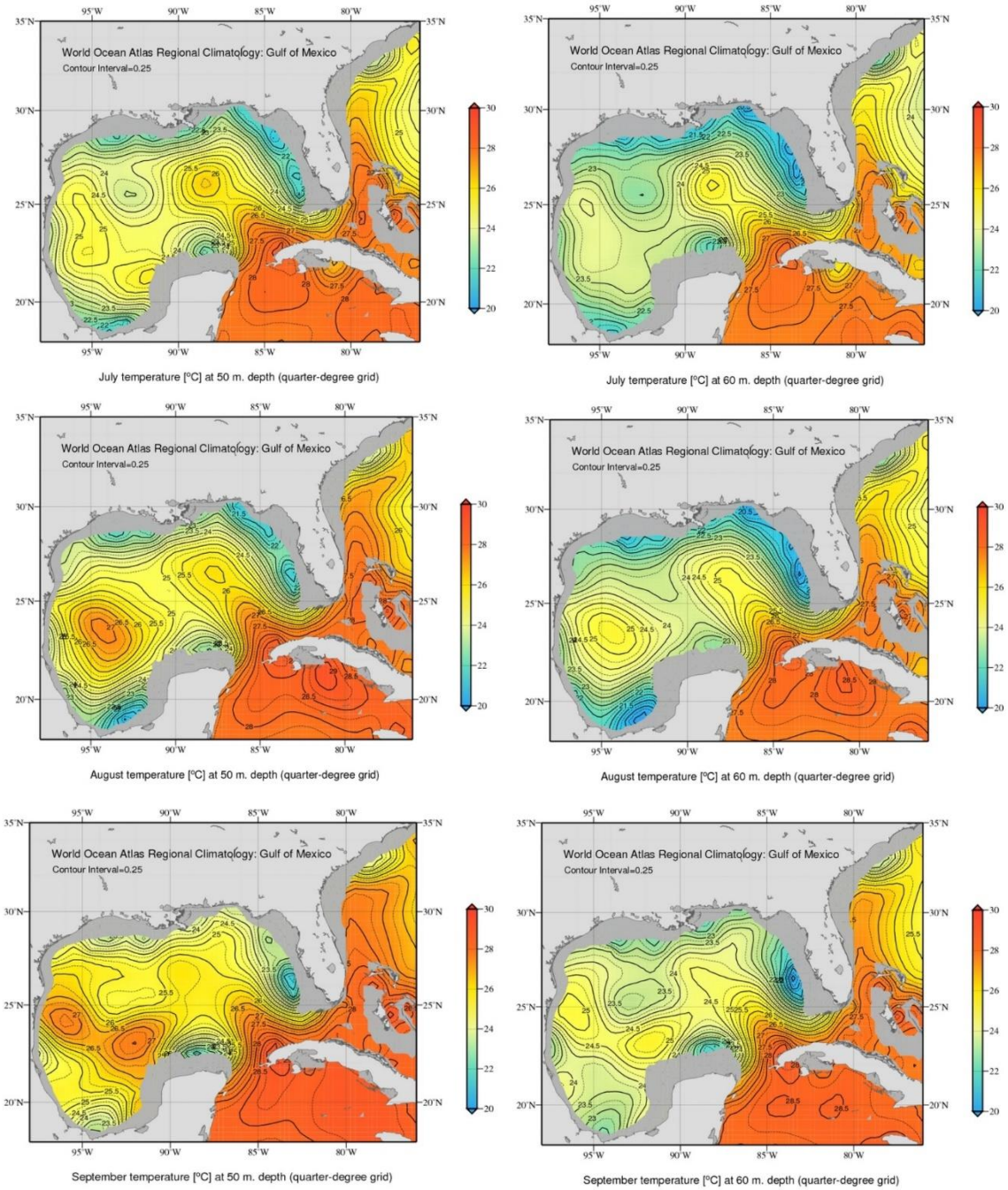

Figure 3-6 Summer temperature at depth: 50 & 60 m

Climatological temperature at depth during the months of July, August, and September, left: 50 m right: 60 m in °C. Because this is a climatological mean, WCEs are not well represented; however, difference between the LC temperature at depth and that of GCW is apparent. Temperatures in September are higher at depth than July and August. (NOAA National Centers for Environmental Information Gulf of Mexico Data Atlas, Boyer et al. 2011)

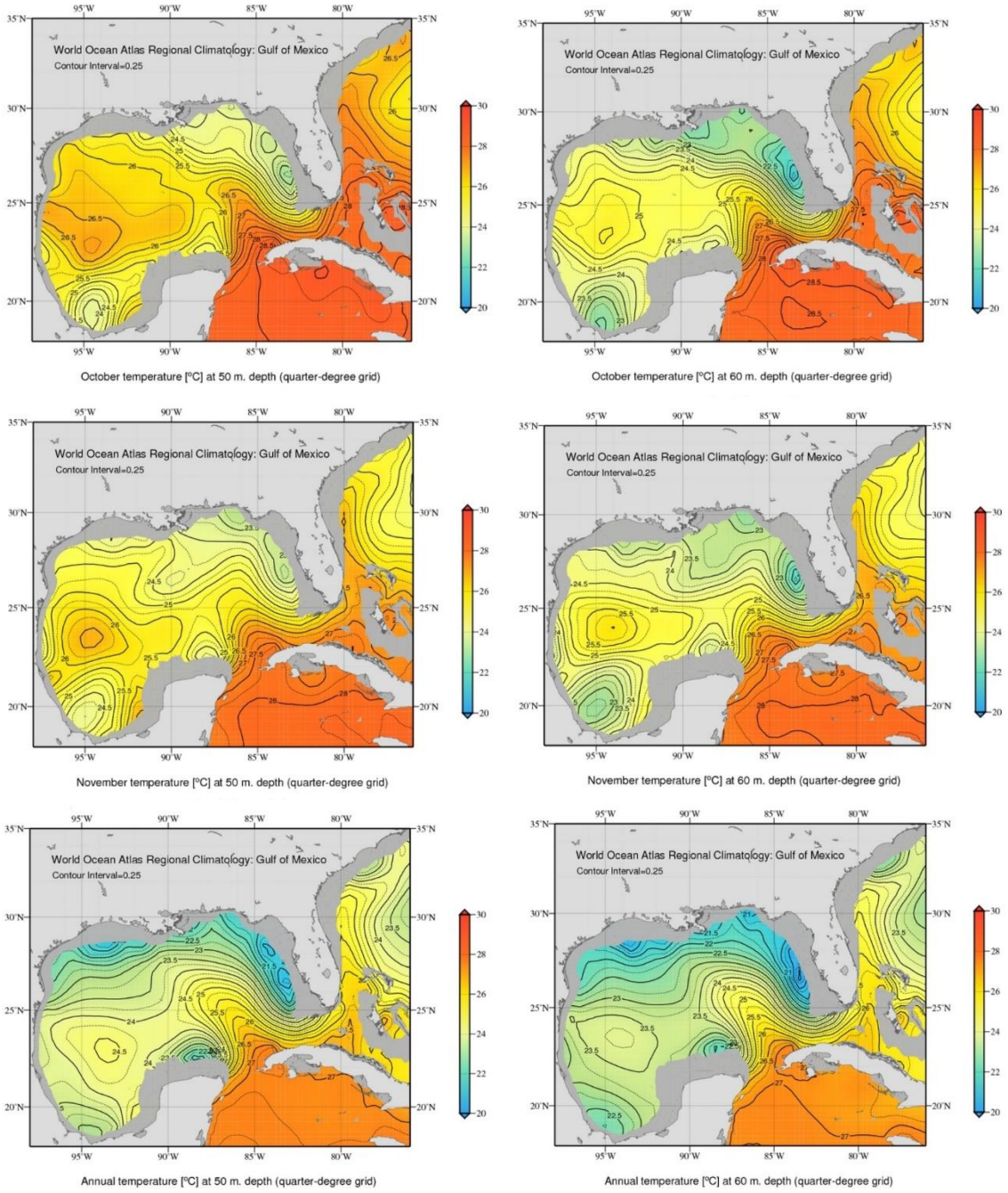

Figure 3-7 Fall and annual temperature at depth:
Climatological temperature at depth during the months of October and November, left: 50 m right: 60 m in °C. Temperatures in October are higher at depth in the LC than in August and September even though the SST is starting to cool. During November, temperatures at depth in the LC start to cool. Bottom row: annual climatological mean temperature at 50 and 60 m. Temperatures in the LC remain warmer than those in the GCW year-round. (Diagrams: NOAA National Centers for Environmental Information Gulf of Mexico Data Atlas, Boyer et al. 2011)

3.2. Hurricane Intensity and MPI

Intensity of a tropical cyclone in the United States refers to its peak 1-minute sustained wind speed at a height of 10 meters (Schott et al., 2012). Tropical cyclones with sustained wind speeds above 118 km/hr are classified as hurricanes and assigned a category between 1 and 5 based on the Saffir Simpson Hurricane Wind Scale (Table 3.1). Those with sustained winds below 118 km/hr but above 63 km/hr are classified as tropical storms (Schott et al., 2012). Central pressure of a hurricane has a negative relationship with sustained wind speed; as pressure drops wind speed generally increases.

Central pressure and predicted storm surge magnitude were previously components of the Saffir Simpson Hurricane Scale. Over time it was found that central pressure and storm surge magnitude may vary between storms of the same category (Schott et al., 2012). Some storms produced larger storm surge than the scale predicted, this was observed in Hurricanes Katrina (Resio and Westerink, 2008) and Ike (Schott et al., 2012). Because of possible variance, predicted storm surge and pressure components were removed from the scale in 2010 (Schott et al., 2012).

Table 3-1 Saffir Simpson Hurricane Wind Scale
(Schott et al., 2012) conversions rounded to whole numbers.

Category	Lower Bound		
	Wind kts	Wind km/hr	Wind mph
TD	20	35	22
TS	35	63	39
1	64	119	74
2	83	154	96
3	96	178	111
4	113	209	130
5	137	252	157

The theoretical maximum upper limit of intensity a hurricane can reach for any given SST is known as its maximum potential intensity (MPI) (Emanuel, 1986; Holland, 1997). Emanuel (1986) contends that hurricanes are basically Carnot heat engines that acquire enthalpy at the sea surface and release latent heat in the upper troposphere or lower stratosphere that is then converted to kinetic energy. MPI is based on the assumption that only a fraction of the latent heat extracted from the ocean surface is converted to kinetic energy, and that all of the kinetic energy produced is then dissipated. Furthermore, it is also assumed that the rate at which the energy is released and dissipated relates to the wind speed. Emanuel's equation for maximum wind speed was created by equating these two rates. MPI calculates (Equation 3-1) the wind speed at which the enthalpy gained equals the energy lost in dissipation caused by friction between the winds and the surface and a steady state is reached (Emanuel, 2003).

Emanuel's equation for MPI is best explained by breaking it down into 4 parts: ratio of the bulk exchange coefficients C_k to C_D, thermodynamic efficiency($\mathcal{E}$),

representation of the Clausius Clapeyron relationship, and relative humidity within the boundary layer. Thermodynamic efficiency (Ɛ) is defined as the ratio of the difference between SST (T_o) in °K and the temperature of the atmosphere at the altitude of outflow (T_a) in °K to the SST (T_o) as shown by the equation: $(T_o-T_a)/T_o$ (Emanuel, 1998). As the difference between the two temperatures increases, thermodynamic efficiency also increases; this enhances the capability of the hurricane to intensify because more water vapor will be condensed liberating latent heat (Emanuel, 1986; Holland, 1997). For most hurricanes the thermodynamic efficiency is equal to approximately 1/3 but fluctuates based on the temperature of the sea surface and at outflow (Emanuel, 1986). Taller convective cloud columns have lower cloud top temperatures increasing the thermodynamic efficiency, as does higher sea surface temperatures.

The ratio of the bulk exchange coefficients is the ratio between the enthalpy transfer coefficient C_k and the momentum coefficient C_D; the ratio of coefficients modifies the rate of transfer of the available heat energy into kinetic energy used for wind momentum (Emanuel, 1986). Because obtaining direct turbulent flux measurements in the hurricane boundary layer in winds speeds above 50 m/s is extremely difficult and unreliable close to the storm's core, inputs for this ratio are currently not well defined (Richter et al., 2016; Holland, 1997; Bell et al., 2012; Jeong et al., 2012). Richter et al. (2016) found significant error in using the flux profile method to estimate C_k/C_D during high winds in 37 tropical cyclones. Emanuel (2003) assumes that the ratio is unity; but a study by Bell et al., (2012) which used 6 CBLAST missions to estimate values for C_k and

C_D for storms with wind speeds above 50 m/s, estimated C_D to be $2.4 \times 10^3 \pm 1.1 \times 10^3$ and C_k to be $1.0 \times 10^3 \pm 0.4 \times 10^3$. Estimations in Bell et al. (2012) could reduce C_k/C_D to as low as possibly 0.4.

The Clausius Clapeyron relationship is represented in the third part of the MPI equation which calculates the latent heat produced in joules by the amount of water vapor in excess of the saturation vapor pressure at the altitude of outflow. The Clausius Clapeyron equation determines how much water vapor air parcels at certain temperatures can hold; this amount changes by approximately 7% per 1°C. The symbol: ϵ is the ratio of the molecular weight of water vapor to dry air which is equal to .622. L_v is the latent heat of vaporization in joules and e* is the saturation vapor pressure (Emanuel, 1986). This is divided by P_m, the atmospheric pressure at the radius of maximum winds.

The total from the third part of the equation is multiplied by $(1-H_a)$. H_a is the relative humidity of the boundary layer; therefore, $1-H_a$ is the amount of additional water vapor that can be evaporated until the relative humidity equals 100%. If the boundary layer is already saturated, no more water can be evaporated and MPI cannot be calculated with this equation, the result becomes 0. Currently, relative humidity in the boundary layer of hurricanes is not well defined, this affects the accuracy of MPI because small changes in the value used for H_a can have a large effect on MPI (Table 3-3) (Emanuel, 1986; Holland, 1997).

Previous studies vary in the input for H_a from .75 to .90; however, most are assumptions because direct measurements of humidity in the hurricane boundary layer are rare. The lack of measured humidity data is because of the difficultly of obtaining it and other factors such as ocean spray and precipitation which can affect the results (Holland, 1997). Wu et al. (2012) used AIRS on the AQUA satellite to obtain environmental relative humidity and found that the near surface average relative humidity during the 198 North Atlantic tropical cyclones they analyzed was ~82% +/- 9% error. The result of the MPI equation (V^2) is wind speed in $(m/s)^2$; taking the square root will give the theoretical maximum wind speed in m/s that the hurricane could achieve.

Equation 3-1 Emanuel's Equation for MPI

$$V^2 = \left(\frac{C_k}{C_D}\right) \frac{T_o - T_a}{T_o} \frac{\in L_V e^*}{P_m} (1 - H_a)$$

Equation is a modified version of Emanuel's MPI equation for wind speed taken from Emanuel's MIT Website: "Physics of Mature Tropical Cyclones, I." Lecture 4: 13 Apr. 1998, 10:50, accessed 02/25/2017

SST below 26.5°C is considered inadequate for sustaining hurricane intensity in the GOM because it is generally equal to or less than the atmospheric temperature of the boundary layer. Emanuel's equation for MPI shown as Equation 3-1, does not account for this limitation because the thermodynamic disequilibrium in the boundary layer is not calculated (Lin et al., 2013). This equation will give a result for SST under 26.5°C, but it is important to note that the result may not be accurate for temperatures that low. The equation for MPI also does not consider other factors that may affect intensity such as eyewall replacement cycles, wind shear, interactions with land, or if the hurricane is developing or decaying (Holland, 1997).

Most hurricanes do not reach MPI during their lifecycle (Holland, 1997; Emanuel, 2003; Kotal et al., 2008; Lin et al., 2013 (a)). A study by Kotal et al. (2008) found that only 18% of the tropical cyclones in the Bay of Bengal reached over 80% of their MPI, and only 38% reached over 50%. Generally, MPI varies little between different storms and along the track of individual storms in the Gulf of Mexico during the summer months.

Table 3-2 Change in MPI per °C

Change in MPI per 1°C SST when temperature at outflow and pressure are held constant. The change is approximately ~7-9 km/hr but increases by an additional ~.1-.3 km/hr per 1°C.

SST °C/ °K	Temperature at Outflow °K	Pressure mb	Ɛ	H	MPI in km/hr	Change from MPI at 27° C in km/hr	Change from MPI at 1°C Lower
27/300.15	190	920	.367	.8	234.2	0	NA
28/301.15	190	920	.369	.8	241.9	7.7	7.7
29/302.15	190	920	.371	.8	249.8	15.6	7.9
30/303.15	190	920	.373	.8	257.9	23.7	8.1
31/304.15	190	920	.375	.8	266.1	31.9	8.2
32/305.15	190	920	.377	.8	274.6	40.4	8.5
33/306.15	190	920	.379	.8	283.3	49.1	8.7
34/307.15	190	920	.381	.8	292.2	58.0	8.9

Table 3-3 Changes in MPI per 10% change in H

Test calculations for MPI to determine change in MPI per 10% change in Ha value when SST and outflow temperature and pressure remain constant. To = 190°K Pm= 920 mb

SST in °C/K	MPI in km/hr per H value			MPI in km/hr Difference from H= .8	
SST	H=.7	H=.8	H=.9	H=.7	H=.9
28/301.15	296.3	241.9	171.1	54.4	-70.8
29/302.15	305.9	249.8	176.6	56.1	-73.2
30/303.15	315.8	257.9	182.3	57.9	-75.6

3.3. Thermodynamic Process of Intensification

A thermodynamic and moisture disequilibrium needs to exist between the ocean surface and near surface boundary layer in order for enthalpy from the ocean to be transferred to the hurricane (Leipper and Volgenau, 1972; Emanuel, 2003; Jaimes et al., 2016). Atmospheric temperature over the subtropical oceans in the near surface boundary layer is ~26°C or higher; therefore, ocean water of 26°C or less has limited to no enthalpy exchange with the atmosphere shutting down thermodynamic processes in hurricanes (Leipper and Volgenau, 1972; Emanuel, 1986 & 2003; Seo and Xie, 2013; Jaimes et al., 2016). Heat exchange between the atmosphere and ocean occurs both convectively and through conduction, although conduction accounts for only a small part of the total energy flux (Leipper and Volgenau, 1972; Jaimes et al., 2016).

As hurricane winds blow over the ocean surface, sensible and latent heat is transferred from the warm water to the air within the near surface boundary layer increasing its potential temperature (Leipper and Volgenau, 1972; Emanuel, 2003: Seo and Xie, 2013; Jaimes et al., 2016). The warm moisture laden buoyant air rises convectively increasing updraft and lowering the central pressure (Jaimes et al., 2016). As the warm air rises in the eyewall it cools, once it reaches its saturation vapor pressure the excess moisture condenses into water droplets releasing latent heat warming the air (Leipper and Volgenau, 1972; Jaimes et al., 2016). The overall pressure gradient steepens increasing the wind speed. Increase in wind speed further increases the enthalpy flux

because turbulent flow excites water molecules on the ocean surface increasing evaporation and advection (Riehl, 1948; Emanuel, 2003; Lin et al., 2013 (a)).

Eventually the air at the cloud column top will cool and sink back to the surface in the eye and between the rain bands, warming and drying as pressure increases (Emanuel, 2003). If this dry air is entrained into the boundary layer it evaporates water from the ocean surface and convectively rises again increasing the energy flux. If this or other dry air is entrained into the mid or upper level of the convective column it can reduce condensation by lowering the relative humidity, this would limit the release of latent heat reducing the net energy flux to the storm. If evaporation cannot occur within the boundary layer or the air cannot convectively rise to the convective condensation level (CCL), enthalpy is not transferred to the storm, effectively cutting the hurricane's energy supply and reducing intensity (Leipper and Volgenau, 1972; Jaimes et al., 2016).

The above thermodynamic processes reduce the heat in the surface layer of the ocean leaving a cold wake under the hurricane's path (Leipper and Volgenau, 1972; Emanuel, 2003; Shay and Uhlhorn, 2008; Lin et al., 2013 (a); Jaimes et al., 2016). Water on the surface cools and sinks being replaced by water from below (Shay and Uhlhorn, 2008; Jaimes et al., 2016). Winds pushing on the ocean surface cause divergence which creates upwelling, turbulence, vertical shear, and mixing. Cooler water from below is entrained and mixes with the surface water, SST cools and the OHC decreases; this reduces the thermodynamic disequilibrium between the ocean and atmosphere limiting

the enthalpy flux (Leipper and Volgenau, 1972; Shay and Uhlhorn, 2008; Uhlhorn and Shay, 2011; Seo and Xie, 2013; Jaimes et al., 2016). If the surface cools to below 26°C the thermodynamic disequilibrium becomes so low that the enthalpy flux is effectively stopped.

If warm water above 26°C continues to a depth greater than the hurricane affects, mixing and upwelling does not greatly reduce the SST and OHC and the ocean is able to maintain the energy flux to the atmosphere (Shay and Uhlhorn, 2008; Uhlhorn and Shay, 2011; Jaimes et al., 2016). This continuous heat flux from the ocean allows for a positive feedback due to a greater net enthalpy transfer, effectively reducing the normal negative feedback of surface cooling; possibly allowing for rapid intensification (Shay and Uhlhorn, 2008; Uhlhorn and Shay, 2011; Lin et al., 2013 (a)). Effects caused by hurricane winds normally extend to depths greater than the depth to the 26°C isotherm, and sometimes in the GCW past the depth of the 20° isotherm. During exceptionally strong hurricanes, mixing up to 100 meters may occur (Lin et al, 2013) with the deepest mixing occurring close to the radius of maximum winds (Jaimes et al., 2016).

Jaimes et al. (2016) found that during hurricane Isaac wind induced convergence of warm water at the surface of a WCE caused downwelling and deepening of the thermocline increasing the OHC. The average temperature to “h”; the depth at which a change in temperature of more than 0.5°C occurs within 2 m, increased by ~0.5°C in the WCE while the GCW and water in the CCE decreased between 0.5 and 1.8°C. The small

increase in temperature could have been caused by other factors besides downwelling including horizontal advection or natural daily temperature fluctuations (Jaimes et al., 2016). Regardless, the data supported that the SST reduced more in the GCW and CCE than it did in the WCE due to hurricane Isaac. Jaimes et al. (2016) concluded that OHC was more correlated to Isaac's intensification from a TS into a category 1 hurricane than SST because Isaac was in close proximity to a WCE and over an area of elevated OHC when the intensification occurred; the SST however, remained relatively stable. The highest observed enthalpy flux during Isaac occurred over the WCE 2 to 3 radial distances outside of Rmax; the radius of maximum winds. Jaimes et al., (2016) concluded that increased wind speed does not influence the enthalpy exchange rate; that increased enthalpy flux is due to increased moisture disequilibrium and potential temperature in the hurricane boundary layer over areas of high OHC.

Shay and Uhlhorn (2008) also observed downwelling and deepening of the 26°C isotherm during Isidore in the eastern Yucatán Straits which increased in OHC by 20 kJ/cm^2; however, over the Yucatán shelf which had a shallower thermocline the OHC reduced by 40 kJ/cm^2 and SST reduced by 4.5°C. The center of the Yucatán Straits where the Loop Current flows to the north, remained stable in OHC and SST. This was attributed to the Loop Current carrying warm water northward which limited the vertical shear due to pressure gradients and velocity (Shay and Uhlhorn, 2008). Within the outer regions of the LC north of Cuba, depth to the 26°C isotherm decreased by ~20 m and the

SST decreased by ~1°C during Isidore; however, the OHC remained over 100 kJ/cm^2 before Lili's arrival (Shay and Uhlhorn, 2008).

During Lili SST changed little in the LC but in the GCW decreases were between 2°C and 6°C (Shay and Uhlhorn, 2008). Shay and Uhlhorn, (2008) concluded that the LC inhibits strong mixing and vertical shear due to its velocity and pressure gradients; furthermore, the mixing that does occur limits cooling due to the temperature profile, depth to the 26°C isotherm, and the high OHC. Bright et al (2002) found that advection from the Gulf Stream limited the negative feedback to cyclones in the North Atlantic. The flow of the warm water in the Gulf Stream replaced the heat lost due to the mixing by advection. Bright et al. (2002) also found that most of the tropical cyclones that traversed over the Gulf Stream or paralleled it intensified.

Hurricane Opal (1995) increased its maximum sustained winds from ~126 km/hr to ~216 km/hr while its pressure decreased from 963 mb to 916 mb within 14 hours while traversing over a WCE (Bosart et al., 1999; Hong et al. 2000; Shay et al., 2000). Rapport et al. (2010) found that a majority of the most intense hurricanes since 1995 reached their lowest pressure or highest maximum wind speed ~6-18 hours after passing over areas of the highest local OHC. Ho and Huang (2011) found a .8 correlation between rapid intensification and tropical cyclone heat potential (TCHP), defined as the OHC integrated to the 26°C isotherm, in 35 typhoons in the Pacific.

Net enthalpy flux depends on translation speed, wind speed, and SST, in addition to the OHC (Shay and Uhlhorn, 2008). Shay and Uhlhorn (2008) measured peak enthalpy flux during hurricanes Lili and Isidore (2002), they found that even though Lili had stronger sustained winds Isidore was able to draw more energy from the ocean. Peak enthalpy flux in Isidore was 1.8 kW/m^2 while in Lili peak surface flux was .4 kW/m^2 less at 1.4 kW/m^2 (Shay and Uhlhorn, 2008). Isidore had a much slower translation speed than Lili: 4 m/s compared to Lili's 7 m/s; furthermore, the SST was ~1°C lower in the LC during Lili than when Isidore passed through just a week prior (Shay and Uhlhorn, 2008).

Slower moving hurricanes stay over a region of ocean water longer and are able to absorb more energy from the ocean and increase in intensity if the TCHP is high and the depth to the 26°C isotherm is deep (Lin et al., 2013 (a)). Alternatively, hurricanes are more negatively affected by the cooling of the ocean surface if the TCHP is low and the depth is shallow (Emanuel, 1999; Lin et al., 2013 (a); Jaimes et al., 2016). Regions with lower TCHP are depleted of available heat faster than regions with higher TCHP. If the hurricane's speed of translation is fast, the effect from the ocean, both positively and negatively, is dampened.

3.4. TCHP and Intensity

OHC to the 26°C isotherm has been hypothesized to be one of the main factors for determining hurricane intensity. This amount of OHC in kilojoules has been given different names in various studies: TCHP (Tropical Cyclone Heat Potential) (Leipper and

Volgenau, 1972; Shay et al., 2000; Ho and Huang, 2011; Lin et al., 2013 (b)), OHC (ocean heat content) (Jaimes et al., 2016), and UOHC (Upper Ocean Heat Content) (Seo and Xie, 2013). OC_PI (Ocean coupling Potential Intensity Index) (Lin et al., 2013 (a)) was another method used in which the subsurface ocean temperature profile was taken into consideration; however, in this method SST was averaged to the 26°C isotherm and the mean temperature value in °C was used in place of SST in Emanuel's MPI equation in order to calculate maximum potential intensity.

The equation below calculates (Q): TCHP in kJ/cm^2. C_ρ is the specific heat of ocean water, ρ is density at the surface, T (Z) is the sea surface temperature, and dZ is the change in depth from the surface to the 26°C isotherm in meters (Leipper and Volgenau, 1972; Seo and Xie, 2013; Jaimes et al., 2016).

Equation 3-2 Equation for TCHP

$$Q = C_\rho \int_{h_{26}}^{\eta} \rho\,(\mathcal{Z})\,[T(\mathcal{Z}) - 26]\;d\mathcal{Z}$$

Taken from Leipper and Volgenau (1972)

OHC is one of the 8 statistically significant predictors used to forecast RI in the RII index created by Kaplan et al. (2010). Mainelli et al. (2008) analyzed OHC as a predictor in the SHIPS Perturbation model for hurricanes that occurred between 1995-2005 and found that OHC becomes significant at a threshold of 50 kJ/cm^2, however, this only reduced the error in the 72-hour forecast for the entire sample by 1%. When applied to regions of OHC over 60 kJ/cm^2 the reduction of error was greater and even more so for

OHC over 100 kJ/cm^2. Areas with greater OHC had the largest error reduction; because of this Mainelli et al. (2008) concluded that OHC may be an important predictor in regions with high OHC. In the Gulf of Mexico, OHC over 100 kJ/cm^2 is currently only found in the LC and the WCEs (Mainelli et al., 2008).

Currently, the TCHP threshold required to induce RI is still unknown (Jaimes et al., 2016). Observations of rapidly intensifying hurricanes have suggested that RI is more likely when the TCHP is ~80 kJ/cm^2 or more (Jaimes et al., 2016). The NHC SHIPS model utilizes a threshold of 50 kJ/cm^2 for possible intensification of tropical cyclones (Jaimes et al., 2016).

3.5. Other Factors that Affect Intensity

3.5.1. Relative Humidity & Dry Air Entrainment

Relative humidity (H) (Emanuel, 1986) is an important component of the MPI equation and its value under the hurricane eyewall is still not well defined and difficult to measure (Wu et al. 2012; Kaplan and DeMaria, 2003). Relative humidity has been hypothesized to be a major factor in hurricane intensity and rapid intensification; therefore, the relationship between intensity and humidity needs to be better understood in order to improve the skill level of intensity forecasting (Holland, 1997; Wu et al. 2012).

Studies have shown that relative humidity needs to be high in the mid and upper troposphere in order for hurricanes to rapidly intensify or reach their maximum potential intensity (Kaplan and DeMaria, 2003; Kaplan et al. 2010; Wu et al., 2012). This is because if the environmental air has lower relative humidity, the drier air will mix with the rising moist air in the convective column reducing condensation (Wu et al., 2012). Mixing and drying of the rising air limits the amount of latent heat released and available to the system to use as kinetic energy. Dry air entrainment also produces cold downdrafts which can infiltrate the core and destabilize the eye by producing asymmetrical convection (Emanuel, 1988; Wu et al., 2012).

Kaplan and DeMaria (2003) found that relative humidity was higher in the lower troposphere but above the boundary layer, as well as the mid and upper troposphere in hurricanes that underwent RI in the North Atlantic. Wu et al. (2012) found that out of the 198 North Atlantic tropical cyclones they analyzed, those that reached category 5 status had larger relative humidity values in the mid and upper troposphere; however, those results were not linear and not statistically significant. Wu et al. et al., (2012) also found that relative humidity stayed fairly constant in the boundary layer but decreased above the boundary layer over the life of the hurricane; but relative humidity increased with increasing intensity.

3.5.2. Vertical and Horizontal Wind Shear

Vertical and horizontal wind shear in excess of 20 kts has detrimental effects on tropical cyclones often elongating the eye, reducing outflow, causing asymmetrical or poor convection, and can cause gaps in the eyewall or even complete eyewall collapse (Willoughby et al., 1982; Kaplan and DeMaria, 2003). Strong horizontal shear can also shear the upper extent of the convective column elongating it or tear it off completely and displace it towards the direction of the shear (Willoughby et al., 1982). These effects reduce the total energy released to the system and thermodynamic efficiency by increasing the cloud top temperature effectively lowering intensity and reducing the capability of the storm to intensify. Studies have shown that hurricanes that underwent rapid intensification had low wind shear (Kaplan and DeMaria, 2003).

During ENSO cycles when an El Niño is present, the Eastern Pacific Ocean is warmer than usual which increases wind shear in the Atlantic, and during a La Niña the tropical Atlantic is warmer than the Eastern Pacific which reduces wind shear (Latif et al., 2007). Latif et al. (2007) contends that the tropical Indian Ocean also has an effect on the tropical North Atlantic Ocean and that it's the temperature difference between the three oceans that determines the amount of wind shear over the Atlantic. Reduced wind shear supports cyclogenesis and cyclone stability. Latif et al. (2007) found that during the 2005 season, which brought hurricanes Dennis, Katrina, Rita and Wilma, SST warmed faster in the Atlantic Ocean than in the tropical Indian Ocean increasing the difference in

temperature between the two oceans, and that this reduced the wind shear creating a favorable environment for tropical cyclones in the Atlantic basin even though ENSO was in a neutral phase.

3.5.3. Eyewall and Inner Core Conditions

The strength, stability, and organization of the eyewall and inner core can also greatly affect hurricane intensity. Eyewall replacement cycles, concentric eyewalls, collapse of the eyewall, elongation of the eyewall, eyewall asymmetry, poor convection, a cloud filled eye, and gaps in the eyewall can all drastically affect the intensity (Willoughby et al.,1982; Emanuel, 2003; Kaplan and DeMaria, 2003; Lin et al., 2013 (a)). Willoughby et al. (1982) found that high rates of intensification occurred after an outer concentric eyewall contracted replacing the smaller diameter inner eyewall during an eyewall replacement cycle. These outer eyewalls have a secondary maximum wind speed which increases as the eyewall contracts (Willoughby et al.,1982; Emanuel, 2003). The outer eyewall eventually over takes the inner eyewall which then collapses and dissipates. Hurricanes that underwent rapid intensification were found to have more symmetrical eyewalls with bands of deep convective clouds around the inner core (Kaplan et al., 2010).

3.5.4. Other Factors

Numerous other factors may influence intensity and rapid intensification. Kaplan et al. (2010) and Bosart et al. (1999) found that tropical cyclones farthest from their MPI had the greatest probability of undergoing rapid intensification. Tropical storms had the highest probability and major hurricanes had the lowest probability of rapidly intensifying (Kaplan and DeMaria 2003; Kaplan et al., 2010).

Favorable upper tropospheric divergence that created good outflow and interaction with an upper level trough contributed to the rapid intensification of hurricane Opal along with traversing over a WCE (Bosart et al., 1999). Interaction with land often has a large effect on intensity, just a portion of the storm being over land can greatly reduce its intensity and weaken the eye because of increased dissipation from drag and lack of a moisture source (Kaplan and DeMaria, 2003). These are just some of the numerous factors that have been found to affect hurricane intensity.

3.6. Research Questions

Based on the previous literature review the following research questions arose and will be addressed in this study:

I. Are changes in hurricane intensity (maximum sustained wind speed) associated with traversing over the LC, WCE, CCE or GCW?

II. Are changes in maximum sustained wind speed associated with high SST, high TCHP, and/or increased depth to the 26°C isotherm?

III. What were the highest maximum sustained wind speeds and percent of MPI achieved? Were these values associated with location type (LC, WCE, CCE, or GCW), or certain thresholds of SST, TCHP, or depth to the 26°C isotherm?

IV. What other factors may affect the hurricane's ability to intensify?

V. Are there threshold values of SST, TCHP, and depth to the 26°C isotherm that are more likely to induce rapid intensification?

3.7. Working Hypotheses

Several working hypotheses were formulated; they are specified below:

I. Tropical cyclones that traverse the LC and its associated WCEs have a greater probability of rapidly intensifying than those over GCW or CCEs, but only if atmospheric and other conditions are conducive for intensification.

II. Tropical cyclones that traverse the LC and its associated WCEs have a greater probability of reaching higher maximum sustained wind speeds than those over GCW or CCEs, but only if atmospheric and other conditions are conducive for intensification.

III. The LC and WCEs are more likely to have sufficient TCHP and depth to the 26°C isotherm for RI than GCW and CCEs.

IV. Tropical cyclones will reach a greater percentage of their MPI, based on pre-storm SST, over ocean water with higher TCHP and greater depth to the 26°C isotherm as long as all other conditions are favorable.

4. DATASETS AND METHODS

4.1. Focus Hurricanes

Eleven hurricanes that traversed the central Gulf of Mexico where the Loop Current and its eddies are normally located were selected for this study (Figure 4-1, Table 4-1). The hurricanes occurred between 2002-2012 and achieved at least a category 1 hurricane status while in the GOM. These years were selected because sufficient data from the same sources were available. Five of the focus hurricanes rapidly intensified including Katrina, Rita, Dennis, Lili, and Isidore. Specific details about each hurricane are included in the results section.

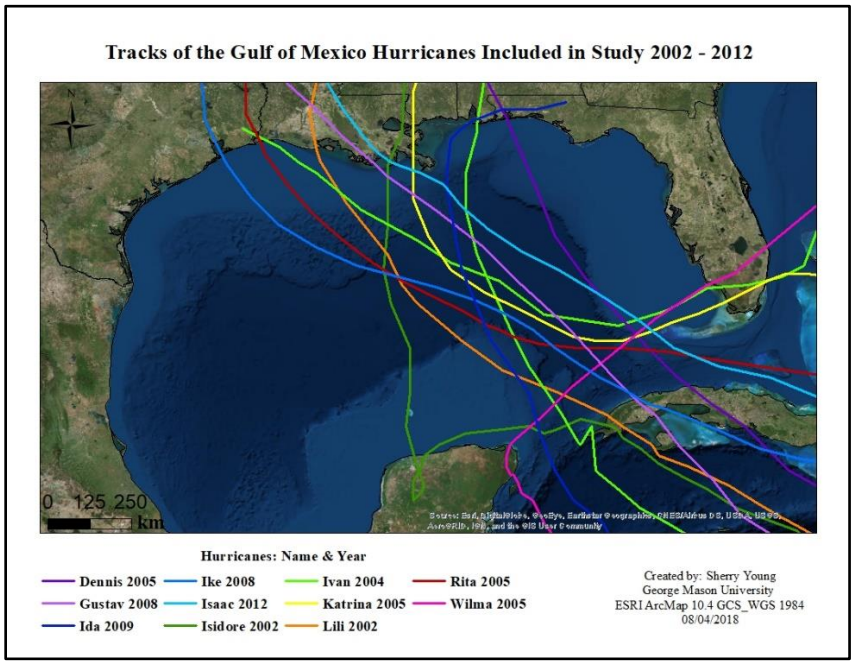

Figure 4-1 Hurricanes included in study

Table 4-1 Hurricanes included in study

Dates listed are the dates included in the study, not the entire length of the lifecycle. Max category is the highest category the storm achieved which may have occurred before it entered the GOM. Study max category is the largest category it achieved during the study period. Max wind speed and lowest pressure are those recorded during this study and may not reflect the maximum during the storm's lifecycle.

Year	Hurricane	Dates Analyzed	Max Category	Study Max Category	Study Max Wind Speed km/hr	Study Lowest Pressure mb
2002	Isidore	09/20-09/26	3	3	204	934
	Lili	10/01-10/03	4	4	232	938
2004	Ivan	09/13-09/16	5	5	260	912
2005	Dennis	07/09-07/10	4	4	232	930
	Katrina	08/25-08/29	5	5	278	902
	Rita	09/20-09/24	5	5	287	895
	Wilma	10/22-10/24	5	3	204	946
2008	Gustav	08/30-09/01	4	4	241	942
	Ike	09/09-09/13	4	2	176	944
2009	Ida	11/08-11/10	2	2	167	975
2012	Isaac	08/26-08/29	1	1	130	966

4.2. Methods & Data Types

The following methods were used:

- Collected data shown in table 4-2 and loaded into ESRI ArcMap 10.4 and an Excel spread sheet.
- The hurricane tracks were layered over rasters containing satellite derived SSH and SST data.
- Layers containing TCHP and depth to the 26°C isotherm were created from Upper Ocean Dynamics Laboratory RMAS graphics and georeferenced into ArcMap. (Shay, 2019)

- Elevation contours were created from the SSH layers designating the location of the Loop Current and associated eddies.
- Detailed hurricane data was recorded from the National Weather Service (NWS) raw text files. 164 observational data records were created in Excel. One record was created for each NWS observational period in which a change occurred in the storm, these ranged from 1-8 hours. Types of information recorded and where it was stored is shown in table 4-3. This was then compared to HURDAT2 data.
- A point shapefile was created for each hurricane using the observational data records. One data point was created for each observational record. Points were layered onto the NHC tracks.
- Satellite and model derived data were added to the 164 observational records including SST under the center, cloud top temperature, depth to the 26 °C isotherm, and TCHP in Excel.
- MPI was calculated for each point. Unity (1) was used for C_k/C_D because of the uncertainty in these variables in the current literature. .8 was chosen for H_a which is used in Emanuel's 1986 study; .8 also coincides with the average relative humidity in the Gulf region during hurricane season. Because the atmospheric pressure at the radius of maximum winds was not known, the low central pressure was used.
- Maps were created in ArcMap to analyze the data geographically while statistics and probabilities were calculated in Excel.

Table 4-2 Sources of data

Parameter	Data Source	Specifications	Limitations
Sea Surface Height Altimeter Data	Sea Surface Height, Absolute, Aviso, 0.25 degrees. Science quality (Ducet et al, 2000)	SSH in meters above the reference ellipsoid including both the height anomaly and mean surface elevation.	Merged data from several satellites, measurements can be taken up to 3 days before or after date on data. 7-day window.
Sea Surface Temperature	MODIS Terra Level 3 SST Thermal IR 8-Day Daytime v2014.0 (OBPG, 2015)	SST measured by radiation emitted in the 11 & 12 µm thermal infrared wave lengths. Collected for before, during and after each storm.	Data was an average over an 8-day period. IR product: cloud coverage can produce "no data" pixels. Accuracy of +/- 0.4°C.
Hurricane Track	NOAA Historical Hurricane Tracks (Knapp et al., 2010)	Storm Tracks were selected by basin, downloaded in NetCDF format then imported into ESRI ArcMap	Lines were created by ESRI ArcMap for point data.
Hurricane Data	Iowa State University Iowa Environmental Mesonet (IEM) Archive NWS Text Products by Issuing Center by Date	National Weather Service Raw Text Product: NHC observation updates for each storm. Data was used to create the data points.	Some observations were missing for earliest storms or not complete. Wind speeds given in 5 knot estimates.
	HURDAT2 Best Track Data Atlantic hurricane database (HURDAT2) 1851-2017 (Landsea and Franklin, 2013)	Reanalysis and best track data for historical hurricanes from 1851-2017.	Wind speeds given in 5 knot estimates.
Cloud Top Temperature	MERRA-2 Model accessed through Earthdata: Giovanni Cloud Top Temperature (K), time average, hourly M2T1NXSLV v5.12.4 (Gelaroa et al., 2017)	Reanalysis combining satellite (microwave and hyperspectral data) and observational data.	None observed for purpose
Precipitation Data	TRMM Near-Real-Time Precipitation Rate (TRMM_3B42RT v7) (Huffman et al., 2014)	TRMM, 3-hour average near real time precipitation rate. Used to observe eye and deep convection.	None observed for purpose
Tropical Cyclone Heat Potential (TCHP) and Depth to 26°C Isotherm	OHC down to the 26° isotherm (TCHP) in kJ/cm² RMAS (Shay, 2019)	Model and satellite derived TCHP and depth to the 26°C isotherm for GOM. These data were provided by the Upper Ocean Dynamics Laboratory at the University of Miami-Rosenstiel School of Marine and Atmospheric Sciences (http://www.rsmas.miami.edu/groups/upper-ocean-dynamics)	Format was graphics with a color-coded key to represent data. Estimations were used to determine values.
	Depth to the 26°C isotherm in meters (Shay, 2019)		
Salinity Data	NOAA salinity figures by month at the surface per 0.25° grid	Used to estimate salinity for the MPI equation based on geographic location and date of the data point.	Climatological mean based on month and location.

Table 4-3 Data types recorded

Type of Data Recorded	Source	Stored
Date & Time of Observation	NWS NHC & HURDAT2	ArcMap Shapefiles & Excel
SST	MODIS Satellite Data	ArcMap Raster Files & Excel
SSH	Aviso Satellite Data	ArcMap Raster Files
Outflow Temperature	MERRA-2 Modeled Data	Excel
Salinity	NOAA Graphics	Excel
Pressure	NWS NHC & HURDAT2	Excel
Sustained Wind Speed	NWS NHC & HURDAT2	ArcMap Shapefiles & Excel
Wind Gusts	NWS NHC	Excel
Change in Wind Speed & Gusts	Calculated	ArcMap Shapefiles & Excel
MPI & % of MPI	Calculated	ArcMap Shapefiles & Excel
Longitude & Latitude	NWS NHC, HURDAT2 & NOAA NHC	ArcMap Shapefiles & Excel
Depth 26°C Isotherm	RMAS Graphics	ArcMap Raster Files & Excel
TCHP	RMAS Graphics	ArcMap Raster Files & Excel
Landfall Location & Time	NWS NHC	Excel
Location LC, WCE, CCE, GCW	Observed in ArcMap using SSH	Excel
Eye Diameter	NWS NHC	Excel
Eyewall Condition & Replacement	NWS NHC	Excel
Wind Shear	NWS NHC	Excel
Translation Speed	NWS NHC	Excel
NHC Notes/Observations	NWS NHC	Excel

4.2.1. Data Specifics

Altimeter SSH

SSH data was downloaded from NOAA's Coast Watch AVISO: Archiving, Validation and Interpretation of Satellite Oceanographic data program. AVISO is a reanalysis project that uses a combination of data collected from: Jason-1, TOPEX/Poseidon, ERS (The European Remote Sensing satellites 1 & 2) and GFO (GEOSAT follow on) satellites. Altimeter data from all the satellites are weight averaged based on accuracy and combined to form a single scientific quality product. Spatial resolution is 0.25° longitude x 0.25° latitude. SSH in this product is defined in the user's manual as the "height of the sea surface above the reference ellipsoid" and includes both the "sea surface height deviation plus the long term mean dynamic height". Data is available to download for individual dates but may have been collected up to 3 days before or after the selected date. SSH data was downloaded in NetCDF format for each hurricane just before the hurricane entered the Gulf Basin.

Sea Surface Temperature

Three raster layers were created for each hurricane with SST data from before, during, and after the hurricane entered the Gulf Basin. MODIS Terra Level 3 SST Thermal IR 8 Day Daytime v2014.0 data was downloaded to create these layers. The Moderate-resolution Imaging Spectroradiometer, MODIS, is a radiometer carried on NASA's Terra satellite. Terra is a sun-synchronous near-polar orbiting satellite; data is

collected with a 1-2-day temporal resolution. SST daytime data is collected during the descending orbit at 10:30 am local time. MODIS can sense radiation in the 11 and 12 μm thermal IR infrared wave lengths which is used to calculate sea surface temperature. One problem with using MODIS data for SST is that available data is an average over 8 days. Often the data available would span both before and after the storm entered the basin in one dataset. In some instances, a dataset that was collected several days to a week before or after the hurricane was in the basin was used to avoid pixels containing "no data" caused by the storm. The spatial resolution of MODIS SST data is 4.63 km; the data was smoothed with a 3-pixel neighborhood circular focus. Often SST varied up to .5°C within the immediate area of the eye, SST with the highest frequency was used for each point.

Temperature at Outflow

Outflow temperature in Kelvins at the cloud top surrounding the eye is required for calculating MPI; this was collected for each data point by using the MERRA-2 data available through NASA's Earthdata Giovanni website. MERRA-2 is a reanalysis product that combines microwave and hyperspectral satellite data and observational data. Cloud top temperature data is available as an hourly time average and was collected for each data point at the exact time the observation was originally recorded by the NHC. Spatial resolution is somewhat coarse at 50 km; however, the center of the storm was easily identifiable and the lowest temperature was recorded.

Precipitation and Convection

TRMM precipitation data was used to identify the central core of the storm in order to evaluate symmetry, convection, strength and shape of the eye, and in order to designate the geographic location for cloud top temperature, and to estimate the overall size of the storm. TRMM data was also accessed from NASA's Earthdata Giovanni website at the same time the MERRA-2 data was collected. TRMM, Tropical Rainfall Measuring Mission satellite, was a joint mission between NASA and the Japan Aerospace Exploration Agency that ended in 2015. TRMM Near-Real-Time Precipitation Rate (TRMM_3B42RT v7) data was collected for each data point of every storm. Spatial resolution of this data is 0.5° x 0.625° and is available as a 3-hour time average.

TCHP and Depth to the 26 °C Isotherm

Tropical cyclone heat potential (TCHP) and depth to the 26°C isotherm data were taken from graphics created by the Upper Ocean Dynamics Laboratory at the University of Miami-Rosenstiel School of Marine and Atmospheric Sciences (RMAS) (Shay, 2019) and made available on their website. Detailed methods and sources of data used to create the graphics are available on the RMAS website. The graphics are available for individual dates and were downloaded and georeferenced into ArcMap. Values along the continental shelf were not specified by RMAS; however, according to graphics available through NOAA/AOML the TCHP is ~20 kJ/cm^2 on the shelf. This study assumed values of 20 kJ/cm^2 for TCHP on the coastal continental shelf and 0 kJ/cm^2 while the tropical

cyclone was over land. RMAS TCHP data was used as the base layer for some of the maps created for each hurricane. These data were authorized for use and provided by the Upper Ocean Dynamics Laboratory at the University of Miami-Rosenstiel School of Marine and Atmospheric Sciences (http://www.rsmas.miami.edu/groups/upper-ocean-dynamics)"

5. RESULTS & DISCUSSION

5.1. Hurricanes

Detailed results for individual hurricanes are given in the following sections; tables 5-1 through 5-5 compare the main results for all of the focus hurricanes. In the Appendix table 8-6 provides detailed data for the complete RI cycles.

5.1.1. 2002: Isidore and Lili

Isidore

Isidore formed off the coast of Venezuela on September 14th, 2002. It made landfall first on the coast of Venezuela and then on Cuba as a category 1 hurricane with ~139 km/hr sustained winds. Zero hour of analysis began while Isidore was over Cuba and beginning an eyewall replacement cycle. Wind shear was low and upper level atmospheric conditions were favorable; therefore, the NHC expected Isidore to intensify once it emerged over the LC. As forecasted, Isidore's sustained wind speed increased by 18.5 km/hr after it emerged off Cuba over the LC beginning a RI cycle; it continued to rapidly intensify while traversing over the current westward. During the RI cycle Isidore's wind speed increased by a total of ~65 km/hr intensifying to a category 3 hurricane with sustained winds of ~204 km/hr (Figure 5-1). Surprisingly, the RI episode occurred while Isidore underwent an eyewall replacement cycle.

Isidore maintained its intensity while it traveled through the Yucatán Channel towards the Yucatán Peninsula. Isidore made landfall on the Yucatán Peninsula as a category 3 hurricane with 204 km/hr sustained winds. It remained over land for the next ~34 hours rapidly losing intensity and suffering a total eyewall collapse. Isidore was a tropical storm with sustained winds of only ~65 km/hr when it emerged off the Yucatán Peninsula over the GOM.

Isidore was able to re-intensify slightly once it was back over warm GCW even though it still lacked an organized central core. Sustained wind speed remained stable as it traveled northward even though the NHC noted that dry air was possibly being entrained into the mid to upper level, no central ring of convection existed, and maximum winds were ~120 nm from the center. Wind speed increased slightly when Isidore encountered an area of elevated SST and TCHP, but it was unable to regain a strong inner core. Isidore made landfall on September 26th near Leeville, Louisiana as a tropical storm with ~102 km/hr sustained winds.

Isidore reached a maximum of 82.2% of its MPI, this was observed following the end of the RI cycle. While over the Yucatán Peninsula Isidore dropped to only 27.3% of its MPI based on SST on the Yucatán shelf. Change in intensity appears to have lagged behind the change in TCHP. This is partially because the change in wind speed is occurring between observation periods, but not observed until the next NHC update. A delay between intensity and high levels of TCHP was noted in Rapport et al. (2010) who

found that hurricanes reached their highest intensity ~6-18 hours after travelling over areas with the highest local OHC. Isidore reached its maximum intensity after travelling over the LC where TCHP values were between 70 and 110 kJ/cm^2 with depths to the 26°C isotherm between 60 and 120 m. Isidore stopped increasing in intensity when the TCHP dropped below 70 kJ/cm^2. The main proposed factor for Isidore's lack of intensification while traversing northward in the GOM is that it never regained a strong central core or eyewall with adequate deep convection; dry air entrainment and the extent of the degradation of the core are possible reasons for this.

The largest change in SST along Isidore's track was ~-7°C which occurred on the continental shelf off the coast of the Yucatán Peninsula where the water was shallow (Figure 5-2). This area was subjected to mixing from Isidore's winds for a much greater period than anywhere else along its path. The smallest change in SST of ~-0.1°C occurred in the Yucatán straits where the flow of the Loop Current has the highest velocity and the depth of the current is the greatest. Change in SST within the Loop Current along the track ranged from -0.1 to -2.2°C, with the largest decreases to the right of the trajectory in areas where the depth to the 26°C isotherm was shallower. This is similar to what was observed by Shay and Uhlhorn (2008) who found that deepening of the 26°C isotherm occurred in the Yucatán Straits and SST and TCHP remained stable where the LC flowed through the Straits; but along the continental shelf of the Yucatán Peninsula TCHP reduced by ~40 kJ/cm^2 and SST decreased by ~4.5°C.

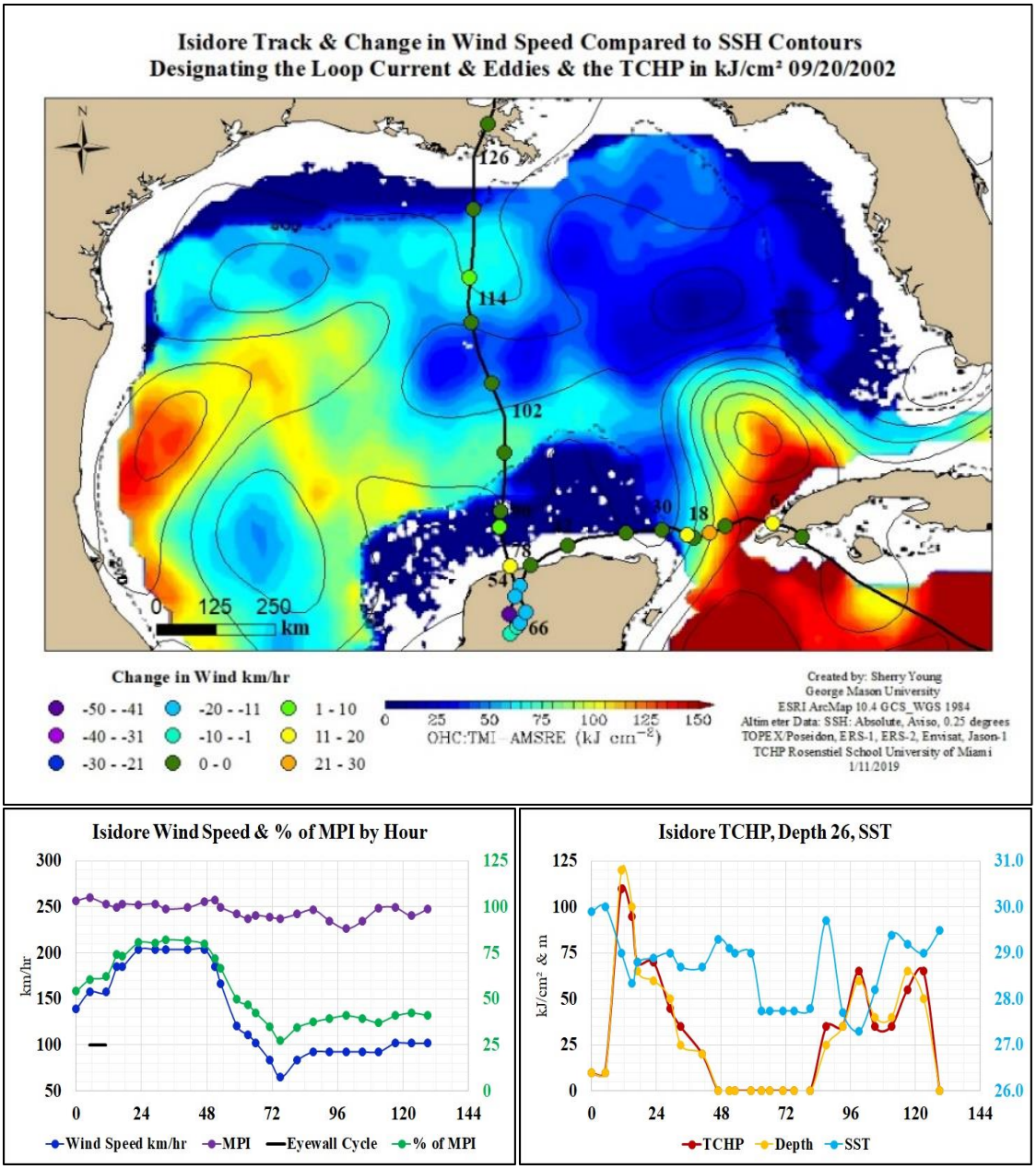

Figure 5-1 Isidore change in wind speed & graphs

Map: Track and change in sustained wind speed compared to TCHP in kJ/cm² on 09/20 and SSH contour lines in meters. Block numbers are hours from zero hour of analysis. Graphs: (left) blue is the actual maximum sustained wind speed km/hr, purple is the calculated MPI wind speed in km/hr, green % of MPI achieved during observation (right) red TCHP in kJ/cm², orange depth to 26°C isotherm in meters, turquoise SST °C.

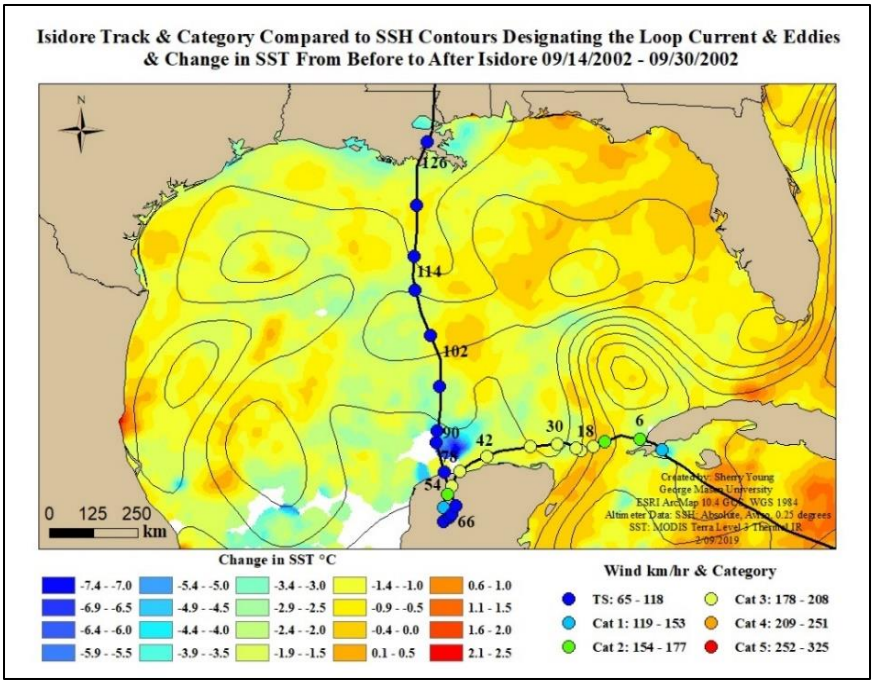

Figure 5-2 Isidore change in SST: cold wake

Isidore's track, category, and sustained wind speed compared to change in SST from before to after Isidore showing the cold wake. SSH contour lines in meters. Block numbers are hours from zero hour of analysis.

Lili

Hurricane Lili formed on September 21st, 2002 northeast of French Guiana. It was a small and fast-moving hurricane, ~13 to 15 kts, with an initial track that was similar to Isidore's. While traversing through the Caribbean Sea, Lili intensified from a tropical storm to a category 2 hurricane with ~167 km/hr sustained winds just before making landfall on Cuba. Zero hour of analysis began at 18:00 UTC on October 1st while Lili was over Cuba (Figure 5-3). Lili had a strong core and atmospheric conditions were favorable for intensification with low wind shear and good outflow; however, SST was ~1.3°C

cooler in the LC than it was during Isidore's passing 11 days earlier because of Isidore's cold wake.

For the first 8 hours after Lili emerged over the LC, sustained winds remained stable as Lili underwent an eyewall replacement cycle. Once the eyewall replacement cycle ended, Lili began a RI cycle. RI continued until hour 26 when Lili became a category 4 hurricane with ~231.5 km/hr sustained winds and achieved ~99% of its MPI. The RI cycle ended when a concentric outer eyewall began to form and outflow became restricted to the west and southwest. At 38 hours the NHC noted an elongated cloud pattern with a partial eyewall collapse and a decrease in sustained wind speed beginning an RDI cycle. Rapid de-intensification continued for the next 9 hours while Lili approached land and shallower continental shelf water. Lili decreased in intensity by a total of ~111 km/hr and made landfall as a category 1 hurricane with ~120 km/hr sustained winds in New Ibera, Louisiana on October 3rd.

It is proposed that Lili's RI was caused by a combination of favorable upper atmospheric conditions along with low wind shear, a strong inner core with deep convection, and traveling over GCW with TCHP over 50 kJ/cm^2 with depth to the 26°C isotherm of more than 50 m. Lili's small size and fast translation speed assisted in limiting the effects from surface cooling by moving Lili before mixing greatly decreased the enthalpy flux; this allowed the moderate levels of TCHP and depth to act as higher levels of TCHP and depth would under a slower moving larger storm. Once the SST,

TCHP, and depth to the 26°C isotherm decreased sufficiently along the continental shelf, Lili rapidly lost intensity and its eyewall began to deteriorate (Figure 5-3).

Changes in SST were hard to determine remotely for Lili due to the effects from Isidore. Some areas showed warming because they were not affected by Lili and had recovered since being cooled by Isidore; such as on the Yucatán shelf (Figure 5-4). In some areas SST data was not available due to Isidore's passing during the satellite's collection period; this created some null values in the before Lili SST raster and an inaccurate value for the calculated difference between the before and after SST rasters. Shay and Uhlhorn (2008) found that SST changed little in the LC after Lili but SST decreased between 2°C and 6°C in the GCW. Based on the satellite data, this study found that SST changed between ~-0.6°C and +1.0°C in the LC on average and between ~-1.3°C and +2.2°C along Lili's immediate track in GCW. Change in SST satellite data (Figure 5-4) is not considered reliable because of the effects of Isidore.

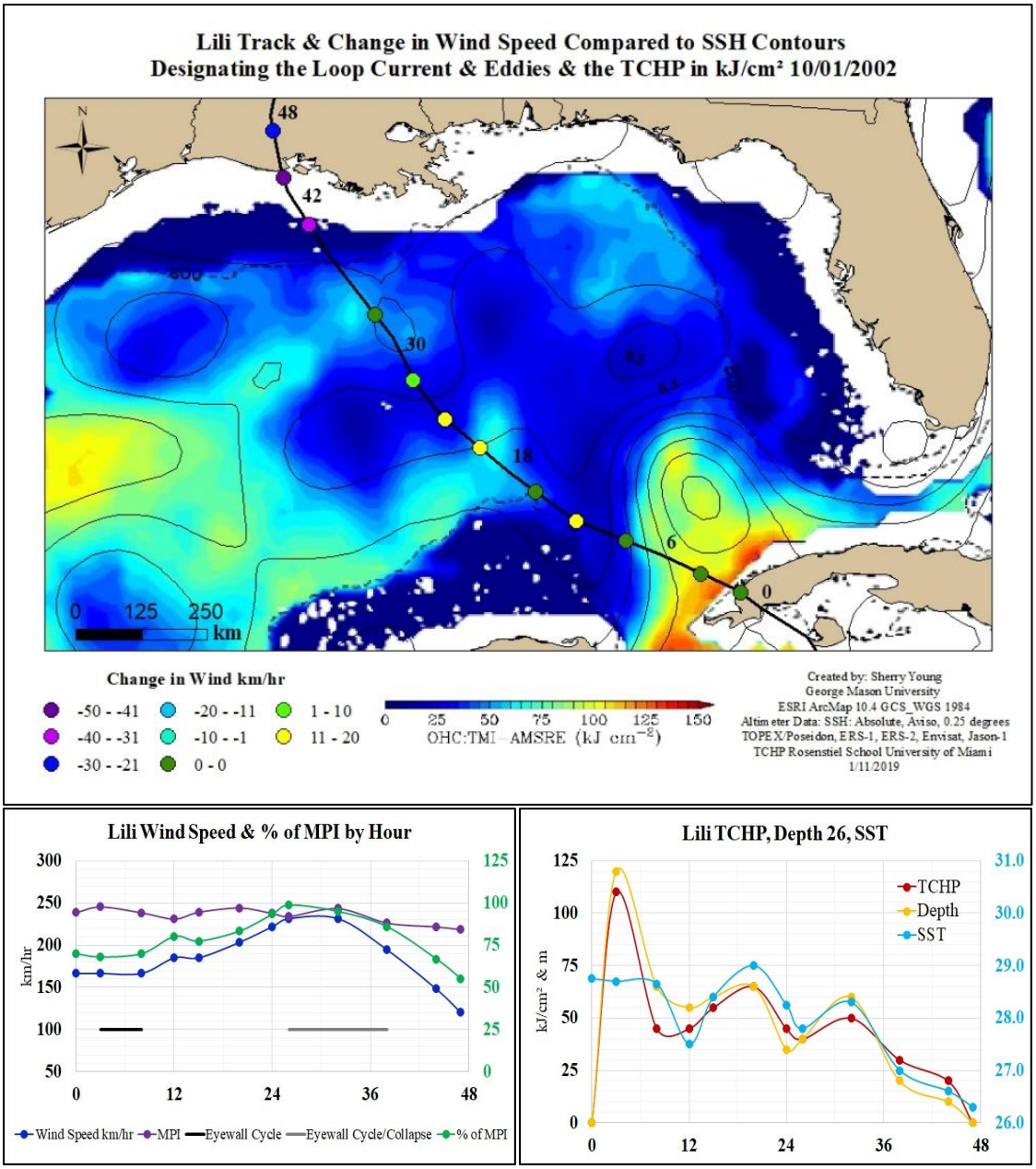

Figure 5-3 Lili change in wind speed & graphs

Map: track and change in sustained wind speed compared to TCHP in kJ/cm^2 on 10/01 and SSH contour lines in meters. Block numbers are hours from zero hour of analysis. Graphs: (left) blue is the actual maximum sustained wind speed km/hr, purple is the calculated MPI wind speed in km/hr, green % of MPI achieved during observation, black and gray lines show periods of adverse eyewall conditions (right) red TCHP in kJ/cm², orange depth to 26°C isotherm in meters, turquoise SST °C.

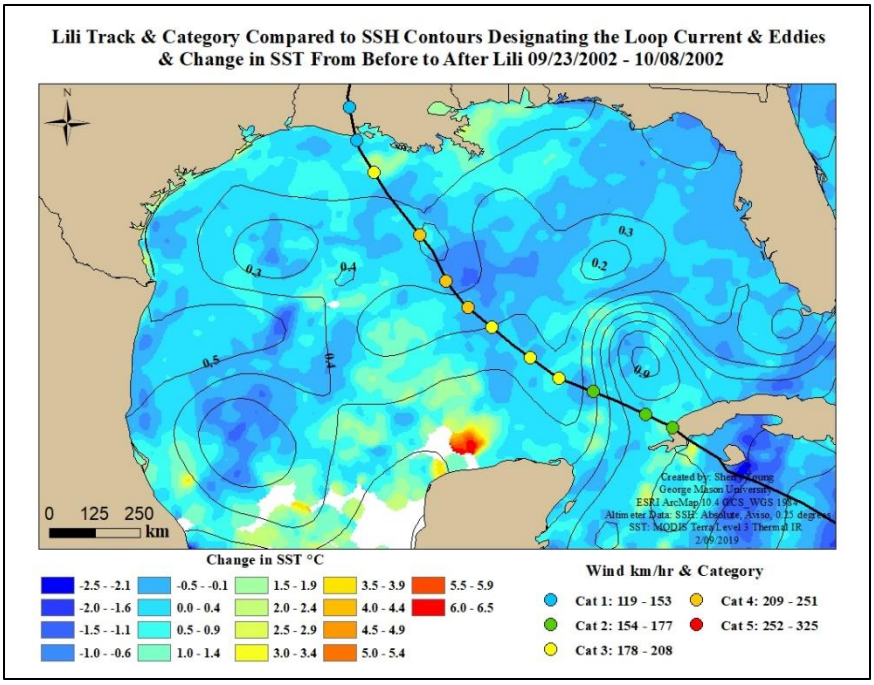

Figure 5-4 Lili change in SST: cold wake

Lili's track, category, and sustained wind speed compared to change in SST from before to after Lili showing the cold wake. This data has been influenced by Isidore's cold wake in addition to Lili. SSH contour lines in meters.

5.1.2. 2004: Ivan

Ivan

Hurricane Ivan formed in the Atlantic Ocean on September 2nd, 2004 and intensified as it traveled through the Caribbean Sea. Zero hour of analysis started at 20:00 UTC on September 13th right before Ivan's landfall on Cuba as a large category 5 hurricane with a strong clear eye, good outflow, and ~260 km/hr sustained winds. Ivan's intensity remained stable while over Cuba and as it traveled through the Yucatán Straits and into the GOM. Ivan reached 100% of its MPI while over the LC at hour 7 even though the sustained wind speed did not increase because the MPI decreased slightly

(Figures 5-5). Between hours 10-18, Ivan's sustained wind speed decreased by a total of 37.1 km/hr when a secondary eyewall formed, outflow to the northwest became restricted because of westerly shear, and dry air began being entrained in the southwest quadrant. Ivan remained stable in intensity from 18-36 hours while passing over a CCE. It is unknown if the eyewall replacement cycle was ongoing or had completed during this time period because it was not mentioned in the NHC observations. NHC reported that Ivan's eye was 45 nm at 30 hours and 25 nm at 36 hours; this would suggest that the replacement cycle completed by 36 hours.

At 36 hours Ivan reached the front edge of a WCE, even though the SST was warm and the TCHP was high, Ivan decreased slightly in intensity by hour 42. NHC reported that it appeared that the westerly shear and dry air was affecting Ivan, also that because of its large size Ivan had a slow response to changes in OHC. Ivan decreased by another 18.6 km/hr in sustained wind speed while it passed over the continental shelf. Ivan made landfall on September 16th at Gulf Shore, Alabama as a category 3 hurricane with ~194 km/hr sustained winds. After landfall Ivan downgraded to a TD as it traveled overland towards the Atlantic Ocean where it intensified into a category 1 hurricane. Ivan then crossed over the southern tip of Florida and entered the GOM as a TD. This study did not analyze Ivan's second pass through the GOM as a TD/TS.

The change in SST due to Ivan ranged between ~-4.3°C to -.3°C with larger decreases occurring in areas that originally had lower TCHP and shallower depths to the

26°C isotherm (Figure 5-6). SST in the LC and WCE also decreased but by a lesser magnitude, ranging between -3.3°C to -.3°C. The greatest reduction in SST occurred in the CCE and on the continental shelf. Satellite data shows SST below 26.5°C in these locations during and after Ivan, which is below the threshold believed to be required to sustain hurricane intensity. This cooling of the ocean surface could have reduced the enthalpy flux reducing Ivan's intensity before landfall. Ivan reached a maximum of 100% of its MPI when it emerged off Cuba over the LC and decreased slowly through the rest of its lifecycle to ~80% of its MPI; however, it remained at ~90% or more of its MPI when the TCHP was between 90 kJ/cm^2 and 135 kJ/cm^2 and the depth to the 26°C isotherm was between 75 m and 115 m.

This study proposes that Ivan's large size, and strong category 4 to 5 intensity allowed it to retain most of its intensity even though it faced some moderate westerly shear, dry air entrainment, concentric eyewalls, and episodic negative feedback due to mixing induced ocean surface cooling. Warm SST of 29°C to 30°C, high TCHP, and increased depth to the 26°C isotherm in the LC and WCE, limited the amount of negative feedback Ivan faced along part of its path allowing it to remain a strong storm with limited intensity loss before landfall.

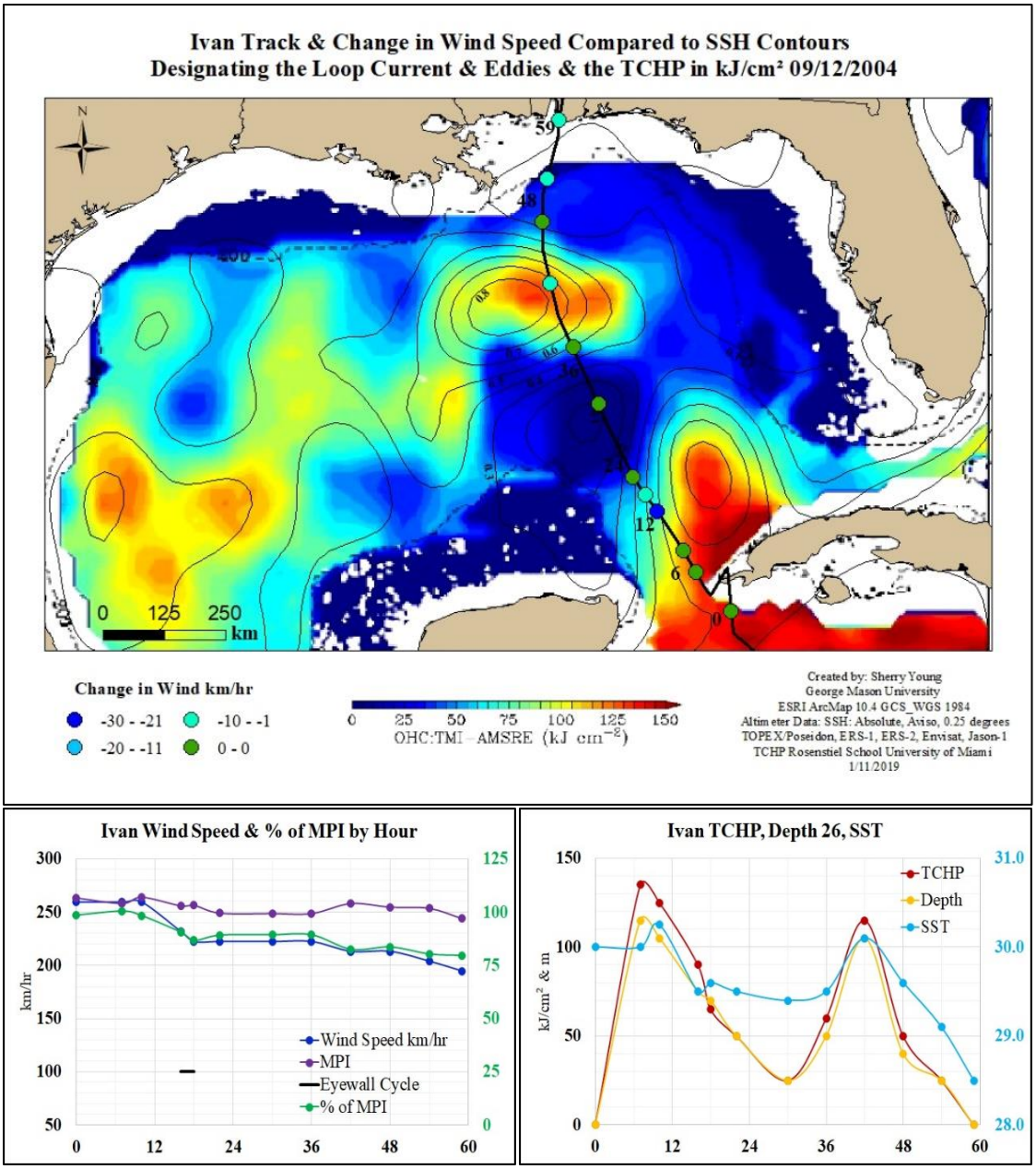

Figure 5-5 Ivan change in wind speed & graphs

Map: track and change in sustained wind speed compared to TCHP in kJ/cm² on 09/12 and SSH contour lines in meters. Block numbers are hours from zero hour of analysis. Graphs: (left) blue is the actual maximum sustained wind speed km/hr, purple is the calculated MPI wind speed in km/hr, green % of MPI achieved during observation, black line shows period of adverse eyewall conditions (right) red TCHP in kJ/cm², orange depth to 26°C isotherm in meters, turquoise SST °C.

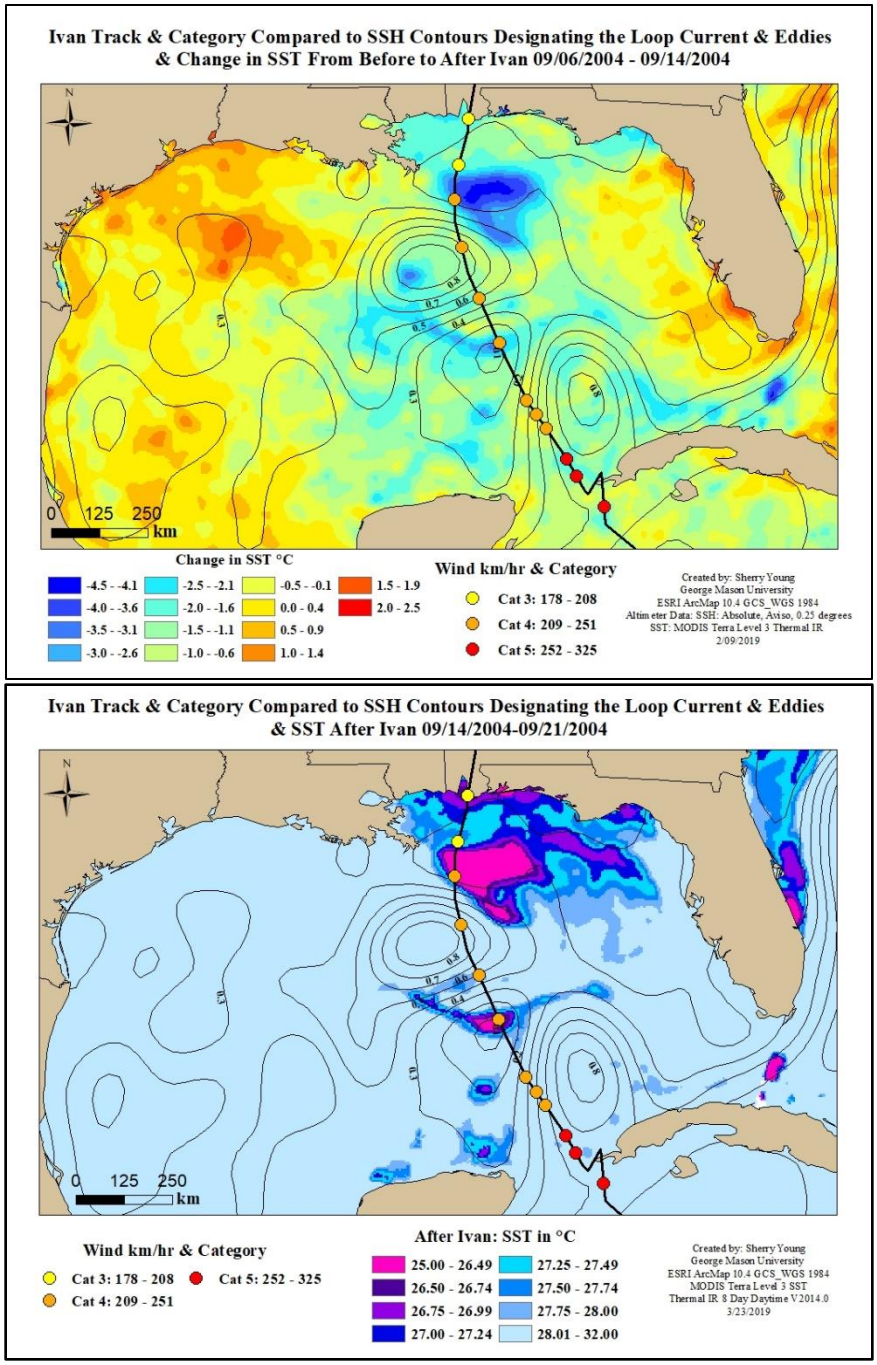

Figure 5-6 Ivan change in SST and SST after Ivan

Top map: track, category, and sustained wind speed compared to change in SST from before to after Ivan showing cold wake. SSH contour lines in meters. Bottom map shows the SST after Ivan in °C symbolized to emphasize areas where SST decreased below the critical value of 26.5°C during Ivan. Areas in the CCE and on the shelf show SST below 26.5°C, some recovery of heat may have occurred during the 8-day satellite collection period.

5.1.3. 2005: Dennis, Katrina, Rita, Wilma

Dennis

Dennis formed as a tropical depression on July 4th, 2005 just north of Venezuela. It intensified as it traveled northward over the Caribbean Sea and made landfall as a category 4 hurricane on Cuba. Zero hour of analysis began at 3:00 UTC on July 9th while Dennis was over Cuba as a category 2 hurricane with ~176 km/hr sustained winds. Dennis emerged off Cuba with a slightly degraded eye; however, the high SST, low wind shear, and good outflow made conditions favorable for Dennis to intensify. As Dennis traveled north along the far-right hand edge of the LC, sustained wind speed decreased and Dennis became a category 1 hurricane (Figure 5-7). The SST was warm and the TCHP was ~65 kJ/cm^2; however, convection was limited due to Dennis's weak eye. Sustained winds increased slightly at hour 8 and Dennis became a category 2 hurricane.

At ~17 hours, Dennis began a RI cycle while over a CCE. The RMAS TCHP diagram for July 9th, shows a tongue of water with TCHP of ~65-75 kJ/cm^2 extending from the LC into the CCE under Dennis's track. It could be possible that Dennis altered the flow of the LC as it passed over; similar effects were observed during Hurricane Matthew in 2016 (Ezer, 2018). Mixing of the ocean surface by Matthew reduced the pressure gradient and thus the geostrophic flow of the Gulf Stream; this allowed water normally transported by the Gulf Stream to pool and become trapped between the shore to the west and the Gulf Stream to the east (Ezer, 2018).

Surprisingly, SST in the middle of the CCE was warmer than the surrounding GCW by ~1°C-2°C. The higher SST should have increased the TCHP slightly even though the depth to the 26°C isotherm was shallow. If the warm tongue continued at depth in the CCE this also would have increased the total TCHP. Dennis's RI cycle continued over the CCE; sustained winds increased by a total of ~74 km/hr. If you include the first increase of ~9 km/hr over the LC, the total increase was ~83 km/hr over 23 hours. The largest increases in intensity began when Dennis's eye became more organized with cold cloud tops when Dennis approached the location of the highest SST in the middle of the CCE. It is possible that Dennis underwent an eyewall replacement cycle up until this time, but it was not noted in the NHC data.

At ~26 hours Dennis's sustained winds reached ~217 km/hr and it became a category 4 hurricane. The last increase in intensity of the RI cycle occurred when Dennis approached another warm tongue of water with increased TCHP; this time extending off the WCE to the west of Dennis's track. As in the previous case, it is possible that Dennis could have altered the geostrophic flow in the WCE offsetting some of the flow to the east under its path. At ~39 hours Dennis decreased in intensity and the NHC reported that Dennis's eye was becoming less distinct and cloud filled due to wind shear. The SST at this location was warm but the water was shallow; Dennis was on the cusp of making landfall with the front bands already inland. On July 10th, Dennis's eye made landfall on Santa Rosa Island, Florida as a category 3 hurricane with sustained winds of ~194.5 km/hr.

Several factors could have contributed to the RI of Dennis, one possible explanation is that Dennis was a compact and moderately fast-moving hurricane at 13 kts. It's compact size and moderate speed of trajectory would have limited the cooling due to mixing and made Dennis more responsive to changes in the heat flux. Another possible factor was the proximity of Dennis to the LC and WCE. This study evaluated ocean conditions directly under the eye of the storm; but as figure 5-8 shows, Dennis acquired energy from the ocean up to distances far from the storm's center under its convective bands. MERRA-2 was used to estimate the positive latent heat flux upward from the ocean surface during observation hour 19 (Figure 5-8). At this time, Dennis was stationed over the center of the CCE and undergoing RI. The model shows that the largest flux was occurring in the right front quadrant; however, strong convection was also occurring over the WCE and the LC. Very little latent heat was being produced within the CCE.

In conclusion, Dennis was unusual in that it underwent a complete RI cycle while the eye was over a CCE; however, warm SST, a consistently sufficient amount of available latent heat, favorable atmospheric conditions, and a strong central core, all contributed to Dennis rapidly intensifying into a category 4 hurricane. This study proposes that TCHP was at or above 50 kJ/cm^2 during most of Dennis's RI cycle. It is further proposed that Dennis's proximity to the LC and WCE allowed large latent heat fluxes from these regions and limited the negative feedback.

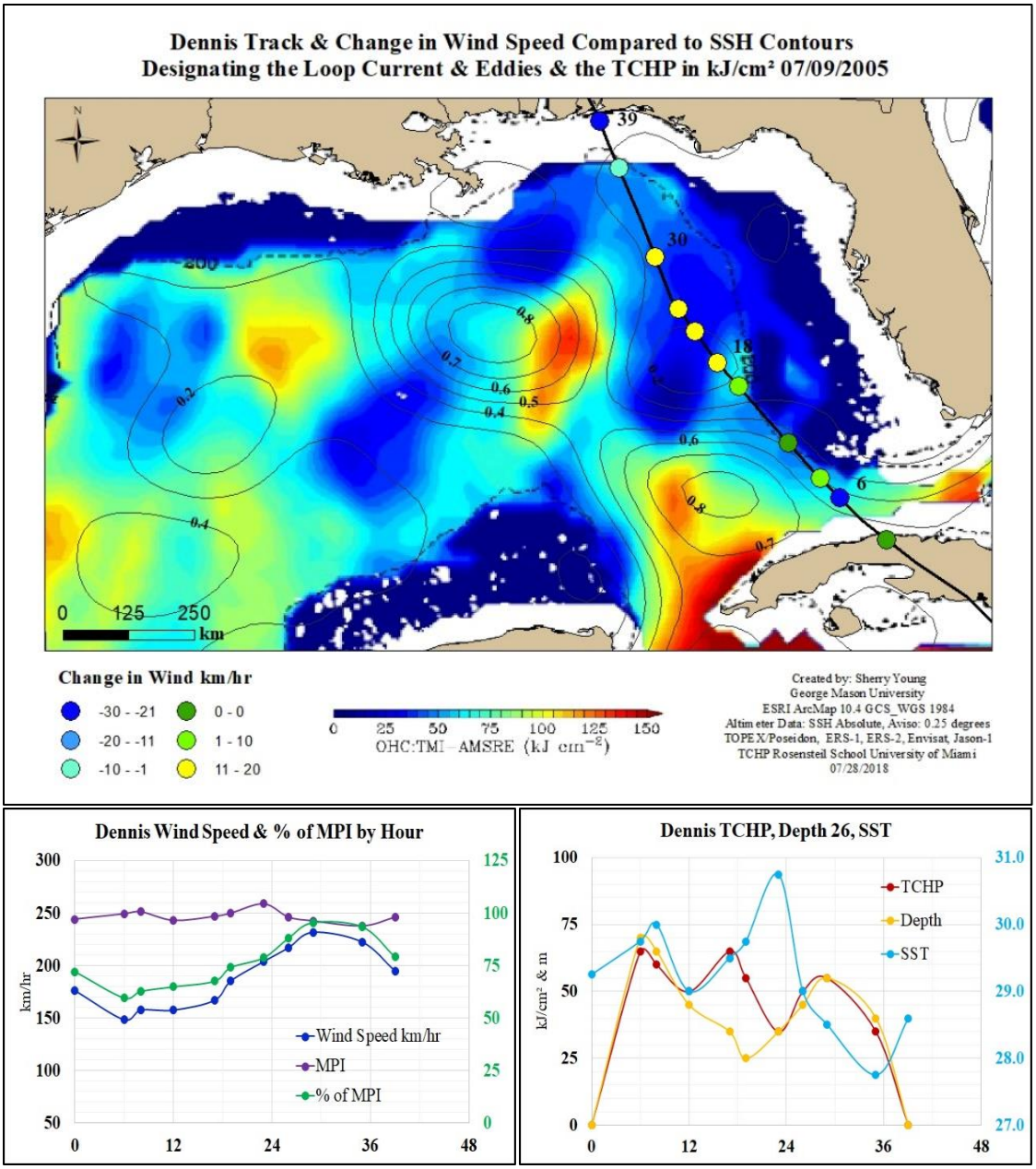

Figure 5-7 Dennis change in wind speed and graphs

Map: track and change in sustained wind speed compared to TCHP in kJ/cm^2 on 07/09 and SSH contour lines in meters. The higher TCHP tongue extending from the LC is shown. Block numbers are hours from zero hour of observation. Graphs: (left) blue is the actual maximum sustained wind speed km/hr, purple is the calculated MPI wind speed in km/hr, green % of MPI achieved during observation (right) red TCHP in kJ/cm², orange depth to 26°C isotherm in meters, turquoise SST °C.

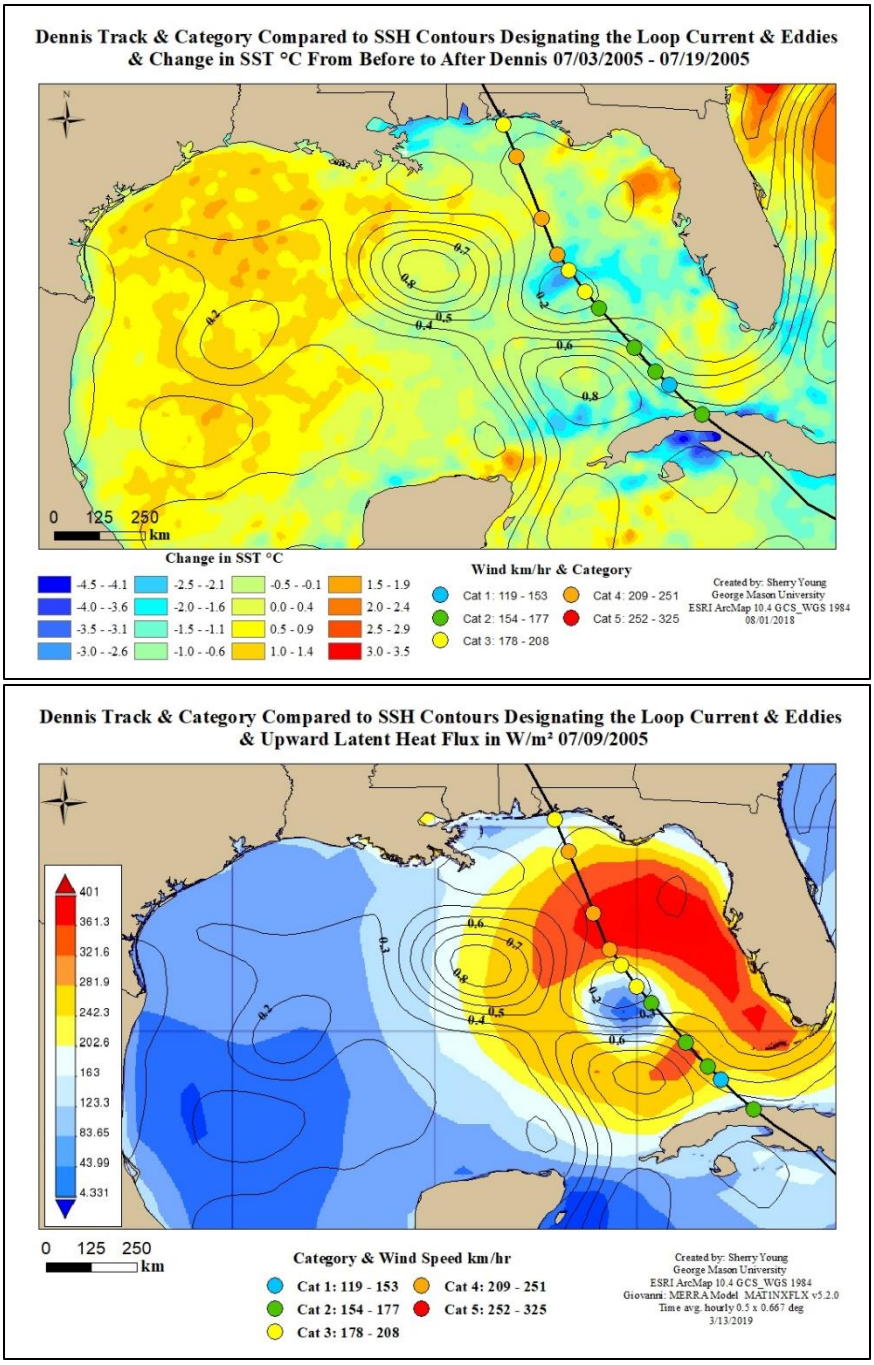

Figure 5-8 Dennis change in SST and latent heat flux

Top map: track, category, and sustained wind speed compared to change in SST from before to after Dennis showing cold wake. SSH contour lines in meters. Bottom map: MERRA modeled latent heat flux on 07/09 between 22:00 and 23:00 UTC, during RI.

Katrina

Katrina formed as a tropical depression off the coast of the Bahamas on August 23rd, 2005. It took a northerly path through the Bahamas then turned westward and made landfall near Hollywood, Florida as a category 1 hurricane with 120 km/hr sustained winds. Zero hour of analysis began on August 25th while Katrina was over southern Florida. Katrina retained its intensity as it traveled over Florida and emerged in the GOM. Conditions were favorable during Katrina's lifecycle; wind shear was low, outflow was good, and SST was warmer than climatological average at 30°C-31°C along Katrina's entire track (McTaggart-Cowan et al., 2007). Katrina began intensifying once it left the continental shelf beginning the first RI cycle. RI ended at 36 hours as an eyewall replacement cycle began; total increase was ~65 km/hr elevating Katrina to a category 3 hurricane with ~185 km/hr sustained winds.

Once the eyewall replacement cycle ended, Katrina's intensity increased by ~46.3 km/hr over the next 6 hours, this began the second RI cycle (Figure 5-9). At hour 60, Katrina became a category 4 hurricane with ~231.5 km/hr sustained winds. During the next hour wind speed increased by another ~28 km/hr followed by another increase of ~18.5 km/hr over the following 5 hours. Katrina became a category 5 hurricane with ~259 km/hr sustained winds at hour 61. At 66 hours the RI cycle ended with a total increase of ~92.6 km/hr over 12 hours. This explosive episode of RI brought Katrina from a category 3 to a category 5 hurricane within just 7 hours and increased the sustained winds from ~185 km/hr to ~278 km/hr within 12 hours. Katrina reached

maximum percentage of its MPI at 66 hours at ~103%. The last 6 hours of the RI cycle occurred while Katrina was at the most northern extent of the LC where it joined the recently shed WCE. Sustained winds remained stable for the next 3 hours as Katrina traveled over the WCE; pressure dropped to its maximum low of 902 mb during this period. Two hours later sustained winds decreased slightly. It is possible that an eyewall replacement cycle was beginning, the eye started to expand in diameter and the southwest eyewall was starting to weaken, but Katrina remained strong at ~99.7% of its MPI.

Once Katrina approached lower TCHP in the northern half of the WCE it started a period of RDI. Seven hours later Katrina's winds decreased by another ~9 km/hr, at this time Katrina's right front quadrant began approaching the continental shelf and the outer bands were starting to come ashore in Louisiana. NHC noted that the eye was less symmetrical and convection was starting to weaken with less hot towers apparent on the satellite imagery. Over the next 11 hours sustained winds decreased by another ~ 65 km/hr for a total decrease of 83.5 km/hr over a 20-hour period as Katrina made landfall. Katrina first made landfall on August 29th near Buras, Louisiana on the Mississippi Delta as a category 3 hurricane. Approximately an hour later Katrina made a second landfall in St. Bernard Parrish, Louisiana, and then finally made a 3rd landfall near the Louisiana-Mississippi border as category 3 hurricane with ~194 km/hr sustained winds.

Change in SST from before to after Katrina ranged from ~-0.1°C to -3.6°C along Katrina's path (Figure 5-10). In the LC the greatest cooling occurred to the right of

Katrina's track; the least amount of cooling occurred in the middle of the LC and to the left of the track. In the WCE the largest decreases in temperature occurred along the northern edge. In general, the most cooling occurred in areas where TCHP was lower and depth to the 26°C isotherm was shallower. SST collected after Katrina shows that SST did not drop below 26.5°C along Katrina's track; however, it came close in two areas: the region along the eastern edge of the LC and the region on the northern edge of the WCE where the RDI cycle began. SST data collected by MODIS is an average over an 8-day period. It is possible that SST was below 26.5°C in these areas during Katrina's passing; advection, mixing and solar insolation possibly restored some heat over the 8-day time frame. Surface cooling might explain why Katrina began an RDI cycle once it reached the northern edge of the WCE.

Almost perfect conditions for intensification existed during Katrina's lifecycle. Wind shear was low, outflow was good, it had a strong central core with deep convection, SST was warmer than climatological, and the LC was in its extended state with a large WCE still attached. Furthermore, Katrina's path took it directly through the middle of the LC and WCE where the explosive RI cycle occurred. It is proposed that favorable atmospheric conditions, high SST, and large areas with high TCHP with greater depths to the 26°C isotherm were all responsible for Katrina's two episodes of RI and allowed it to obtain 103% of its MPI. SST data shows that along most of Katrina's track SST remained above the critical temperature of 26.5°C providing sufficient heat energy to fuel intensification.

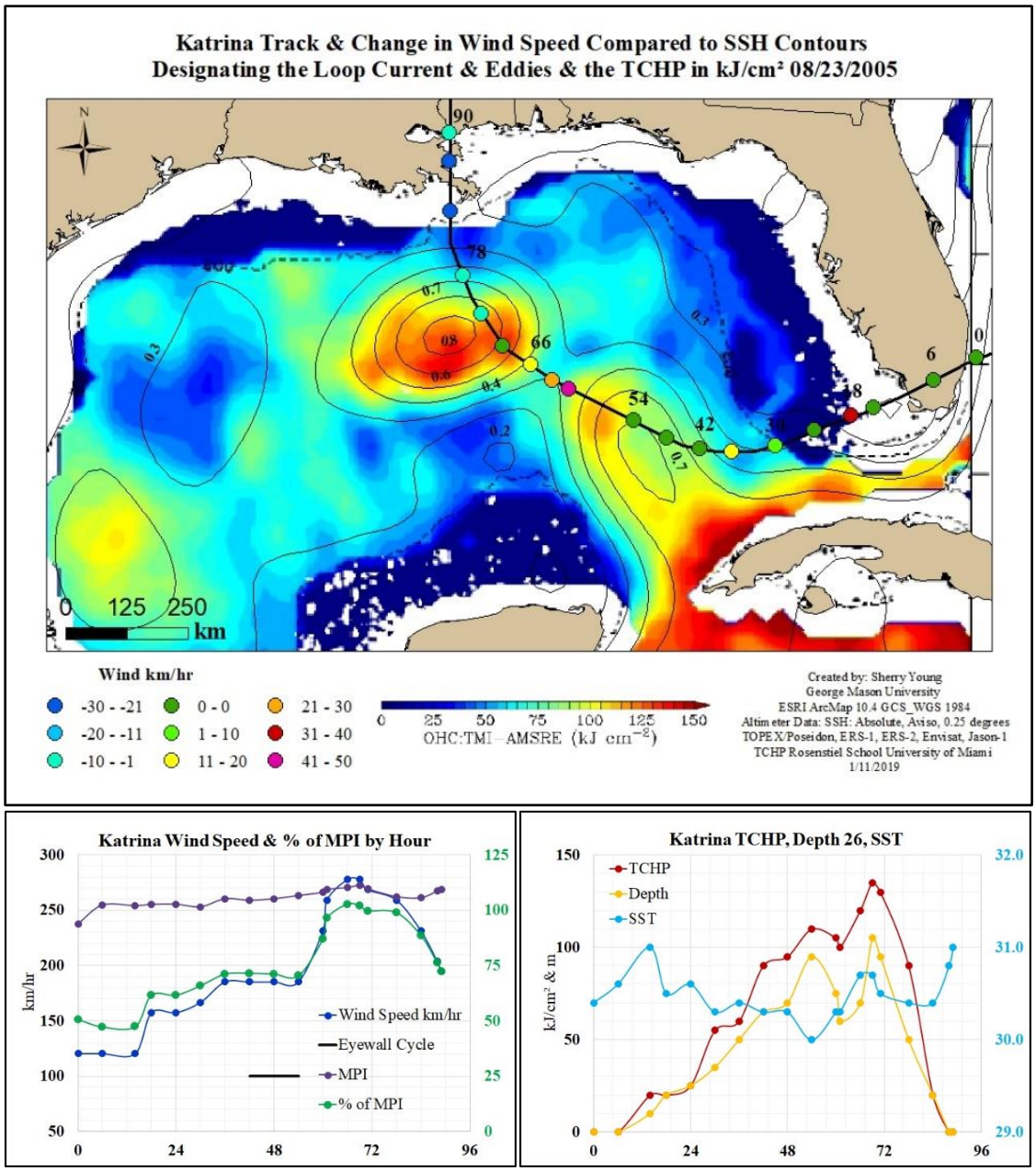

Figure 5-9 Katrina change in wind speed and graphs

Map: track and change in sustained wind speed compared to TCHP in kJ/cm² on 08/23 and SSH contour lines in meters. Block numbers are hours from zero hour of observation. Graphs: (left) blue is the actual maximum sustained wind speed km/hr, purple is the calculated MPI wind speed in km/hr, green % of MPI achieved during observation, black line shows period of adverse eyewall conditions (right) red TCHP in kJ/cm², orange depth to 26°C isotherm in meters, turquoise SST °C.

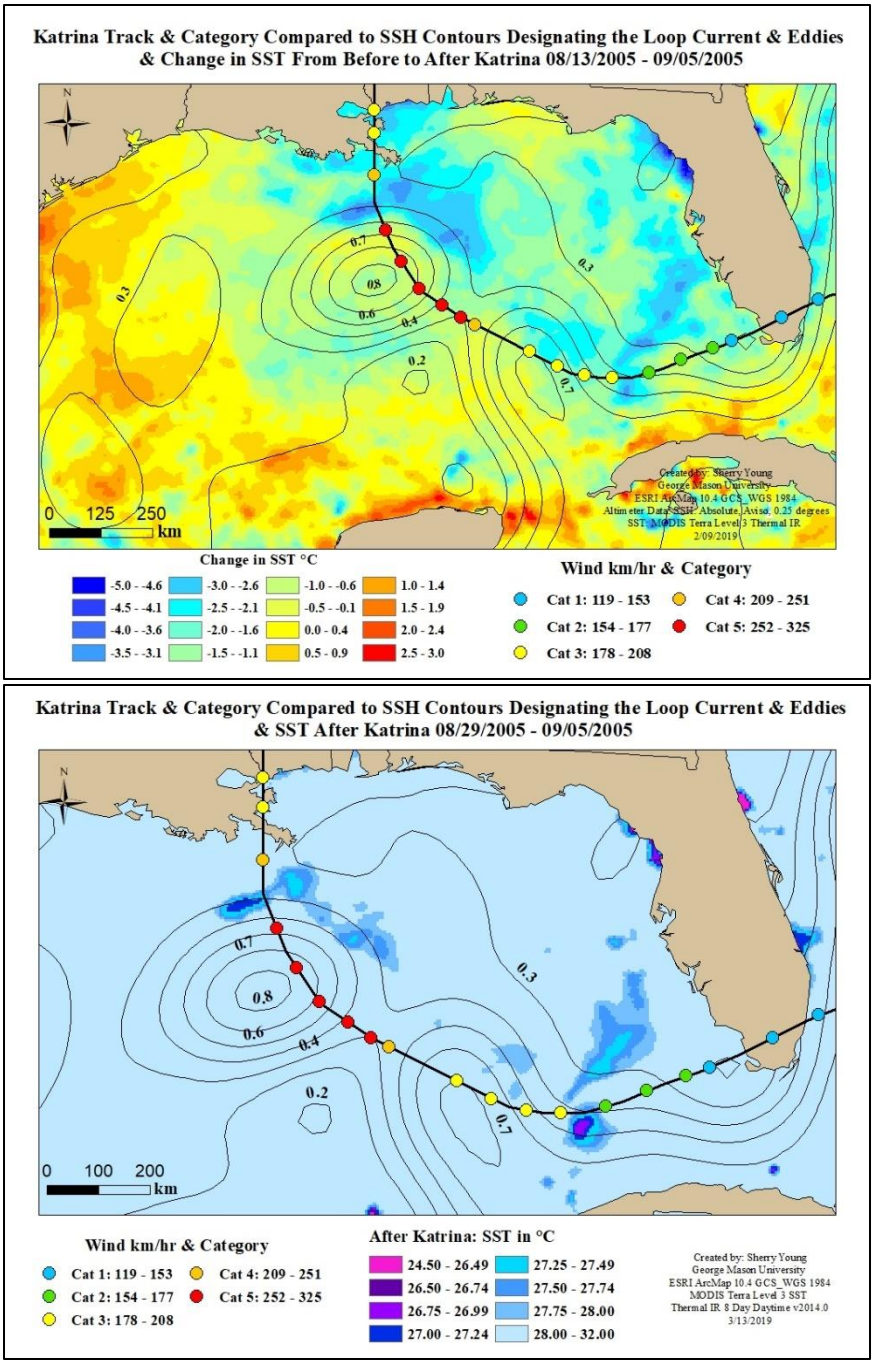

Figure 5-10 Katrina change in SST and SST after Katrina

Top map: track, category, and sustained wind speed compared to change in SST from before to after Katrina showing cold wake. SSH contour lines in meters. Bottom map shows the SST after Katrina in °C symbolized to emphasize areas where SST may have decreased below the critical value of 26.5°C during Katrina. No areas along Katrina's path show SST below 26.5°C, but some recovery of heat may have occurred during the 8-day satellite collection period.

Rita

Rita formed as a tropical depression east of the Turks and Caicos Islands on September 18th, 2005. Zero hour of this study began at 09:00 UTC on September 20th when tropical storm Rita was north of Cuba entering the Florida Straits with ~111 km/hr sustained winds. At hour 6, Rita became a category 1 hurricane in the Florida Straits and began a RI cycle (Figure 5-11). Upper atmospheric conditions were favorable with good outflow and wind shear was low; however, the NHC reported that the eye was slightly disorganized but improving and deep convection was occurring.

Rita traveled over the Florida Current towards the LC while continuing to rapidly intensify. By hour 24, Rita reached the eastern side of the LC and had increased by ~102 km/hr becoming a category 4 hurricane. Rita wasn't finished rapidly intensifying yet, it continued while travelling across the LC; by hour 36 Rita increased by another 55.6 km/hr to a category 5 hurricane. At this point Rita reached the farthest extent of the LC where it was attached to a WCE. Rita continued to intensify increasing by another 18.6 km/hr while it approached the WCE. The RI cycle ended at hour 41; the total increase in intensity was ~176.1 km/hr of which ~83.5 km/hr occurred within the previous 17 hours over the LC. Rita reached its maximum intensity as a category 5 hurricane with 287 km/hr sustained winds and 110% of its MPI at hour 41. Katrina and Rita both reached their maximum intensity at the farthest extent of the LC where it attached to the WCE; both storms achieved category 5 and over 100% of their MPI at this location.

Over the next 16 hours Rita crossed the western edge of the WCE while it underwent an RDI cycle. The largest decrease in intensity of 37 km/hr occurred at the WCE/CCE interface at hour 57 where the TCHP dropped to 60 kJ/cm^2 and the depth to the 26°C isotherm decreased to 55 m. Rita remained above 100% of its MPI until this time when it decreased to 89.7% and became a category 4 hurricane with ~231 km/hr sustained winds; an eyewall replacement cycle also began. Sustained winds decreased by another ~18.6 km/hr as Rita traveled along the eastern edge of the CCE and the eyewall replacement cycle completed. Rita crossed a second WCE along its eastern side; but the NHC noted that the eyewall was getting less distinct and convection was not as strong. Rita was downgraded to a category 3 hurricane with ~204 km/hr sustained winds. As Rita approached the continental shelf intensity decreased by another 18.6 km/hr. Rita made landfall between Sabine Pass and Johnson Bayou, Louisiana as a category 3 hurricane with ~185 km/hr sustained winds on September 24th.

Change in SST from before to after Rita ranged from -3.6°C to +0.7°C with the largest decreases occurring in GCW in areas originally with lower TCHP and shallower depth to the 26°C isotherm (Figure 5-12). In the LC cooling increased towards the shore of Cuba while cooling in the WCEs was greatest towards the outer edges. The largest decreases in temperature occurred in the GCW between the two WCEs and CCE in areas close to where Rita decreased in intensity. As with Katrina, SST collected after Rita shows that SST did not drop below 26.5°C along Rita's track; however, it came close in areas between the WCEs and CCE where the largest decreases in SST occurred. As

figure 5-12 shows, these regions are located near the data points where Rita began to RDI. As stated previously, because MODIS data is an 8-day average, it is possible that SST was below 26.5°C in these areas during Rita's passing and surface cooling could have limited the energy flux resulting in decreases in intensity.

As with Katrina, it is proposed that favorable atmospheric conditions, high SST, and large areas of high TCHP with greater depths to the 26°C isotherm were all responsible for Rita's episode of RI and allowed it to obtain 110% of its MPI. Change in SST data shows that along Rita's track SST remained above the critical temperature of 26.5°C limiting the negative feedback effect during the RI cycle. Rita underwent RDI when TCHP and depth to the 26°C isotherm decreased to the left of its track in the GCW near the CCE and on the continental shelf. GCW between the two WCEs and CCE had the largest decrease in SST and possibly lowered below the critical value of 26.5°C limiting the energy flux causing a reduction in intensity before landfall.

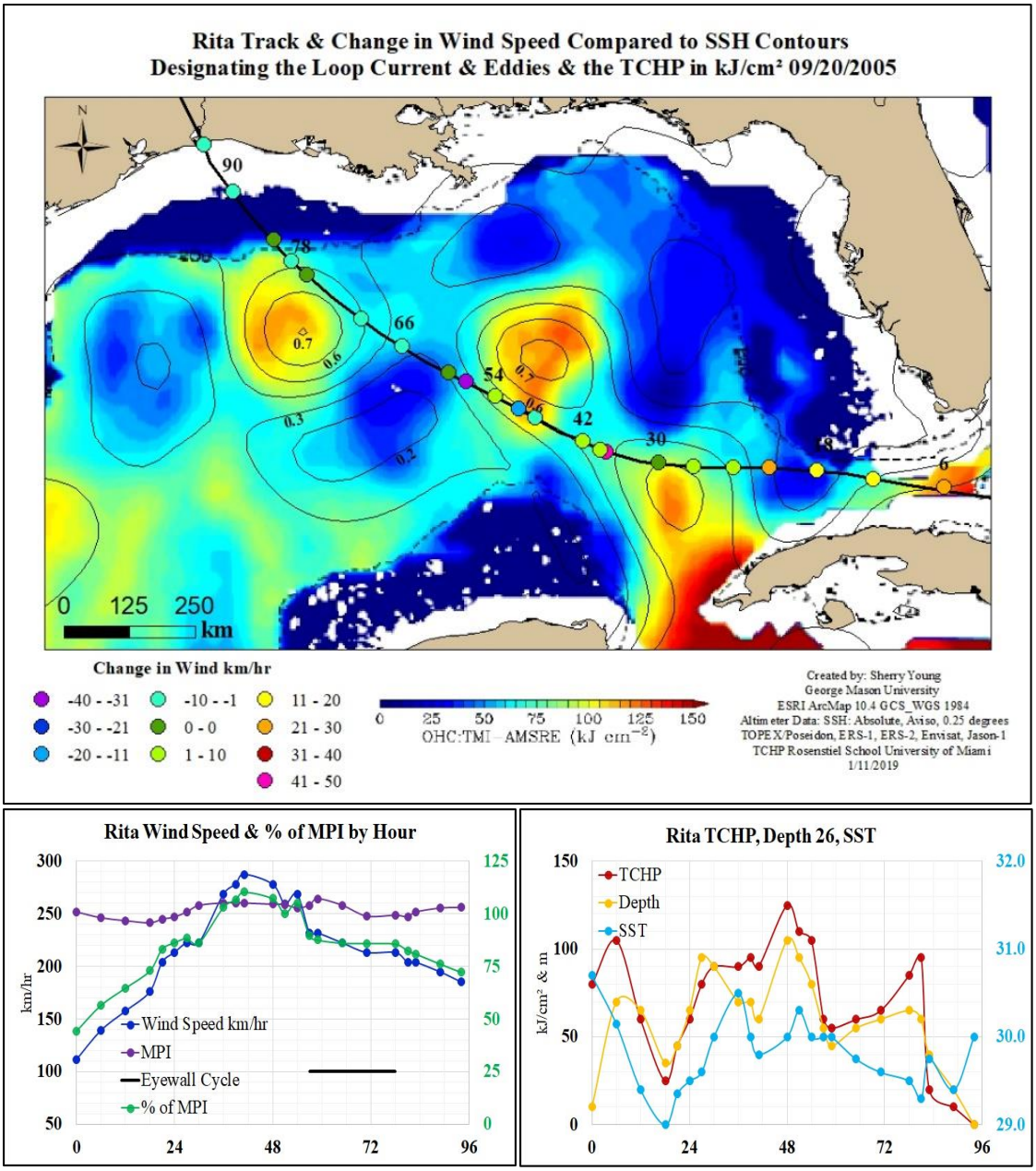

Figure 5-11 Rita change in wind speed and graphs

Map: track and change in sustained wind speed compared to TCHP in kJ/cm^2 on 09/20 and SSH contour lines in meters. Block numbers are hours from zero hour of observation. Graphs: (left) blue is the actual maximum sustained wind speed km/hr, purple is the calculated MPI wind speed in km/hr, green % of MPI achieved during observation, black line shows period of adverse eyewall conditions (right) red TCHP in kJ/cm², orange depth to 26°C isotherm in meters, turquoise SST °C.

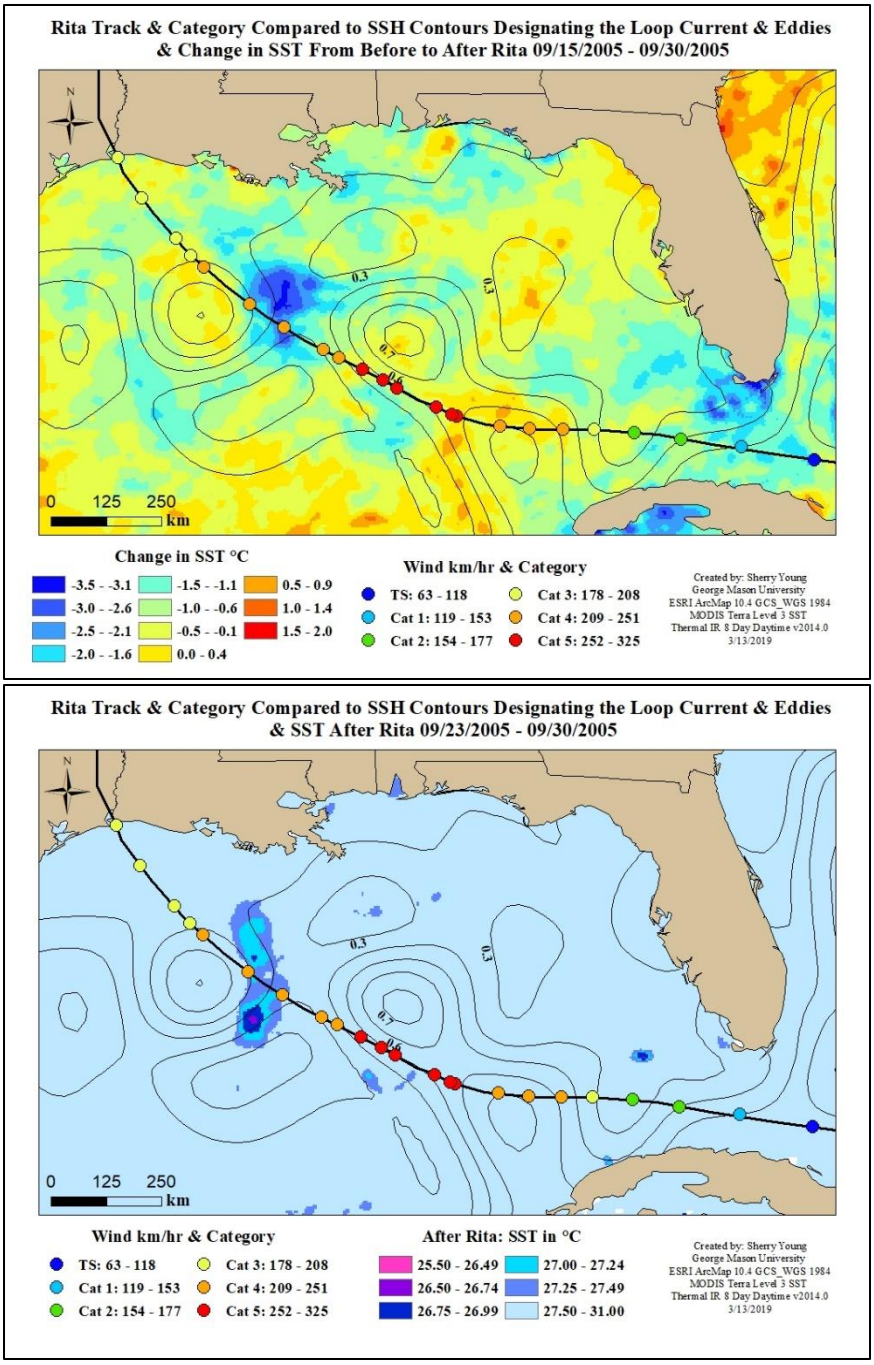

Figure 5-12 Rita change in SST and SST after Rita

Top map: track, category, and sustained wind speed compared to change in SST from before to after Rita showing cold wake. SSH contour lines in meters. Bottom map shows SST after Rita in °C symbolized to emphasize areas where SST may have decreased below the critical value of 26.5°C during Rita. No areas along Rita's path show SST below 26.5°C, but some recovery of heat may have occurred during the 8-day satellite collection period.

Wilma

Wilma formed as a tropical depression just southwest of Jamaica on October 15th, 2005. It took a northwesterly path through the Caribbean Sea where it intensified and became a category 5 hurricane with ~298 km/hr sustained winds and a central pressure of ~882 mb; currently the lowest pressure ever recorded for an Atlantic tropical cyclone (Mainelli et al., 2008). Wilma made landfall at Playa del Carmen, Mexico on October 22nd as a category 4 hurricane and spent the next 21 hours on the Yucatán Peninsula. Zero hour of analysis began when Wilma was on the Yucatán Peninsula at 15:00 UTC on October 22nd as a category 3 hurricane with ~185 km/hr sustained winds (Figure 5-13).

Wilma emerged off the Yucatán Peninsula as a category 2 hurricane and headed through the Yucatán Channel towards the GOM. Conditions were somewhat unfavorable because of moderate westerly shear and a weak disorganized eye; an eyewall replacement cycle began as Wilma entered the LC. Wilma began to intensify as it approached the middle of the LC. By 39 hours, deep convection resumed around the eye and it was becoming better organized, but Wilma was over shallow water only 30 nm from the Florida coast and stopped intensifying. Wilma increased by a total of 46.3 km/hr by hour 39 becoming a category 3 hurricane with ~204 km/hr sustained winds. This episode of intensification did not qualify as a full RI cycle because it fell short of the 56.5 km/hr increase required. The NHC noted that Wilma's eye was becoming more organized but it was still large and being affected by increasing westerly shear. By 42 hours, Wilma reached its maximum intensity while in the GOM of ~204 km/hr sustained winds with a

central pressure of 950 mb at ~85% of its MPI. Wilma's sustained winds decreased by 9.3 km/hr as it made landfall at 10:30 UTC on October 24th near Marco Island, Florida as a category 3 hurricane with ~194 km/hr sustained winds.

Change in SST from before to after Wilma ranged from -6.9°C to +0.1°C. The largest decreases in SST occurred along Florida's coast to the right of the track where the original TCHP was lower and depth to the 26°C isotherm was shallower. Another area with large changes in SST was on the Yucatán shelf. SST in the LC changed little, the largest decrease of ~-2.4°C occurred where the depth to the 26°C isotherm was shallower. SST data collected after Wilma shows that SST dropped below 26.5°C along Wilma's track in most areas of GCW; while SST in the LC remained above 27°C.

This study proposes that several factors contributed to Wilma's lack of a full RI cycle and reaching its MPI while in the GOM. First, moderate wind shear, an eyewall replacement cycle, and a large disorganized eye, made conditions unfavorable for intensification. Secondly, the cooling of the ocean surface lowered the SST below 26.5°C limiting the enthalpy flux. Another factor is that Wilma's forward speed of translation increased from 2-3 kts to 16-17 kts. This decreased the enthalpy flux while Wilma was over the eastern side of the LC, but also decreased the amount of negative feedback while over shallow low TCHP water. Wilma was able to intensify in the LC and on the Florida shelf in areas where the SST remained above 27°C limiting the negative feedback, but not enough to reach its MPI or complete a full RI cycle.

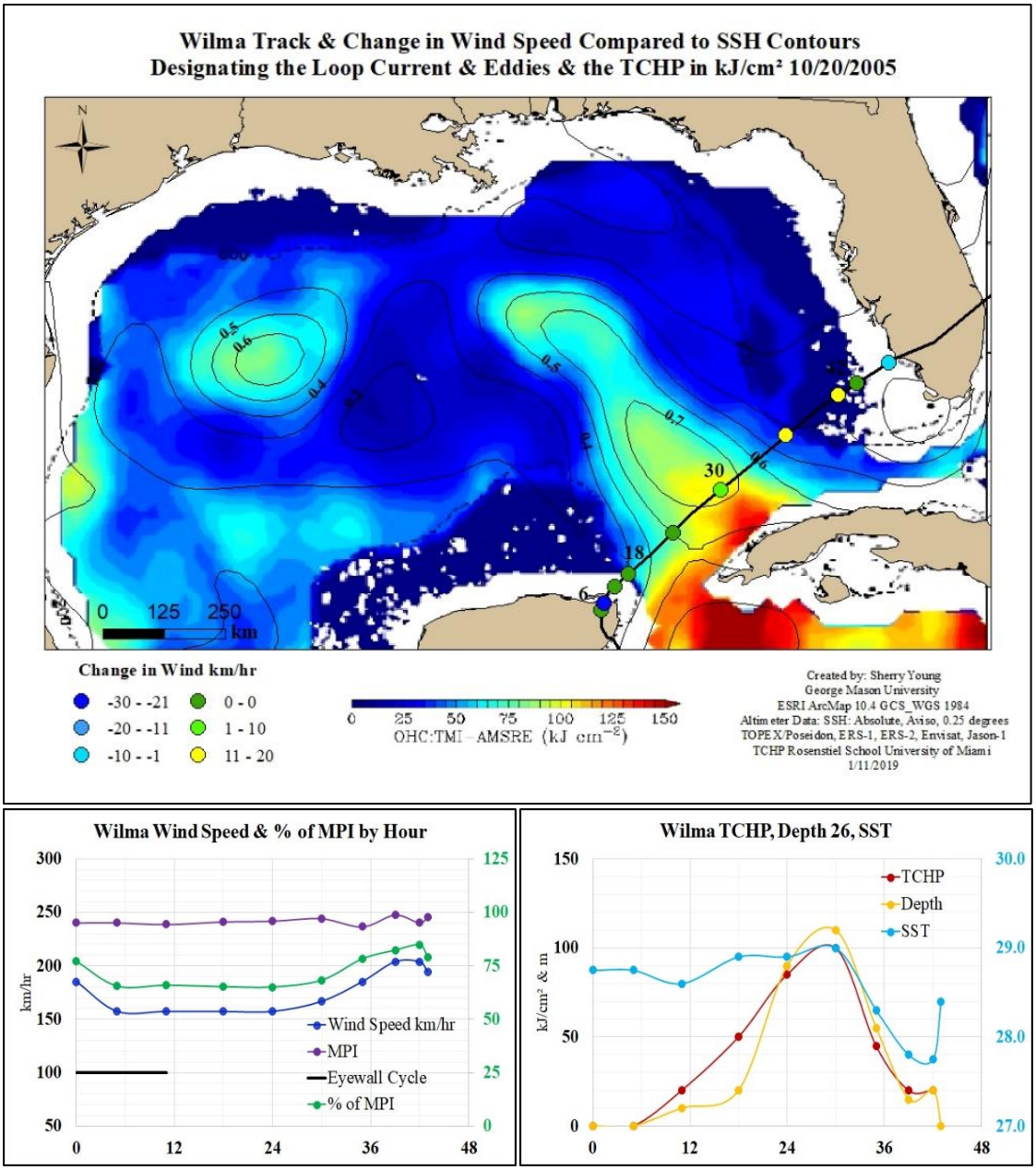

Figure 5-13 Wilma change in wind speed and graphs

Map: track and change in sustained wind speed compared to TCHP in kJ/cm² on 10/20 and SSH contour lines in meters. Block numbers are hours from zero hour of observation. Graphs: (left) blue is the actual maximum sustained wind speed km/hr, purple is the calculated MPI wind speed in km/hr, green % of MPI achieved during observation, black line shows period of adverse eyewall conditions (right) red TCHP in kJ/cm², orange depth to 26°C isotherm in meters, turquoise SST °C.

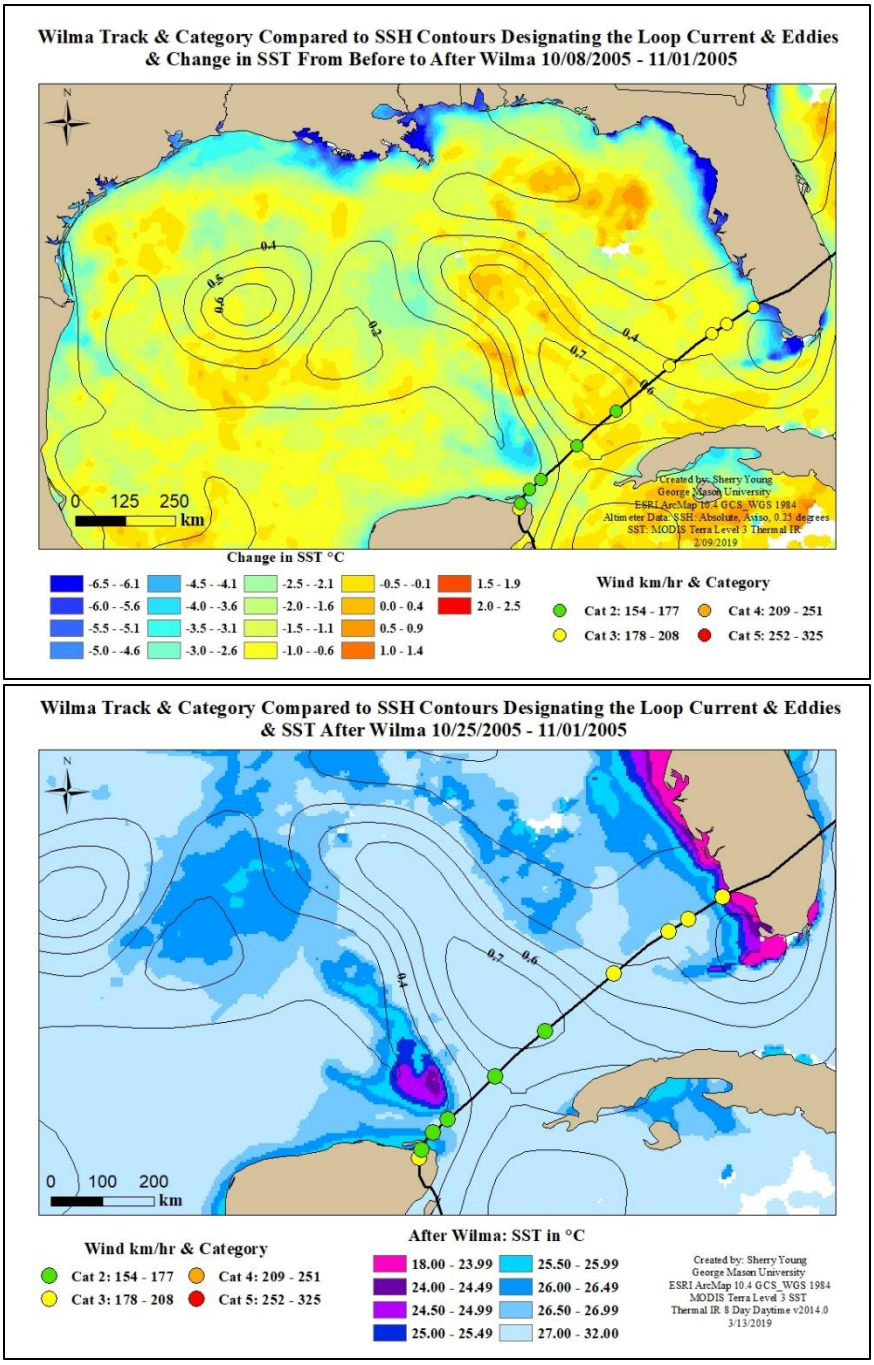

Figure 5-14 Wilma change in SST after Wilma

Top map: track, category, and sustained wind speed compared to change in SST from before to after Wilma showing cold wake. SSH contour lines in meters. Bottom map shows the SST after Wilma in °C symbolized to emphasize areas where SST may have decreased below the critical value of 26.5°C during Wilma. MODIS data is an 8-day average of SST, so additional areas may have been below 26.5°C.

5.1.4. 2008: Gustav and Ike

Gustav

Tropical depression Gustav formed north of the Antilles Islands on August 25th, 2008. It traveled through the Caribbean Sea and made landfall on Haiti as a category 1 hurricane with ~130 km/hr sustained winds on August 26th. After traveling along Jamaica's southern shore, tropical storm Gustav headed towards Cuba while intensifying. Hour zero of this study began at 21:00 UTC on August 30th as Gustav was approaching Cuba. Approximately an hour later, Gustav made landfall on Cuba as a strong category 4 hurricane with ~250 km/hr sustained winds (Figure 5-15).

Gustav emerged off Cuba over the LC with a slightly weakened eye. The NHC noted that the LC had high levels of OHC and that the SST was high. They expected Gustav to intensify while over the LC and then be affected by increasing shear of 20 kts from the south; however, it was expected to remain at least a category 3 hurricane until landfall. Even though conditions appeared to be favorable for Gustav to intensify while over the LC, an RDI cycle began between 0-5 hours. By hour 24, sustained winds decreased by a total of ~64.8 km/hr. Gustav's eye became ragged, elongated and open to the southeast by hour 18. Gustav was large in diameter and continued to expand in size while approaching land. Gustav made landfall at Cocodrie, Louisiana on September 1st at 15:00 UTC as a category 2 hurricane with ~167 km/hr winds.

Change in SST from before to after Gustav ranged from -2.9°C to +0.8°C with the largest decreases in SST occurring in areas where TCHP was less than 65 kJ/cm^2 and depth to the 26°C isotherm was less than 50 m (Figure 5-16). Cooling in the LC along the track was up to 2°C but on average was between 1°C-1.6°C. SST after Gustav shows no areas below 26.5°C along Gustav's path. To the right of where the largest change in SST occurred, SST measured ~27.5°C-27.75°C after Gustav; it unknown if this area may have dropped below 26.5°C during Gustav. Because the MODIS SST after Gustav data was collected partially during Ike, it is possible that the change in SST data is inaccurate.

It is proposed that Gustav's degraded eyewall limited convection and the enthalpy flux affecting Gustav's capability to intensify. Other factors that affected Gustav's intensity was wind shear of 20 kts, dry air entrainment, and interaction with Cuba; all of which affected deep convection and the strength of the central core. Speed of translation was between 13-16 knots, which also may have affected the net enthalpy flux. Satellite data suggests that SST did not reduce to below 26.5°C under Gustav's path; therefore, surface cooling doesn't appear to be a strong factor in Gustav's lack of intensification.

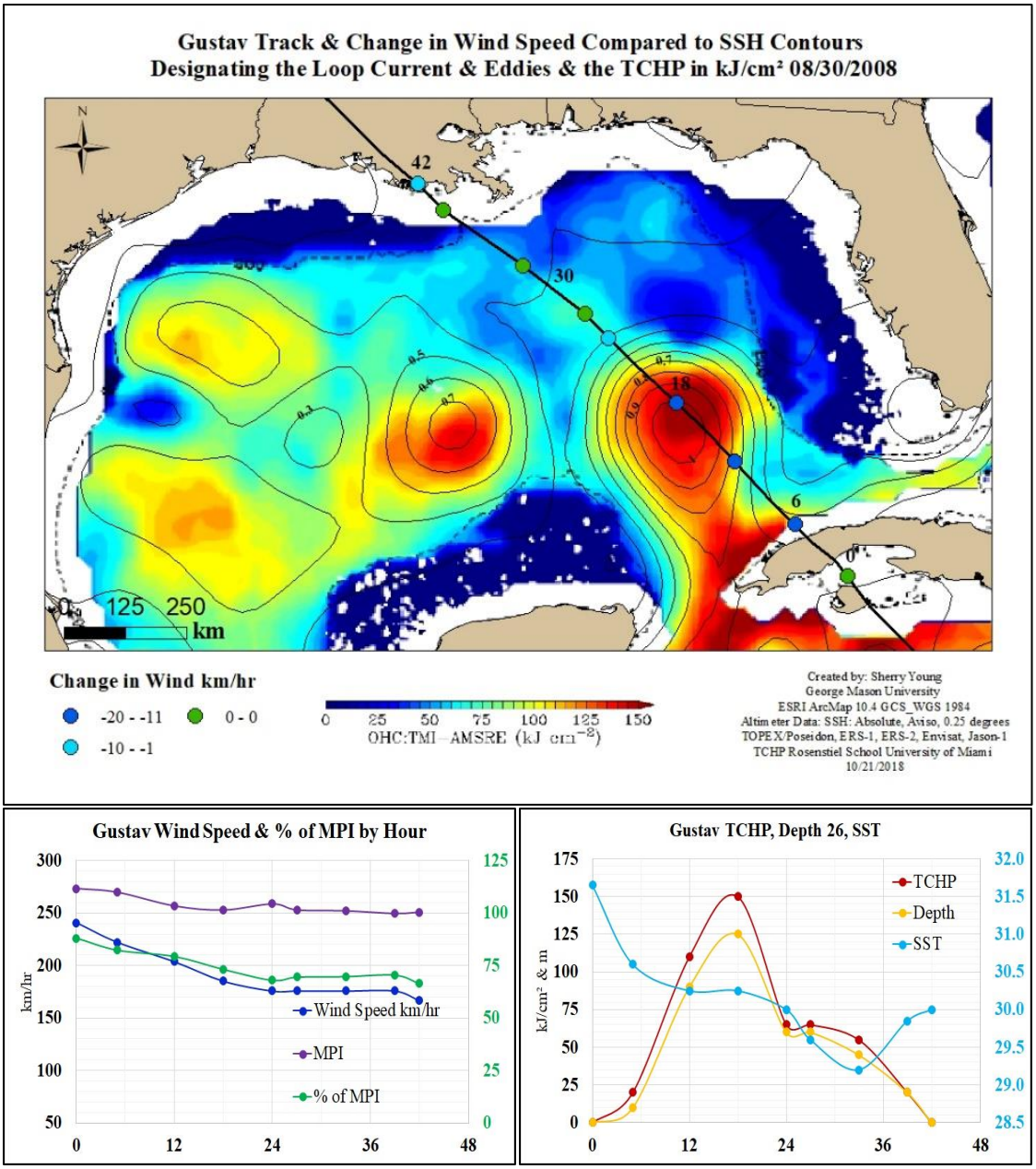

Figure 5-15 Gustav change in wind speed and graphs

Map: track and change in sustained wind speed compared to TCHP in kJ/cm^2 on 08/30 and SSH contour lines in meters. Block numbers are hours from zero hour of observation. Graphs: (left) blue is the actual maximum sustained wind speed km/hr, purple is the calculated MPI wind speed in km/hr, green % of MPI achieved during observation (right) red TCHP in kJ/cm², orange depth to 26°C isotherm in meters, turquoise SST °C.

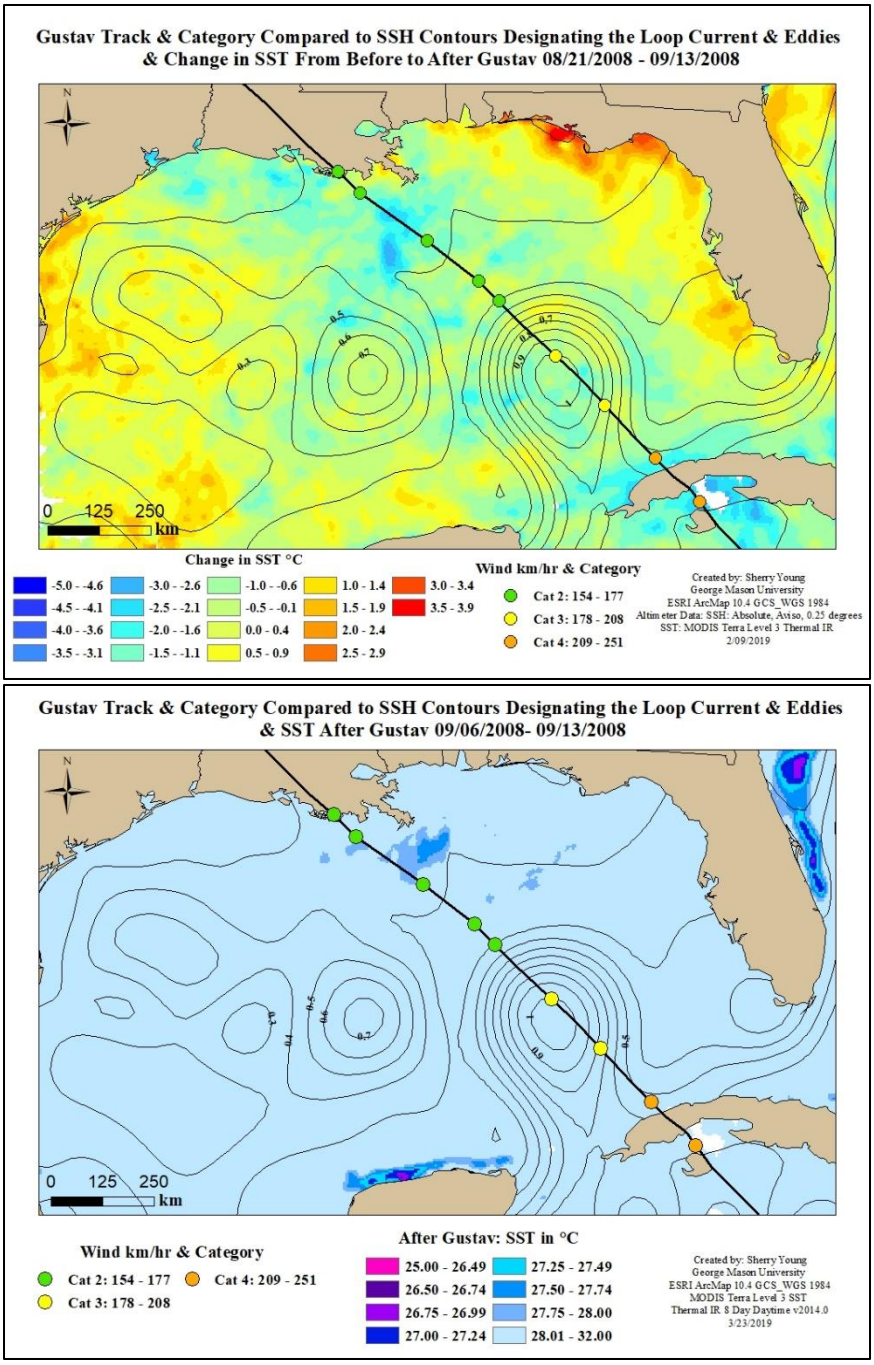

Figure 5-16 Gustav change in SST and SST after Gustav

Top map: track, category, and sustained wind speed compared to change in SST from before to after Gustav showing cold wake. SSH contour lines in meters. Bottom map shows the SST after Gustav in °C symbolized to emphasize areas where SST may have decreased below the critical value of 26.5°C during Gustav. No areas along Gustav's path show SST below 26.5°C, but some recovery of heat may have occurred during the 8-day satellite collection period.

Ike

Ike formed over the Atlantic Ocean while Gustav made landfall in the Gulf. Ike formed as a tropical depression on September 1st, 2008 over the tropical Atlantic Ocean. Ike intensified while traveling westward towards Cuba and made landfall on September 8th in Punta de Maisi, Cuba as a category 4 hurricane with ~212 km/hr sustained winds. Over the next day, Ike crossed over Cuba into the Caribbean Sea and made a second landfall near the San Cristobal-Candelaria border at 15:00 UTC September 9th as a category 1 hurricane with ~130 km/hr sustained winds; analysis of Ike began at this time.

Even though SST was warm, TCHP was high, and depth to the 26°C isotherm was more than 75 m in the LC, Ike intensified slowly by a total amount of ~37 km/hr over 21 hours while over the LC. Another small episode of intensification occurred between hours 59 and 71 after Ike passed over a WCE. Besides the two episodes of intensification, Ike's sustained winds remained stable. Ike made landfall on September 13th near Galveston, Texas as a category 2 hurricane with ~176 km/hr sustained winds.

Ike was a large storm with an atypical wind structure; it had a large wind field with a small 8-10 nm inner eyewall with a larger outer concentric eyewall throughout most of its lifecycle in the GOM. The eyewall replacement cycle was unable to complete until ~5 hours before landfall. Tropical storm force winds expanded out to 275 nm and hurricane winds out to 120 nm from the center. The NHC center also noted that the air in the upper troposphere was warm because of a high pressure over Texas and some dry air

existed to Ike's west. The NHC expected Ike to intensify to at least a category 3 hurricane before landfall and observed that the pressure lowered to what would be expected of a category 3 or 4 hurricane while the sustained winds remained that of a category 2. Wind shear of 15 kts affected Ike around 65 hours and Ike lost its inner core. In the last few hours before landfall, Ike organized a singular stronger 40 nm eyewall that was contracting and the upper level winds increased to that of a category 4 storm, but the winds at the surface only increased by 9.3 km/hr. It is proposed that Ike's atypical wind structure and its inability to complete the eyewall replacement cycle until just before landfall limited Ike's ability to intensify. Ike was still strong enough to be able to intensify slightly while over the LC and WCE and maintain its intensity until landfall in spite of its large size, atypical wind structure and lack of a strong central core with deep convection.

Before Ike SST MODIS satellite data was collected from August 29th to September 6th, during this time SST was at least partially affected by hurricane Gustav. MODIS SST data was unusable for the after Ike period from September 14th to the 21st because of large areas containing no data (Figure 5-19). During Ike SST data had to be used instead for the change in SST map, this data was collected between September 6th to the 13th. Clouds from Ike likely prohibited satellite observation during some of this period; however, very few pixels with no data existed in this data set. Because of possible lapses in SST data collection, SST change shown in figure 5-19 is considered unreliable.

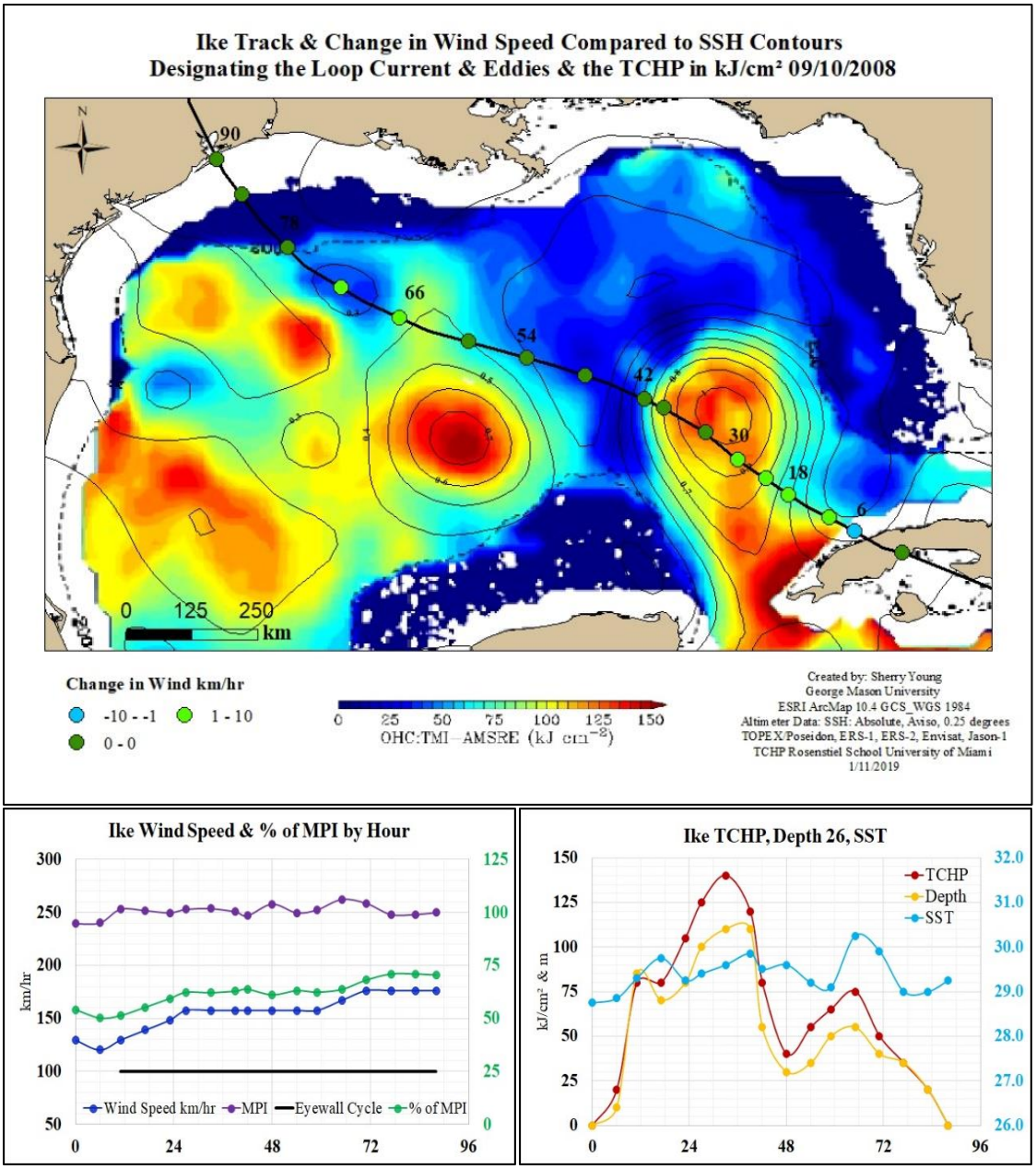

Figure 5-17 Ike change in wind speed and graphs

Top map: track and change in sustained wind speed compared to TCHP in kJ/cm^2 on 09/10 and SSH contour lines in meters. Block numbers are hours from zero hour of observation. Graphs: (left) blue is the actual maximum sustained wind speed km/hr, purple is the calculated MPI wind speed in km/hr, green % of MPI achieved during observation (right) red TCHP in kJ/cm², orange depth to 26°C isotherm in meters, turquoise SST °C.

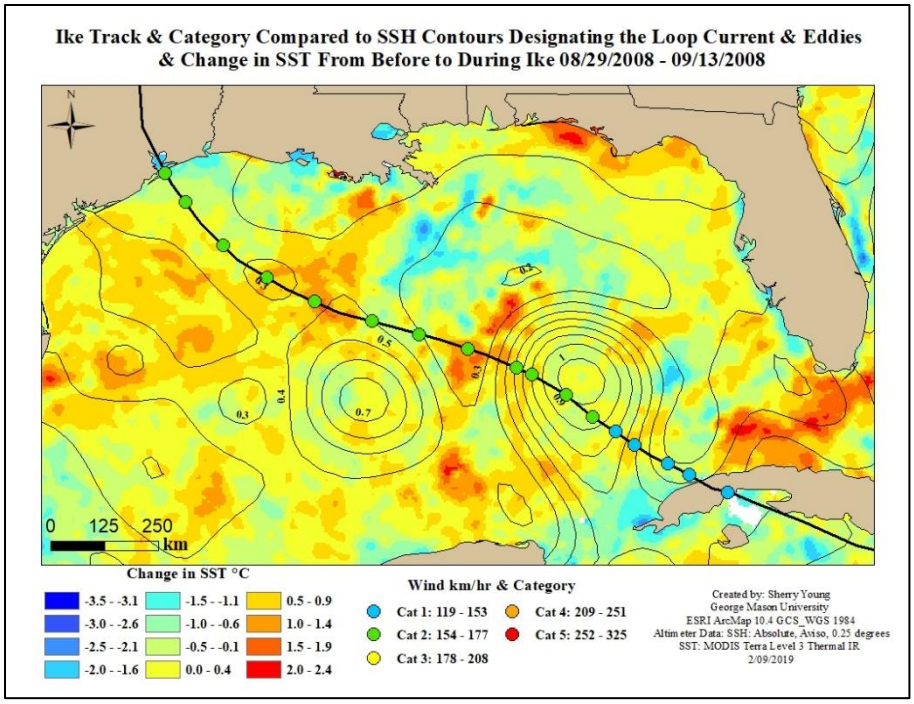

Figure 5-18 Ike change in SST

Map: Ike's track, category, and sustained wind speed compared to change in SST from before to during Ike. Change in SST data has been potentially affected by lapses in data collection.

5.1.5. 2009: Ida

Ida formed as a tropical depression on November 4th, 2009 east of Costa Rica at ~11°N latitude and 81.3°W longitude. Ida took a northwesterly path and made landfall as a category 1 hurricane in Nicaragua on November 5th. A day later, Ida emerged over the Caribbean Sea from Honduras as a tropical depression. Ida began to intensify as it continued north over warm Caribbean water; zero hour of analysis began at 12:00 UTC on November 8th when Ida was entering the Yucatán Channel as a category 2 hurricane with ~157 km/hr sustained winds (Figure 5-20).

The LC was in the retracted state and a large CCE was directly northwest of the LC under Ida's path, a weak WCE existed to the west. Ida's sustained winds increased slightly by 9.3 km/hr while over the LC; but once Ida moved over the CCE it began to rapidly de-intensify. Between hours 12 and 24 Ida's sustained wind speed decreased by a total of 55.5 km/hr. By 26 hours the top of Ida's cloud column was being sheared off towards the northeast restricting deep convection and the eyewall collapsed. At 38 hours SST decreased to 25°C and Ida began its second RDI cycle; over the next 10 hours Ida's sustained winds decreased by another 74 km/hr while the SST and TCHP continued to drop (Figure 5-20). Ida made landfall at 12:00 UTC on November 10th as barely a tropical storm with no central core and ~65 km/hr sustained winds on Dauphin Island, Alabama.

Change in SST from before to after Ida ranged from -4.7°C to +2.0°C; the largest decreases in SST occurred on the continental shelves and in the CCE where TCHP was lower and depth to the 26°C isotherm was shallower (Figure 5-21). SST was low in the GCW and CCE before Ida with surface temperatures below 26°C on the continental shelves; after Ida along most of its path SST was at or below 26°C except for in the LC. Ida was a late season storm that was affected by significant wind shear of 20-30 kts, low SST in the northern GOM below 26.5°C, and TCHP below 35 kJ/cm^2 along most of its path. It is proposed that these factors limited deep convection and the enthalpy flux from the ocean surface affecting Ida's capability of sustaining its intensity.

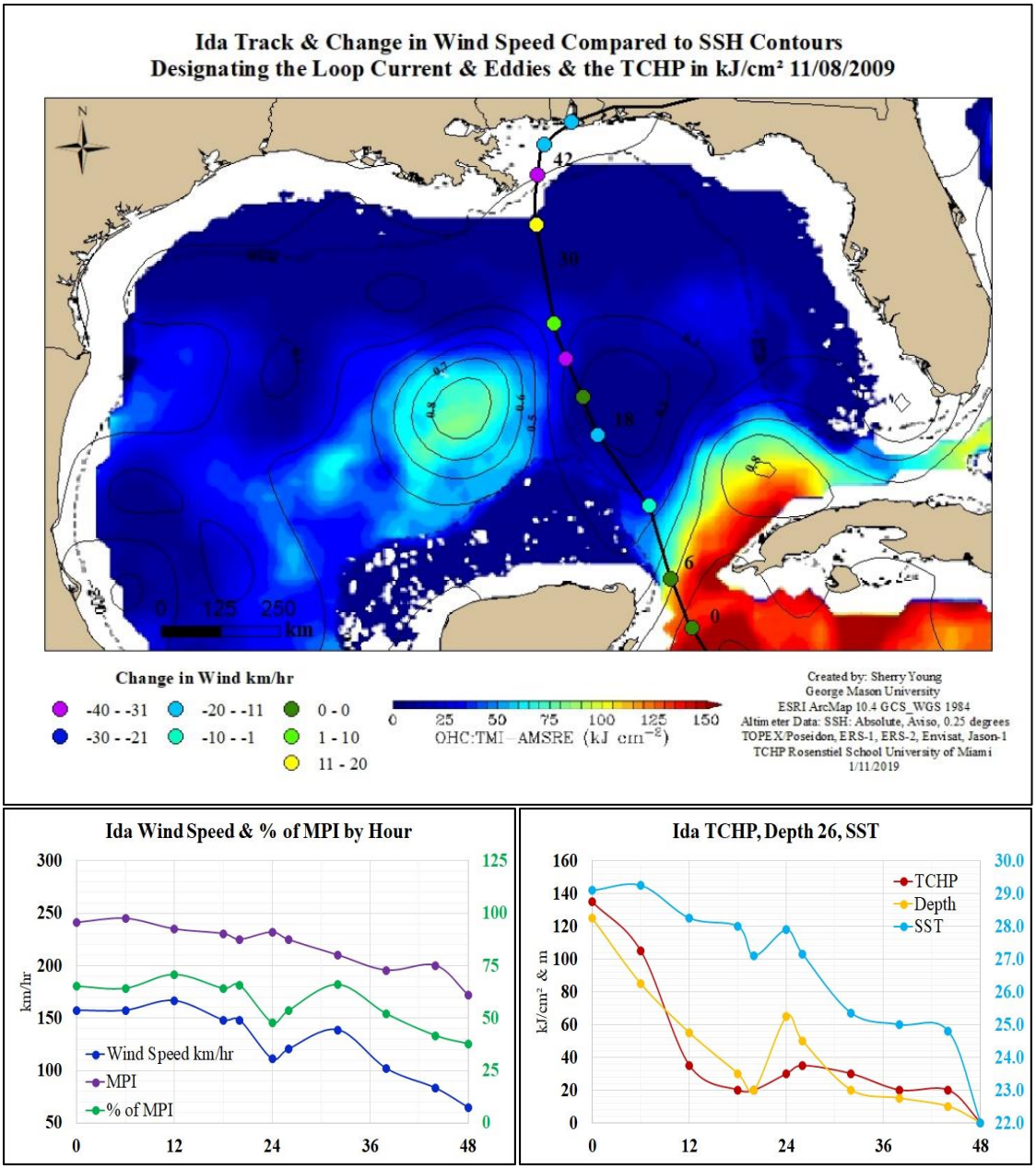

Figure 5-19 Ida change in wind speed and graphs

Map: track and change in sustained wind speed compared to TCHP in kJ/cm² on 11/08 and SSH contour lines in meters. Block numbers are hours from zero hour of observation. Graphs: (left) blue is the actual maximum sustained wind speed km/hr, purple is the calculated MPI wind speed in km/hr, green % of MPI achieved during observation (right) red TCHP in kJ/cm², orange depth to 26°C isotherm in meters, turquoise SST °C.

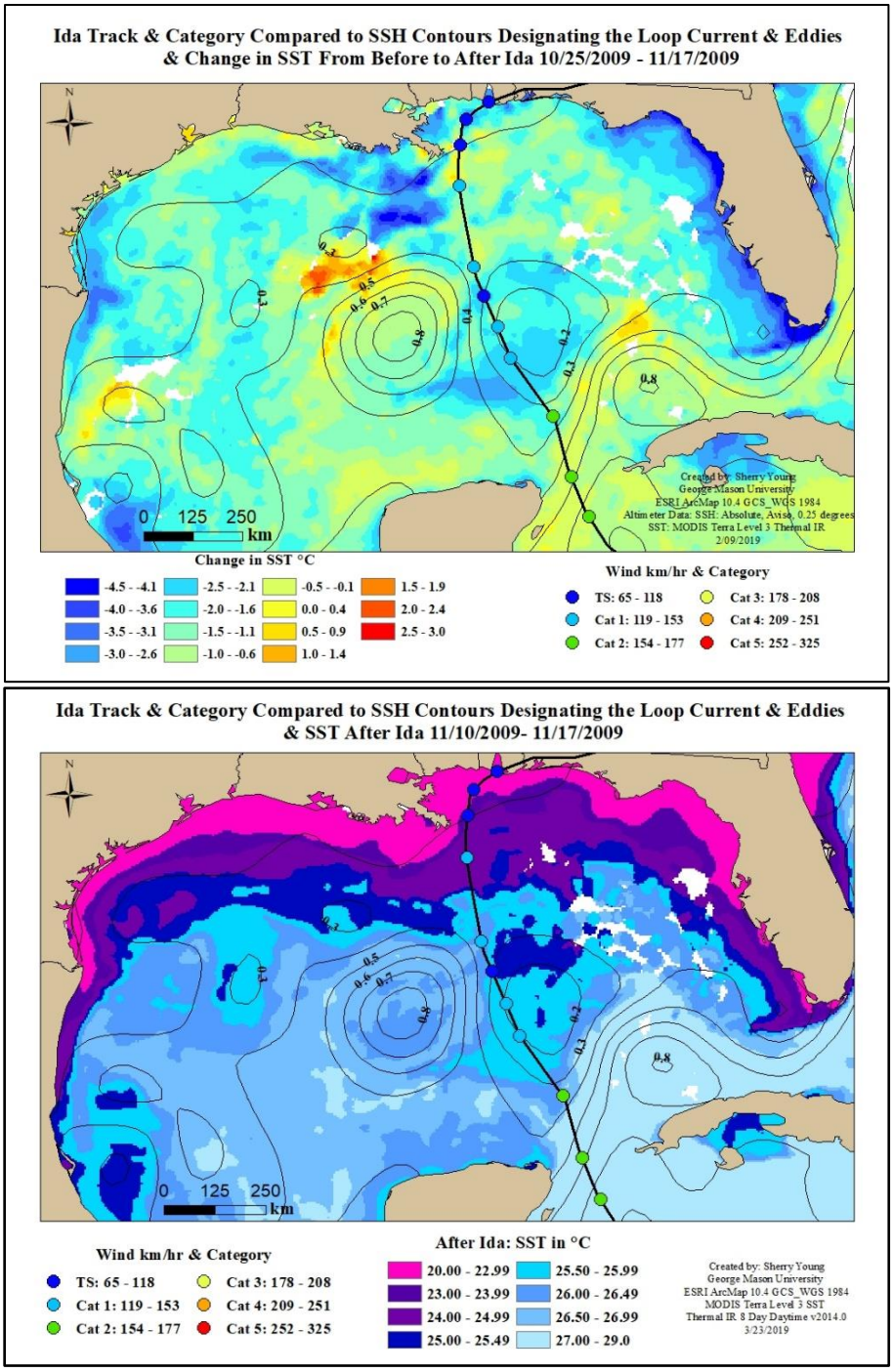

Figure 5-20 Ida change in SST and SST after Ida

Top map: Ida's track, category, and sustained wind speed compared to change in SST from before to after Ida. Bottom map shows SST after Ida in °C symbolized to emphasize areas where SST may have decreased below the critical value of 26.5°C during Ida. Large areas along Ida's path shows SST below 26.5°C. White pixels contain no data.

5.1.6. 2012: Isaac

Isaac began as a tropical depression over the Atlantic Ocean at ~15.7°N latitude and 44.8°W longitude on August 20th, 2012. It took a westerly path through the Caribbean Sea and then turned northwestward and made landfall east of Trou Mahot, Haiti on August 25th as a tropical storm. Isaac continued towards the northwest and made a second landfall near Imias, Cuba and then followed the northern coast of Cuba into the Florida Straits. Zero hour of observation began at 12:00 UTC on August 26th when Isaac was north of Cuba entering the Florida straits as a tropical storm with ~93 km/hr sustained winds (Figure 5-22). Isaac lacked an organized inner core with deep convection at this time.

SST was very warm along Isaac's path between 29.6°C-31.9°C; however, the LC was in a retracted state close to the shore of Cuba with lower than average TCHP. A large CCE was positioned to the west of Isaac's path with a WCE to the northwest of the CCE. Atmospheric conditions were unfavorable for intensification, there was moderate wind shear from the southeast and dry air was being entrained into the mid-level layer from the northeast; furthermore, Isaac's wind radius was large with the maximum winds were located far from the center.

Ivan intensified by 18.6 km/hr between hours 18-30, and again at hour 50 by 9.3 km/hr; at this time Isaac became at category 1 hurricane. An eyewall began developing several times, but each time a partial eyewall appeared on satellite imagery it was eroded

by dry air restricting deep convection. Isaac became a little better organized at hour 56 when it passed the WCE to its west and increased by another 9.3 km/hr. Isaac made landfall twice, first on the Mississippi Delta in Plaquemines Parish, Louisiana and then on Elmer's Island as a category 1 hurricane with ~130 km/hr sustained winds.

The cold wake from Isaac was widespread because Isaac mostly traveled over CCEs and GCW with lower TCHP and shallower depths to the 26°C isotherm. Change in SST along Isaac's path ranged from -3.7°C to +0.25°C (Figure 5-23). The LC and WCE had the least amount of cooling but were still affected; however, because the initial SST was so high, after Isaac SST remained above 26.5°C along Isaac's entire path. It doesn't appear that surface cooling affected Isaac's intensity.

It is proposed that Isaac's intensification was restricted because of a lack of a strong eyewall with deep convection which limited the enthalpy flux from the ocean to the storm. Moderate wind shear and dry air entrainment prohibited Isaac from organizing a strong central core with deep convection. Isaac did improve and strengthen slightly over the LC and WCE but not enough to allow for significant intensification and to obtain more than 52% of its MPI.

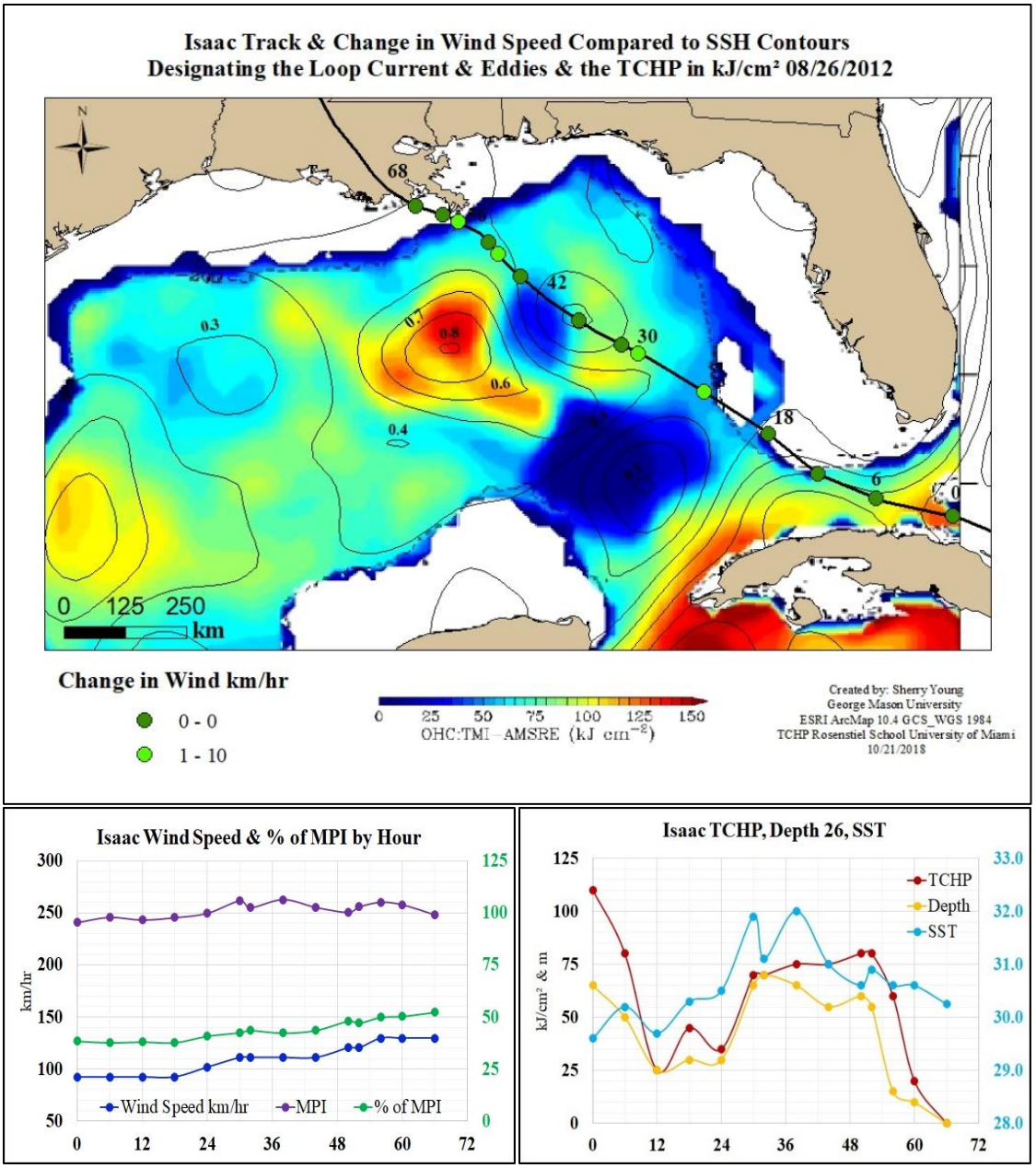

Figure 5-21 Isaac change in wind speed and graphs

Map: track and change in sustained wind speed compared to TCHP in kJ/cm^2 on 08/26 and SSH contour lines in meters. Block numbers are hours from zero hour of observation. Graphs: (left) blue is the actual maximum sustained wind speed km/hr, purple is the calculated MPI wind speed in km/hr, green % of MPI achieved during observation (right) red TCHP in kJ/cm², orange depth to 26°C isotherm in meters, turquoise SST °C

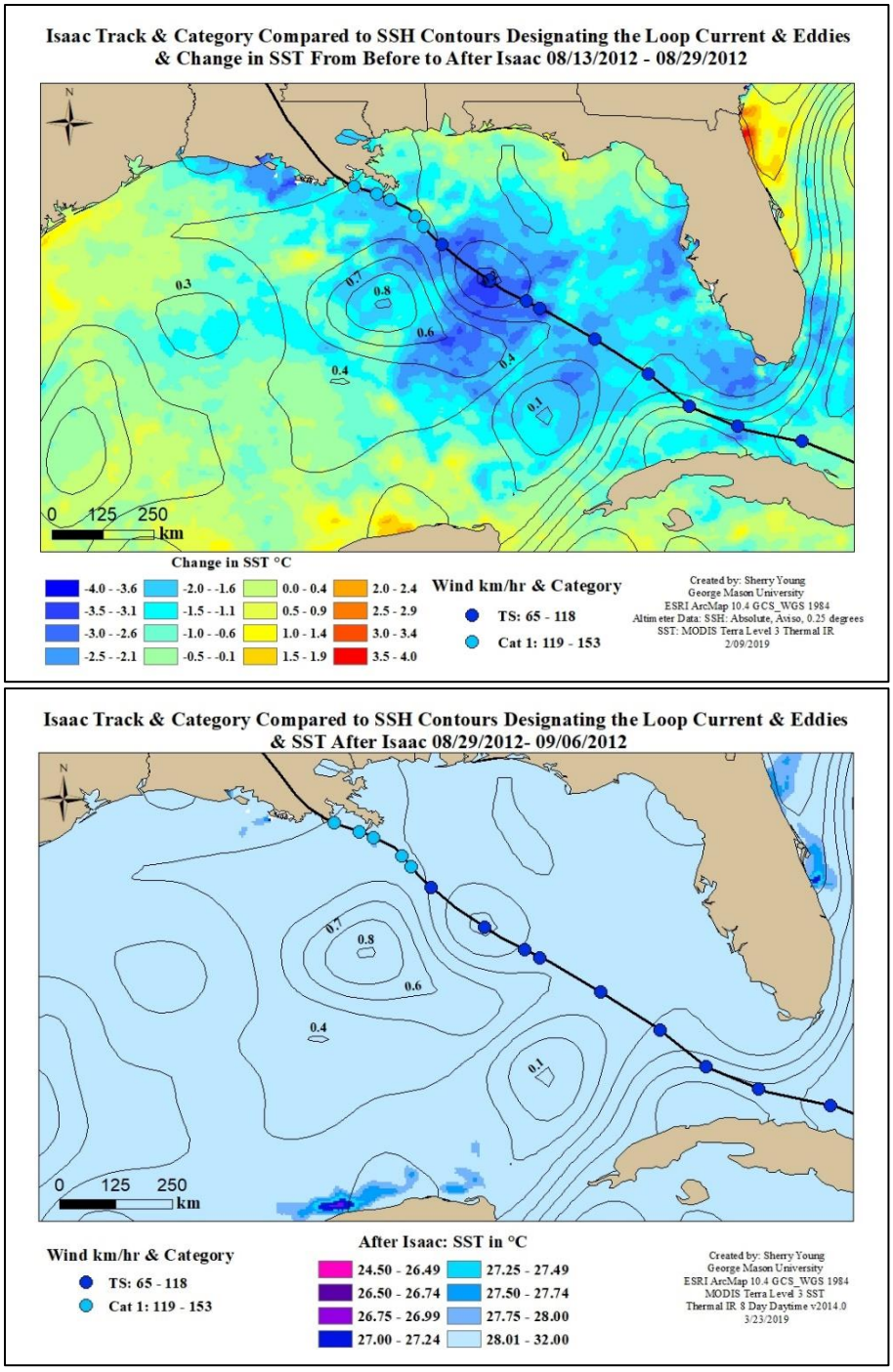

Figure 5-22 Isaac change in SST and SST after Isaac

Top map: Isaac's track, category, and sustained wind speed compared to change in SST from before to after Isaac. Bottom map shows the SST after Isaac in °C symbolized to emphasize areas where SST may have decreased below the critical value of 26.5°C during Isaac. No areas along Isaac's path show SST below 26.5°C, but some recovery of heat may have occurred during the 8-day satellite collection period.

Table 5-1 Summary of hurricanes: formation & starting conditions

Storm			Formation		Beginning Study Conditions	
Year	Name	Zero hour of study	Location	Date	Atmosphere	Eye
2002	Isidore	21:00 UTC 09/20/2002	Off coast Venezuela	09/14/2002	Low wind shear, favorable upper atmosphere	Eyewall replacement cycle over Cuba
	Lili	18:00 UTC 10/01/2002	Northeast of French Guiana	09/21/2002	Low wind shear, good outflow, favorable conditions	Eyewall replacement over LC
2004	Ivan	20:00 UTC 09/13/2004	Atlantic Ocean	09/02/2004	Some westerly shear, favorable upper atmosphere, good outflow	Strong eye with deep convection
2005	Dennis	03:00 UTC 07/09/2005	Off the coast of Venezuela	07/04/2005	Low wind shear, good outflow, favorable conditions	Slightly degraded eye
	Katrina	21:00 UTC 08/25/2005	Near the Bahamas	08/23/2005	Low wind shear, good outflow, favorable conditions, warm SST	Strong eye with deep convection
	Rita	09:00 UTC 09/20/2005	Turks and Caicos Islands	09/18/2005	Low wind shear, good outflow, favorable conditions	Slightly disorganized with deep convection
	Wilma	15:00 UTC 10/22/2005	Southwest of Jamaica	10/15/2005	Moderate shear, slightly unfavorable	Weak disorganized eye, eyewall replacement
2008	Gustav	21:00 UTC 08/30/2008	North of Antilles Islands	08/25/2008	Moderate wind shear, dry air entrainment	Weak degraded eye
	Ike	15:00 UTC 09/09/2008	Atlantic Ocean	09/01/2008	Low wind shear, favorable upper atmosphere	Eye appeared strong over Cuba
2009	Ida	12:00 UTC 11/08/2009	Off Costa Rica	11/04/2009	Moderate to strong wind shear, cool GCW	Weak elliptical eye
2012	Isaac	12:00 UTC 08/26/2012	Atlantic Ocean	08/20/2012	Moderate wind shear, dry air entrainment, unfavorable	No organized core/eye

Table 5-2 Summary of hurricanes: RI & RDI cycles

Hours are from zero hour of study and coincide with hours on the maps, MSWS is the maximum sustained wind speed at the end of the cycle, where: is the location where the eyewall was when the changes occurred. Some storms had multiple cycles while some had none.

Storm	RI				RDI			
Name	Total km/hr	Hours	Where	MSWS km/hr	Total km/hr	Hours	Where	MSWS km/hr
Isidore	64.8	0-23	LC	203.7	120.4	47-75	Yucatán	64.8
Lili	64.8	8-26	GCW	231.5	111.1	32-47	GCW/Land	120.4
Ivan	N/A	N/A	N/A	N/A	N/A	N/A	N/A	N/A
Dennis	83.4	6-29	LC/CCE	231.5	N/A	N/A	N/A	N/A
Katrina	64.8	14-36	GCW/LC	185.2	83.5	69-89	WCE/GCW	194.5
	92.6	54-66	LC/WCE	277.8				
Rita	176.1	0-41	GCW/LC	287.1	74.1	41-57	WCE	231.5
Wilma	N/A	N/A	N/A	N/A	N/A	N/A	N/A	N/A
Gustav	N/A	N/A	N/A	N/A	64.8	0-24	LC	175.9
Ike	N/A	N/A	N/A	N/A	N/A	N/A	N/A	N/A
Ida	N/A	N/A	N/A	N/A	55.5	12-24	CCE	111.1
					74.0	32-48	GCW/Land	64.8
Isaac	N/A	N/A	N/A	N/A	N/A	N/A	N/A	N/A

Table 5-3 Summary of hurricanes: adverse conditions

Hours are from zero hour of study and coincide with hours on the maps

Storm		Adverse Conditions	
Year	Name	What	Hours
2002	Isidore	Concentric eye, eyewall replacement	0-29
		Over land	41-81
		No core/eye collapse	63-129
	Lili	Eyewall replacement	0-8
		Concentric eyewall, elongated eye, wind shear, dry air entrainment	24-32
		Partial eyewall collapse	38-47
2004	Ivan	Eyewall replacement	10-18
		Some westerly shear & dry air	10-42
2005	Dennis	Slightly degraded eye	0-19
	Katrina	Eyewall replacement	36-54
	Rita	Disorganized eye	0-12
		Eyewall replacement	54-78
	Wilma	Eyewall replacement	0-11
		Over land	0-5
		Westerly shear, weak eye	0-39
2008	Gustav	Weak elongated eye	0-27
		Eye open on south	27-42
		Wind shear, dry air entrainment	0-42
	Ike	Concentric eyewalls	11-77
		Large radius, winds far from center, atypical wind structure	11-88
2009	Ida	Moderate to strong wind shear	0-48
		Elongated weak eye	0-24
		No eye, core, or deep convection	24-48
2012	Isaac	Moderate wind shear, dry air entrainment, lack of core/eye, large wind field	0-66

Table 5-4 Summary of hurricanes: maximum wind speed, % of MPI & pressure

Hours are from zero hour of study and coincide with hours on the maps, maximums are those recorded during the study and may not reflect the storm's lifetime maximum, where: is the location of the eyewall during the observation, lowest pressure did not always occur at the same time as the maximum wind speed. LA= Louisiana TX= Texas

Storm		Study Maximum Wind Speed & Category					Study Maximum % of MPI		
Year	Name	Max Wind Speed km/hr	Lowest Central Pressure	Max Cat	Hours	Where	%	Where	Hours
2002	Isidore	203.7	934	3	23-47	LC GCW	82.2	GCW	33
	Lili	231.5	938	4	26-32	GCW	98.8	GCW	26
2004	Ivan	259.3	912	5	0-10	Cuba LC	100.4	LC	7
2005	Dennis	231.5	932	4	29	CCE GCW	95.5	CCE GCW	29
	Katrina	277.8	902	5	61-69	LC WCE	102.7	WCE	66
	Rita	287.1	895	5	41	LC	110.3	LC	41
	Wilma	203.7	950	3	39-42	GCW	84.7	GCW	42
2008	Gustav	240.8	942	4	0	Cuba	88.0	Cuba	0
	Ike	175.9	944	2	88	CCE	70.9	TX	88
2009	Ida	166.7	975	2	12	LC	70.9	LC	12
2012	Isaac	129.6	966	1	56-66	GCW LA	52.2	LA	66

Table 5-5 Summary of hurricanes: landfall locations
Hours are from zero hour of study and coincide with hours on the maps

Storm	Landfalls Observed During Study			
	Hour from Zero Study Hour	Where	MSWS km/hr	Category
Isidore	0-5	Cuba	139-157	1-2
	41-75	Yucatán Peninsula	204-65	3-TS
	129	Leeville, Louisiana	102	TS
Lili	0	Cuba	167	2
	47	New Ibera, LA	120	1
Ivan	0-7	Cuba	259	5
	59	Gulf Shore, AL	194	3
Dennis	N/A	Cuba	222	4
	39	Santa Rosa Island, FL	194	3
Katrina	0	Hollywood, FL	120	1
	88	Buras, LA	204	3
	89	St. Bernard Parrish, LA	194	3
	N/A	LA/MI border	194	3
Rita	94	Sabine Pass and Johnson Bayou, LA	185	3
Wilma	N/A	Playa del Carmen, MX	213	4
	43	Marco Island, FL	194	3
Gustav	0-5	Cuba	250	4
	42	Cocodrie, LA	167	2
Ike	N/A	Cuba	212	4
	0	Cuba	130	1
	88	Galveston, TX	176	2
Ida	N/A	Nicaragua	130	1
	48	Dauphin Island, AL	65	TS
Isaac	N/A	Haiti	102	TS
	N/A	Cuba	93	TS
	60	Plaquemines Parish, LA	130	1
	66	Elmer’s Island	130	1

5.2. Statistical Analysis

5.2.1. Probabilities of Intensification

Observations from the 11 focus hurricanes were statistically analyzed by using bins based on location, changes in intensity, and other factors that could affect intensity. First, all points were sorted into groups based on if the eye was over the LC, WCE, CCE, or the GCW during the observation. Then each group was sorted into bins based on whether they intensified, de-intensified, or remained stable. Intensification was defined as the sustained wind speed increased by 1 km/hr or more from the last observation data point, de-intensification was a reduction in sustained wind speed by 1 km/hr or more, and stable was defined as no change in sustained wind speed. Calculations were completed to analyze if the location type, and by proxy the TCHP and depth to the 26°C isotherm, affected the probability of the hurricane intensifying, de-intensifying, or remaining stable.

Analysis began with all data points including those that occurred during favorable and unfavorable conditions. Unfavorable conditions were defined as wind shear of 15 knots or more, an active eyewall replacement cycle, lack of an organized central core or eyewall or other adverse eyewall conditions, eye over land, or dry air entrainment into the mid or upper level; however, already reaching or exceeding MPI and being over shallow water on the continental shelf were not considered unfavorable conditions. Favorable conditions were defined as an absence of unfavorable conditions. In order for a data point to be identified as having occurred during unfavorable conditions, adverse conditions had

to be specifically noted by the NHC as being a factor during the observation period in their raw text documents.

Table 5-6 includes the results for all data points, including those that occurred during favorable and unfavorable conditions. 38.8% of the data points that occurred over the LC intensified, 14.3% de-intensified, and 46.9% remained stable. 25.3% of data points that occurred over GCW intensified, 31.3% de-intensified, while 43.4% remained stable. Based on these results, a larger probability exists of intensification over the LC than GCW while de-intensification is more probable over the GCW.

Analysis of all data points over WCEs and CCEs produced interesting results; this was because of additional factors beyond TCHP, SST, depth to the 26° isotherm, and unfavorable conditions that were not isolated in this study. For example, Dennis heavily skewed the CCE results, even though Dennis's eye was over the CCE its convective bands were over an adjacent WCE and the LC. Dennis accounted for 4 of the 5 data points that intensified while over a CCE. Katrina and Rita heavily skewed the WCE data accounting for 7 of the 8 data points that de-intensified and 3 that remained stable. Both storms had already reached over 100% of their MPI over the LC before approaching the WCE.

The above examples of how the WCE and CCE data was skewed based on extenuating factors explains why attempts at a broad statistical analysis of hurricane

intensity without isolating other relevant factors rarely produces significant results. However, even with this simplistic first level analysis there does appear to be a slightly increased probability of hurricanes over the LC and WCEs intensifying compared to those over GCW and CCEs. 33.3% of all data points over the LC and WCEs intensified and 43.9% remained stable, for a total probability of 77.3% of intensifying or remaining stable when over the LC or WCE. 26.5% of those over GCW and CCEs intensified and 43.9% remained stable, for a total probability of 70.4% of hurricanes intensifying or remaining stable when over GCW or CCEs. Approximately 61.6% of all the data points occurred during unfavorable conditions which possibly affected the storm's ability to intensify.

Table 5-6 Results summary all conditions

Total runs down column per location type and across the row for total for all location types per type of change. % location type gives the % of each change type for that location while % all gives the percent for that type of change at that location out of all of the points. # total gives the total number for each change type and the % of the total points. The way to read this is as follows: there were 164 total data points, 49 (29.9%) of these occurred over the LC, out of those 49, 19 intensified: 38.8% of the 49, 39.6% of the total 48 (29.3%) that intensified

Favorable & Unfavorable Conditions	Over LC			Over WCE			Over CCE			Over GCW			Total	
Change	#	% LC	% All	#	% WC	% All	#	% CC	% All	#	% GC	% All	#	%
Intensified	19	38.8	39.6	3	17.6	6.2	5	33.3	10.4	21	25.3	43.8	48	29.3
De-Intensified	7	14.3	15.9	8	47.1	18.2	3	20.0	6.8	26	31.3	59.1	44	26.8
Stable	23	46.9	32.0	6	35.3	8.3	7	46.7	9.7	36	43.4	50.0	72	43.9
Total	49	100	29.9	17	100	10.4	15	100	9.1	83	100	50.6	164	100

In order to determine how much of an effect other factors had on probabilities of intensifying, de-intensifying, or remaining stable at each location type, data points were

next binned by occurring during favorable or unfavorable conditions and then by location type and type of intensity change. As table 5-7 demonstrates, LC and GCW data points had a larger variance in probabilities during favorable conditions. For data points that occurred over the LC: 61.9% intensified, 4.8% de-intensified, and 33.3% remained stable; for a total probability of 95.2% of remaining stable or intensifying. While data points over the GCW intensified 48% of the time, de-intensified 20% of the time, and remained stable 32% of the time; for a total probability of 80% of remaining stable or intensifying. Out of all of the data points that occurred during favorable conditions 49.2% intensified, 19.1% de-intensified, and 31.7% remained stable; data points over the LC had a greater than average probability of intensifying. As in the first analysis, WCE and CCE statistics were skewed by Katrina, Rita and Dennis; 5 of the 6 data points that de-intensified and 2 of the 4 that remained stable while over the WCE were during Katrina and Rita. Dennis accounted for 4 of the 4 that intensified over the CCE.

Table 5-7 Results summary favorable conditions

Total runs down column per location type and across the row for total for all location types per type of change. % location type gives the % of each change type for that location while % all gives the percent for that type of change at that location out of all of the points. # total gives the total number for each change type and the % of the total points. The way to read this is as follows: 63 data points occurred during favorable conditions, 21(33.4%) of these occurred over the LC, out of those 21, 13 intensified: 61.9%, 41.9% of the total 31 (49.2%) that intensified.

Favorable Conditions	Over LC			Over WCE			Over CCE			Over GCW			Total	
Change	#	% LC	% All	#	% WC	% All	#	% CC	% All	#	% GC	% All	#	%
Intensified	13	61.9	41.9	2	16.7	6.5	4	80.0	12.9	12	48.0	38.7	31	49.2
De-Intensified	1	4.8	8.3	6	50.0	50.0	0	0.0	0.0	5	20.0	41.7	12	19.1
Stable	7	33.3	35.0	4	33.3	20.0	1	20.0	5.0	8	32.0	40.0	20	31.7
Total	21	100	33.4	12	100	19.0	5	100	7.9	25	100	39.7	63	100

Table 5-8 shows results for data points that occurred during unfavorable conditions. The first obvious difference is that the WCE and CCE data is no longer skewed by Katrina and Dennis, 2 of the WCE and 2 of the CCE points do belong to Rita however. The results suggest that hurricanes over the LC and WCEs were able to maintain or increase their intensity during unfavorable conditions more often than those over GCW. 21.4% of the data points over the LC intensified, 21.4% de-intensified, and 57.2% remained stable; for a total of 78.6% that intensified or remained stable in intensity. For data points over the GCW, 15.5% intensified, 36.2% de-intensified, and 48.3% remained stable; for a total of 63.8% that remained stable or increased in intensity. Combining data points over WCEs with those over the LC shows that 75.8% intensified or remained stable compared to 64.7% of data points over the GCW and CCE that intensified or remained stable.

Table 5-8 Results summary unfavorable conditions

Total runs down column per location type and across the row for total for all location types per type of change. % location type gives the % of each change type for that location while % all gives the percent for that type of change at that location out of all of the points. # total gives the total number for each change type and the % of the total points. This table includes only the 101 data points that occurred during unfavorable conditions.

Unfavorable Conditions	Over LC			Over WCE			Over CCE			Over GCW			Total	
Change	#	% LC	% All	#	% WC	% All	#	% CC	% All	#	% GC	% All	#	%
Intensified	6	21.4	35.3	1	20.0	5.9	1	10.0	5.9	9	15.5	52.9	17	16.8
De-Intensified	6	21.4	18.7	2	40.0	6.3	3	30.0	9.4	21	36.2	65.6	32	31.7
Stable	16	57.2	30.8	2	40.0	3.8	6	60.0	11.5	28	48.3	53.9	52	51.5
Total	28	100	27.7	5	100	5.0	10	100	9.9	58	100	57.4	101	100

Next, the data points were binned by whether they underwent RI, RDI, or had little to no change in sustained wind speed. Because the data is evaluated by a single datapoint consisting of observation periods of differing lengths of time, RI and RDI was defined as an average increase or decrease of 2.3 km/hr per hour or more during the observation period. Completing a RI or RDI cycle, achieving a net increase/decrease in sustained wind speed of 56.5 km/hr within 24 hours, was not a requirement for this classification; the threshold of 2.3 km/hr per hour was determined by dividing 56.5 km/hr by 24 hours and rounding down. Average changes in wind speed between +2.3 and -2.3 km/hr per hour were considered stable to small changes in intensity, the kind of change that could possibly be explained by changes in SST alone.

Table 5-9 shows results for all data points, during both favorable and unfavorable conditions, based on magnitude of intensity change and type of location. Out of all 164 data points, 19.5% qualified as RI, 18.9% qualified as RDI, and 61.6% qualified as stable or small changes in intensity. Out of the 49 data points that occurred over the LC, 26.5% qualified as RI, 12.3% qualified as RDI, and 61.2% qualified as stable or small changes in intensity. However, 40.6% of all RI occurred over the LC. 83 data points occurred over GCW but a smaller percentage achieved RI at 16.9%, while a larger percentage 22.9% achieved RDI, and slightly less 60.2% remained stable or had small changes in intensity. WCE and CCE statistics were again skewed by Katrina, Rita, and Dennis.

Table 5-9 Results percent of RI and RDI all conditions

Results for all data points, favorable and unfavorable. Total runs down column per location type and across the row for total for all location types per type of change. % location type gives the % of each change type for that location while % all gives the percent for that type of change at that location out of all of the points. # total gives the total number for each change type and the % of the total points.

Favorable & Un-Favorable Conditions	Over LC			Over WCE			Over CCE			Over GCW			Total	
Change	#	% of LC	% of All	#	% of WC	% of All	#	% of CC	% of All	#	% of GC	% of All	#	%
RI > 2.3 km/hr/hr^{-1}	13	26.5	RI 40.6	2	11.8	RI 6.3	3	20.0	RI 9.4	14	16.9	RI 43.7	32	19.5
RDI > -2.3 km/hr/hr^{-1}	6	12.3	RDI 19.4	4	23.5	RDI 12.9	2	13.3	RDI 6.4	19	22.9	RDI 61.3	31	18.9
Between 2.3 & 2.3 km/hr/hr-	30	61.2	Other 29.7	11	64.7	Other 10.9	10	66.7	Other 9.9	50	60.2	Other 49.5	101	61.6
Total of all:	#	LC	All	#	WC	All	#	CC	All	#	GC	All	164	100
	49	100	29.9	17	100	10.4	15	100	9.1	83	100	50.6		

Table 5-10 shows results based on magnitude of change per location during favorable conditions. As with the combined data set, percentage of data points that underwent RI was greater over the LC than GCW. 57.1% of data points over the LC qualified as RI, 4.8% qualified as RDI, and 38.1% remained stable or had small changes in intensity. Over GCW, 40% underwent RI, 4.0% underwent RDI, and 56% remained stable or had small changes in sustained wind speed. Data suggests that during favorable conditions, RI is more probable over the LC than GCW. Data points over the LC had a greater probability of undergoing RI than remaining stable or changing intensity by small amounts; data points over GCW had a greater probability of remaining stable or changing intensity by small amounts than undergoing RI. It appears that RDI is not significantly probable at ~4-4.8% during favorable conditions over the LC or GCW. Over the WCE and CCE data is skewed by Katrina, Rita, and Dennis, and includes little data from other

storms, therefore, data is not sufficient to determine RI or RDI probability in these locations.

Table 5-10 Results percent of RI and RDI favorable conditions

Results for all data points occurring during favorable conditions. Total runs down column per location type and across the row for total for all location types per type of change. % location type gives the % of each change type for that location while % all gives the percent for that type of change at that location out of all of the points. # total gives the total number for each change type and % of total points.

Favorable Conditions	Over LC			Over WCE			Over CCE			Over GCW			Total	
Change	#	% of LC	% of All	#	% of WC	% of Total	#	% of CC	% of All	#	% of GC	% of All	#	%
RI > 2.3 km/hr/hr^{-1}	12	57.1	RI 44.4	2	16.7	RI 7.4	3	60.0	RI 11.1	10	40.0	RI 37.0	27	42.9
RDI > -2.3 km/hr/hr^{-1}	1	4.8	RDI 12.5	6	50.0	RDI 75.0	0	0.0	RDI 0.0	1	4.0	RDI 12.5	8	12.7
Between 2.3 & -2.3 km/hr/hr^{-1}	8	38.1	Other 28.6	4	33.3	Other 14.3	2	40.0	Other 7.1	14	56.0	Other 50.0	28	44.4
Total of all:	# 21	LC 100	All 33.3	# 12	WC 100	All 19.1	# 5	CE 100	All 7.9	# 25	GC 100	All 39.7	63	100

Table 5-11 shows results for all data points that occurred during unfavorable conditions. RI was not significantly probable during unfavorable conditions for any location at 3.6–6.9%; however, RDI was more probable in GCW at 31% than over the LC at 17.8%. 78.6% of all data points of the LC remained stable or had small changes in intensity; while 62.1% remained stable or had small changes in intensity over GCW. Results for the WCE and CCE were not skewed by Katrina and Dennis during unfavorable conditions, although Rita is responsible for 4 of the CCE data points. It does appear that in both the CCE and WCE it was more probable that hurricanes maintained their intensity or only had small changes in intensity; although Rita did have an effect on

the CCE data and part of Rita was over a WCE during this time. Tables 8-1 through 8-5 in the appendix provide more complete results and detailed analysis including binning by various unfavorable conditions.

Table 5-11 Results percent of RI and RDI unfavorable conditions

Results for all data points occurring during unfavorable conditions. Total runs down column per location type and across the row for total for all location types per type of change. % location type gives the % of each change type for that location while % all gives the percent for that type of change at that location out of all of the points. # total gives the total number for each change type and the % of the total points.

Un-Favorable Conditions	Over LC			Over WCE			Over CCE			Over GCW			Total	
Change	#	% of LC	% of All	#	% of WC	% of All	#	% of CC	% of All	#	% of GC	% of All	#	%
RI > 2.3 km/hr/hr^{-1}	1	3.6	RI 20.0	0	0.0	RI 0.0	0	0.0	RI 0.0	4	6.9	RI 80.0	5	5.0
RDI > -2.3 km/hr/hr^{-1}	5	17.8	RDI 19.2	1	20.0	RDI 3.8	2	20.0	RDI 7.7	18	31.0	RDI 69.2	26	25.7
Between 2.3 & 2.3 km/hr/hr-	22	78.6	Other 31.4	4	80.0	Other 5.7	8	80.0	Other 11.4	36	62.1	Other 51.5	70	69.3
Total of all:	# 28	LC 100	All 27.7	# 5	LC 100	All 5.0	# 10	CC 100	All 9.9	# 58	GC 100	All 57.4	101	100

5.2.2. Correlation Graphs

Data was then graphed to analyze possible relationships between intensity, SST, TCHP, and depth to the 26°C isotherm. As with the probability statistics, data was first analyzed under all conditions and then binned to isolate factors. The first set of graphs compared all data points from all storms under all conditions and compared sustained wind speed and % of MPI to TCHP, depth to the 26°C isotherm, and SST. As seen in

Figure 5-24, little correlation exists when all data points are included because of scatter; however, a weak positive correlation is apparent. R^2 was the largest between sustained wind speed and TCHP at .1076, with sustained winds to depth with the second largest R^2 of .0985. % of MPI had the lowest correlation to SST at .0256.

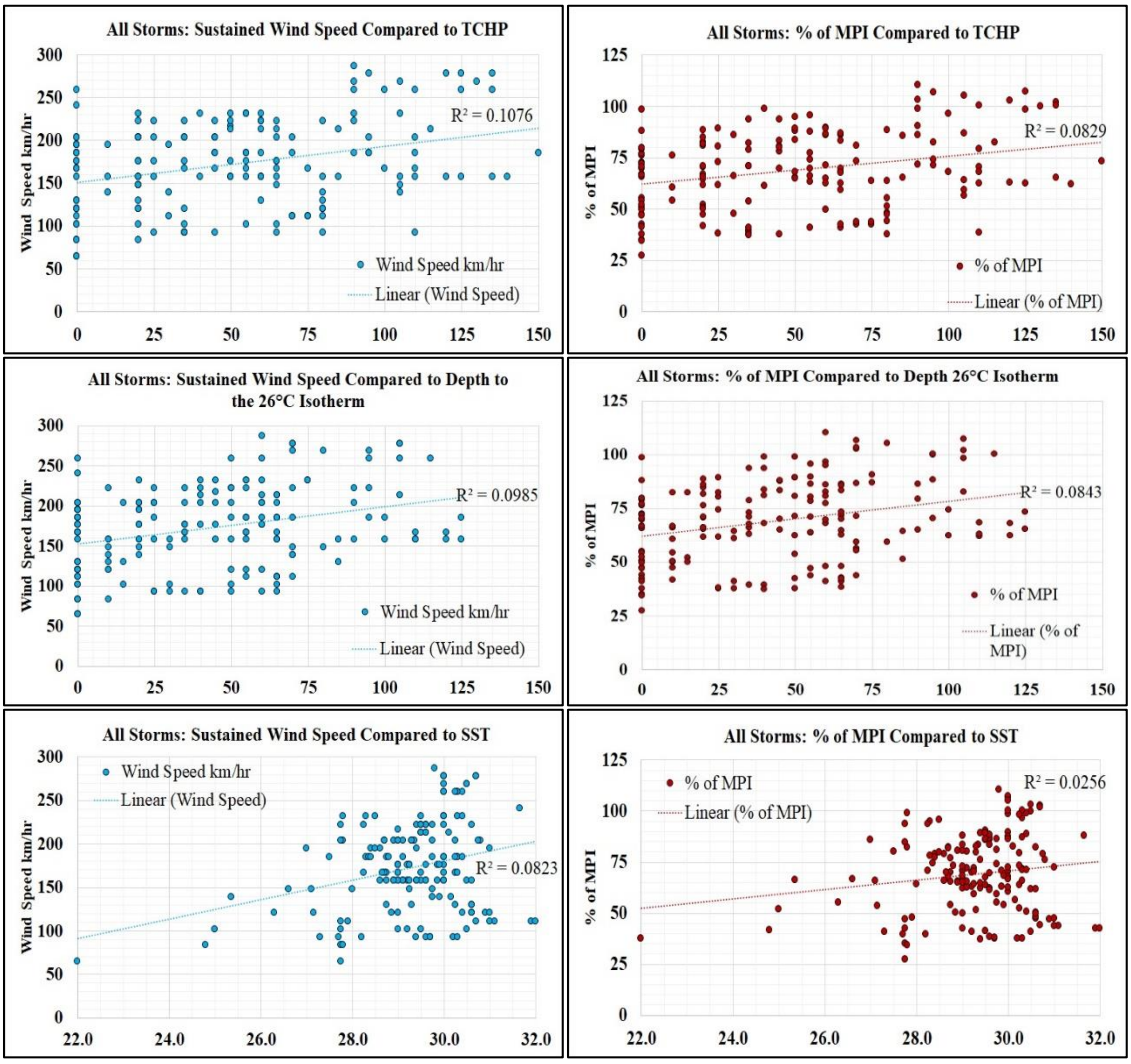

Figure 5-23 Correlation graphs: all storms & conditions

Next all data points including those over land were graphed but grouped by favorable and unfavorable conditions (Figure 5-25).

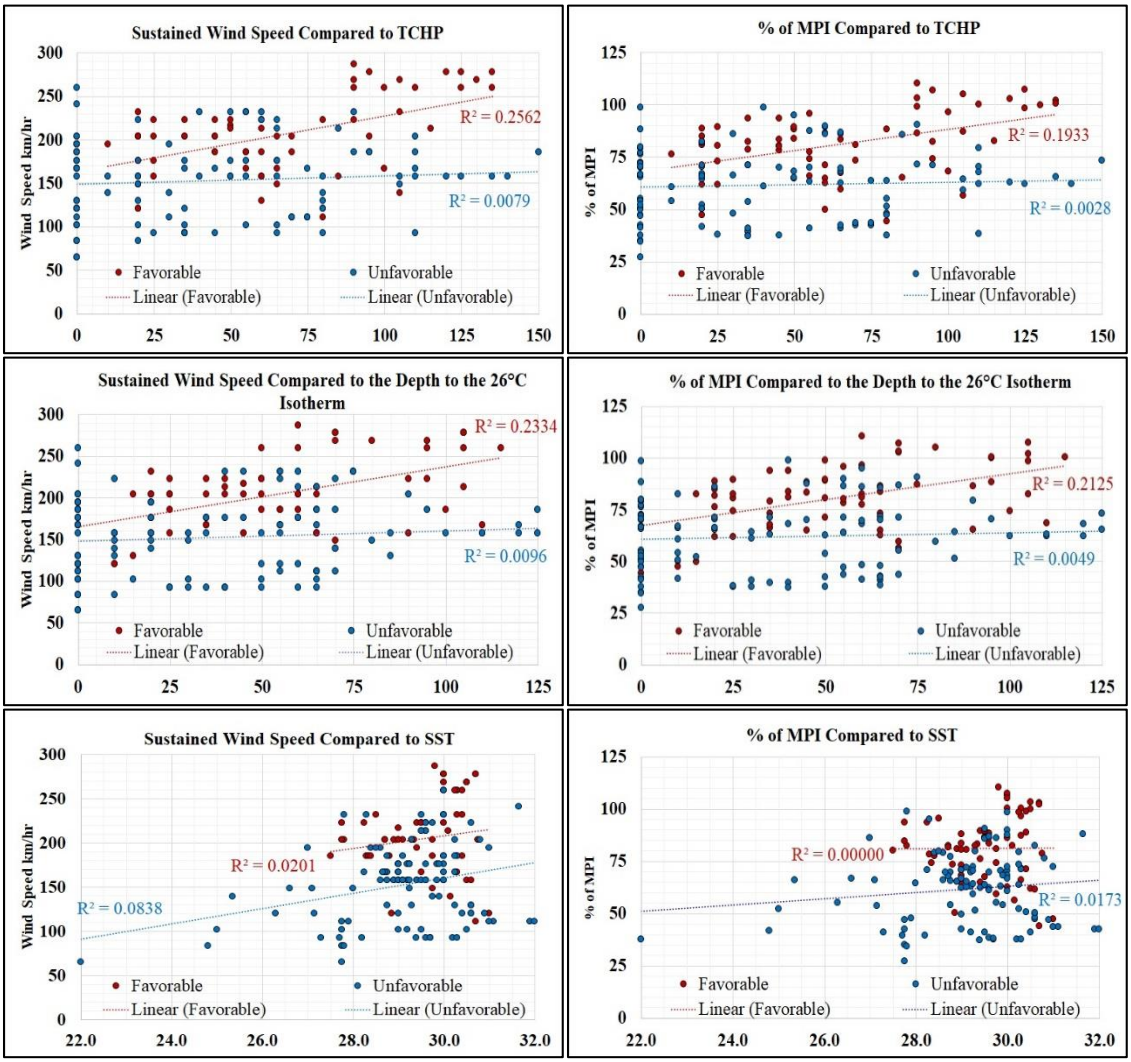

Figure 5-24 Correlation graphs: all storms by conditions

Correlation increased for both sustained wind speed and % of MPI to TCHP and depth during favorable conditions; during unfavorable conditions all R^2 values remained

low. Sustained wind speed during favorable conditions had the highest correlations, TCHP at 25.6% and depth at 23.3%. R^2 remained low for SST to sustained wind and % of MPI. Next data points for all hurricanes during both favorable and unfavorable conditions were grouped based on location: LC & WCE and CCE & GCW. Data points when the eye was over land were removed (Figure 5-26).

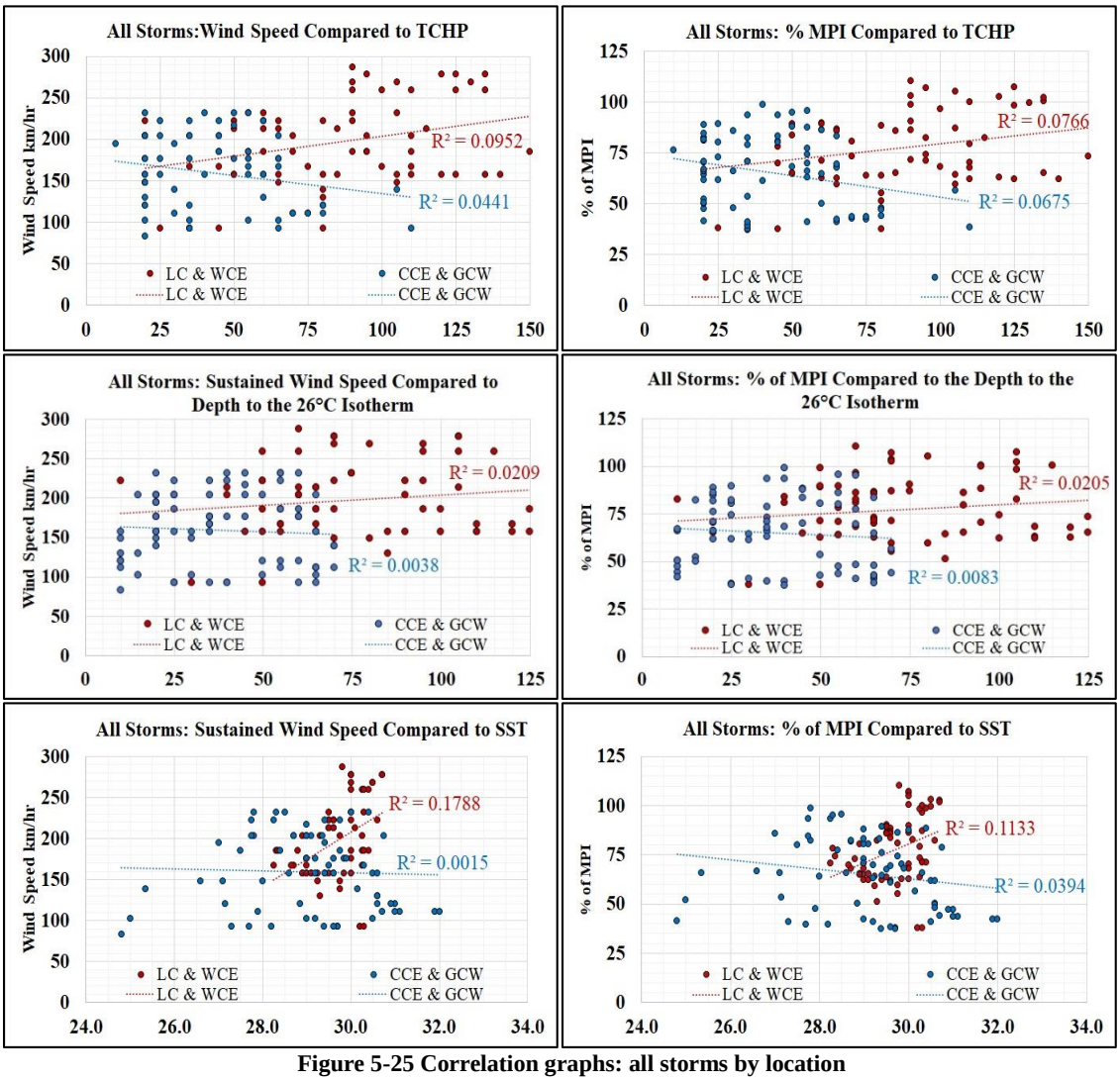

Figure 5-25 Correlation graphs: all storms by location

Correlation is not significant for TCHP and depth for sustained wind speed and % of MPI; however, it was slightly better for the LC and WCE for SST compared to sustained wind speed at R^2 of .1788 and for % of MPI at .1133. It is proposed that this is because SST increases MPI. Next, in an attempt to remove effects from adverse factors, the same correlations were graphed during only favorable conditions (Figure 5-27).

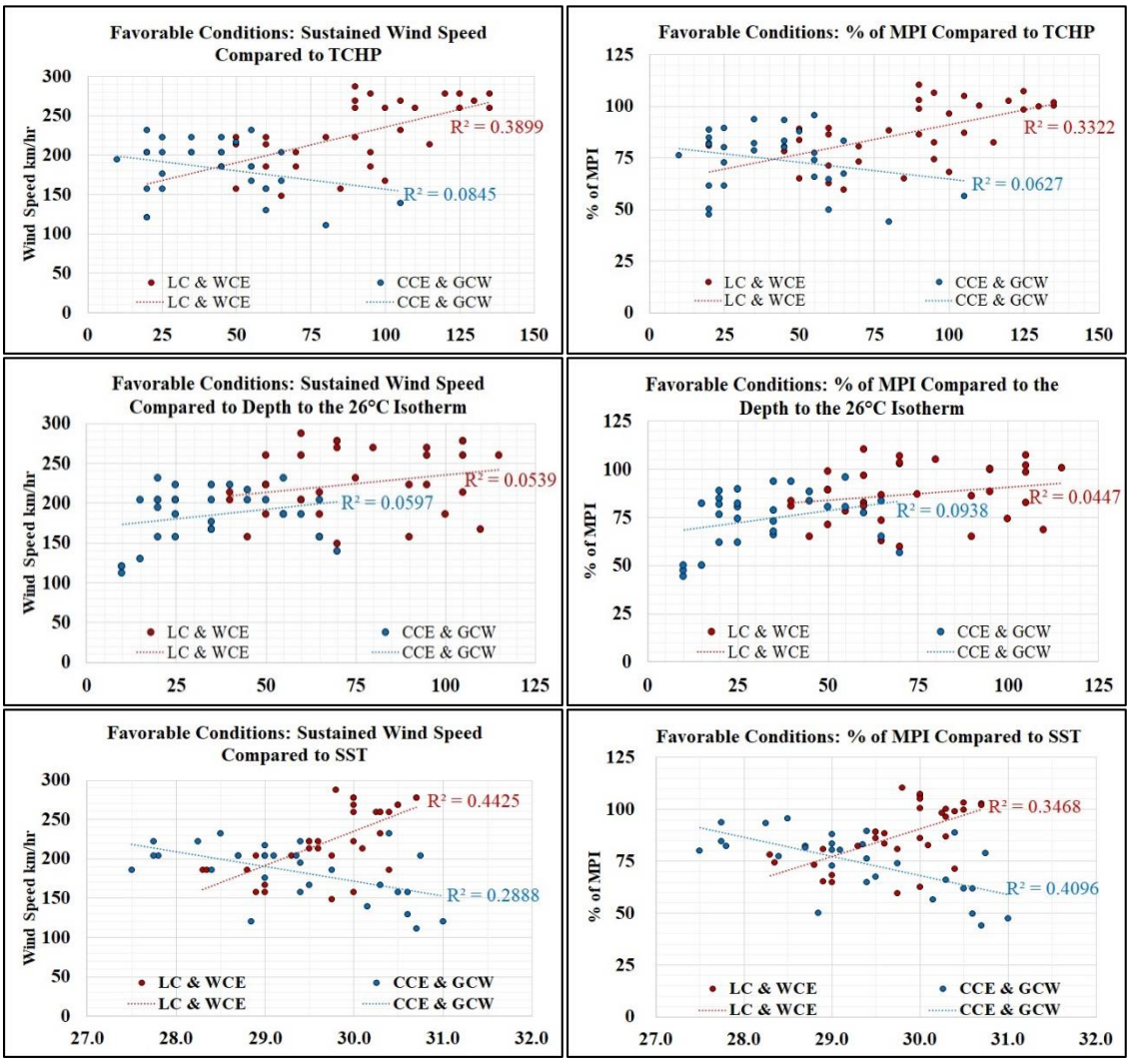

Figure 5-26 Correlation graphs: all storms by location & favorable conditions.

Several important observations are shown by this set of graphs. First, correlation between sustained wind speed and % of MPI to TCHP in the LC and WCE is much greater at ~.39 and .33 respectively; but not in the CCE and GCW. Secondly, data points over the LC and WCE obtained higher sustained wind speeds and a greater percentage of their MPI. All data points that reached 100% or more of their MPI or had a sustained wind speed of 250 km/hr or more, occurred over the LC or WCE when TCHP was 90 kJ/cm^2 or more.

The correlation between sustained wind speed and % of MPI to depth to the 26°C isotherm was not significant between .05-.09 for all locations. Suggesting that intensity doesn't continue to increase with increasing depth; however, there appears to be a threshold depth for the achieving maximum intensity. All data points that achieved 250 km/hr or more sustained wind speed and 100% or more of their MPI, did so when depths to the 26°C isotherm were 50 m or more. It should be noted that some of the data points with a depth to the 26°C isotherm of 50 m or more that had a lower sustained wind speed and % of its MPI, occurred when the hurricane moved over the LC from Cuba early in its lifecycle, this probably affected the R^2.

The last set of graphs in Figure 5-27 shows sustained wind speed and % of MPI compared to SST. There appears to be a negative correlation between SST and sustained wind speed and % of MPI in the CCE and GCW. The negative R^2 for sustained wind speed to SST is probably because there are less data points at the lower SSTs not because

of an actual negative correlation; a greater spread exists at the higher SSTs. However, the negative R^2 for % of MPI to SST appears to be accurate. MPI increases with SST, but the sustained winds do not appear to have increased, this would result in a lower % of MPI. The positive correlation between sustained wind speed and % of MPI to SST is ~.44 and .35 respectively in the LC and WCE. Because MPI has a positive relationship with SST; it is logical that maximum sustained wind speed would increase with SST if the hurricane was able to meet a large percentage of its MPI. Another observation to note is that data points that had sustained winds over 250 km/hr and 100% or more of their MPI all occurred in the LC or WCE with SSTs at or above 29.75°C.

Figure 5-28 shows all data points that occurred over the LC and WCE during both favorable and unfavorable condition. This is similar to data shown in Figure 5-27 but also includes data points during unfavorable conditions, data points recorded when the eye was over land were removed. Results show that during unfavorable conditions the correlations that were observed during favorable conditions no longer apply. During unfavorable conditions sustained wind speed did not reach 250 km/hr or more even when TCHP was above 90 kJ/cm^2 and depth to the 26°C isotherm was more than 50 m. SST also had no apparent correlation to sustained wind speed or % of MPI, even at temperatures greater than 29.75°C during unfavorable conditions. The spread in the data is possibly related to the degree of how unfavorable the conditions were. This data suggests that conditions must be favorable with low wind shear and a strong central core

and eyewall with deep convection in order for the hurricane to make full use of the available energy in the ocean surface layer (Figure 5-28).

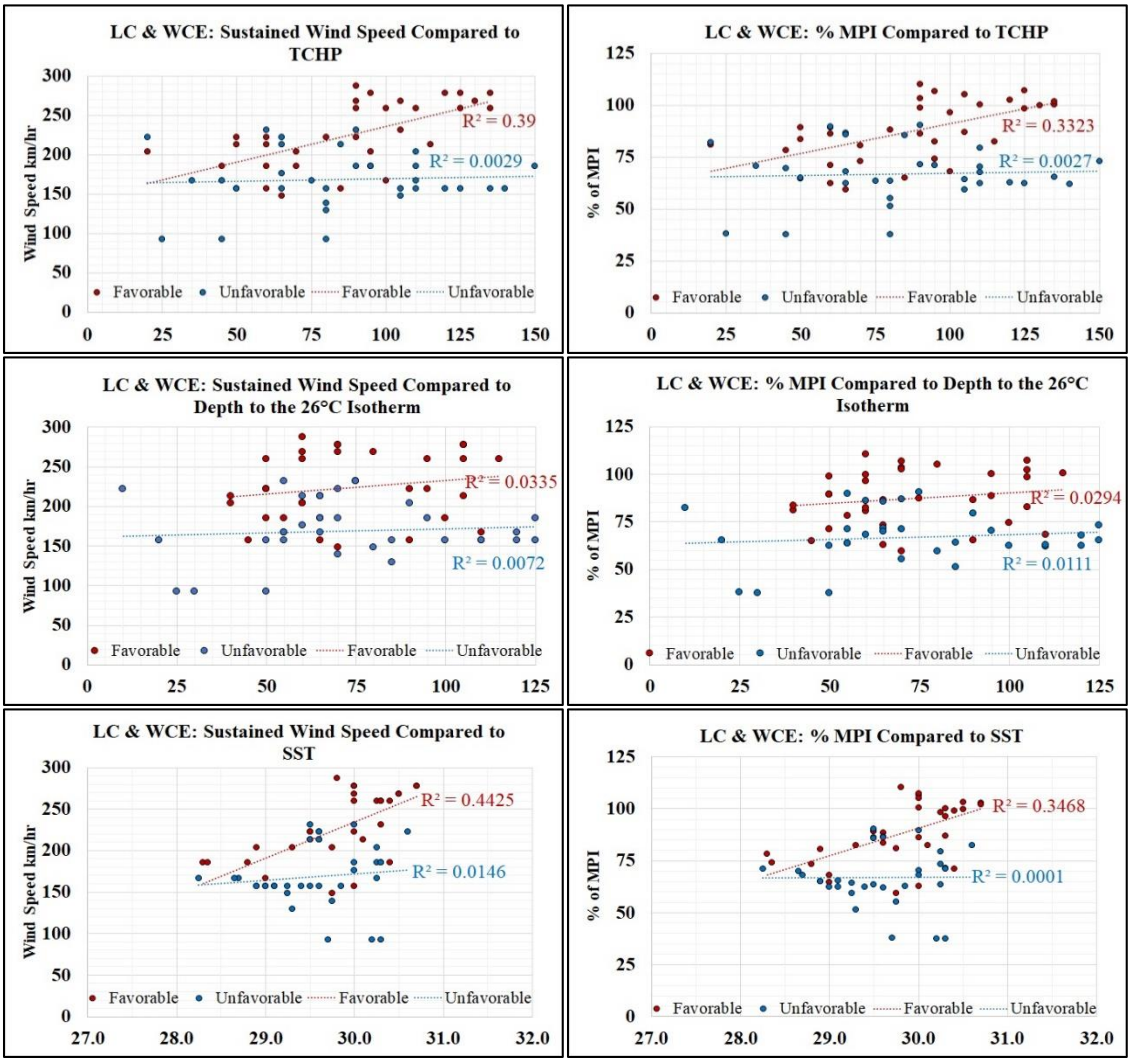

Figure 5-27 All storms LC & WCE favorable & unfavorable conditions.

The same correlation analysis was completed for data points over GCW and CCEs (Figure 5-29). The most noticeable observation, is that no significant correlation exists between TCHP, depth to the 26°C isotherm, or SST and the sustained wind speed or % of MPI. Depth to the 26°C isotherm to sustained wind speed and % of MPI during favorable conditions have the largest correlations of .096 and .054 respectively. Sustained wind speed and % of MPI both appear to increase with increasing depth, but they appear to be capped at 240 km/hr and 95% of MPI. Four of the data points that achieved over 90% of its MPI and 5 of the data points with sustained wind speed above 194 km/hr, belonged to Lili who reached 99% of its MPI during an RI cycle which occurred over GCW with higher than average TCHP and depth to the 26°C isotherm.

Data points that were part of RI cycles that occurred over all locations were graphed in figure 5-30. Only one point was during unfavorable conditions; that was for Lili which occurred over GCW with TCHP of 40 kJ/cm^2 and with 40 m depth.

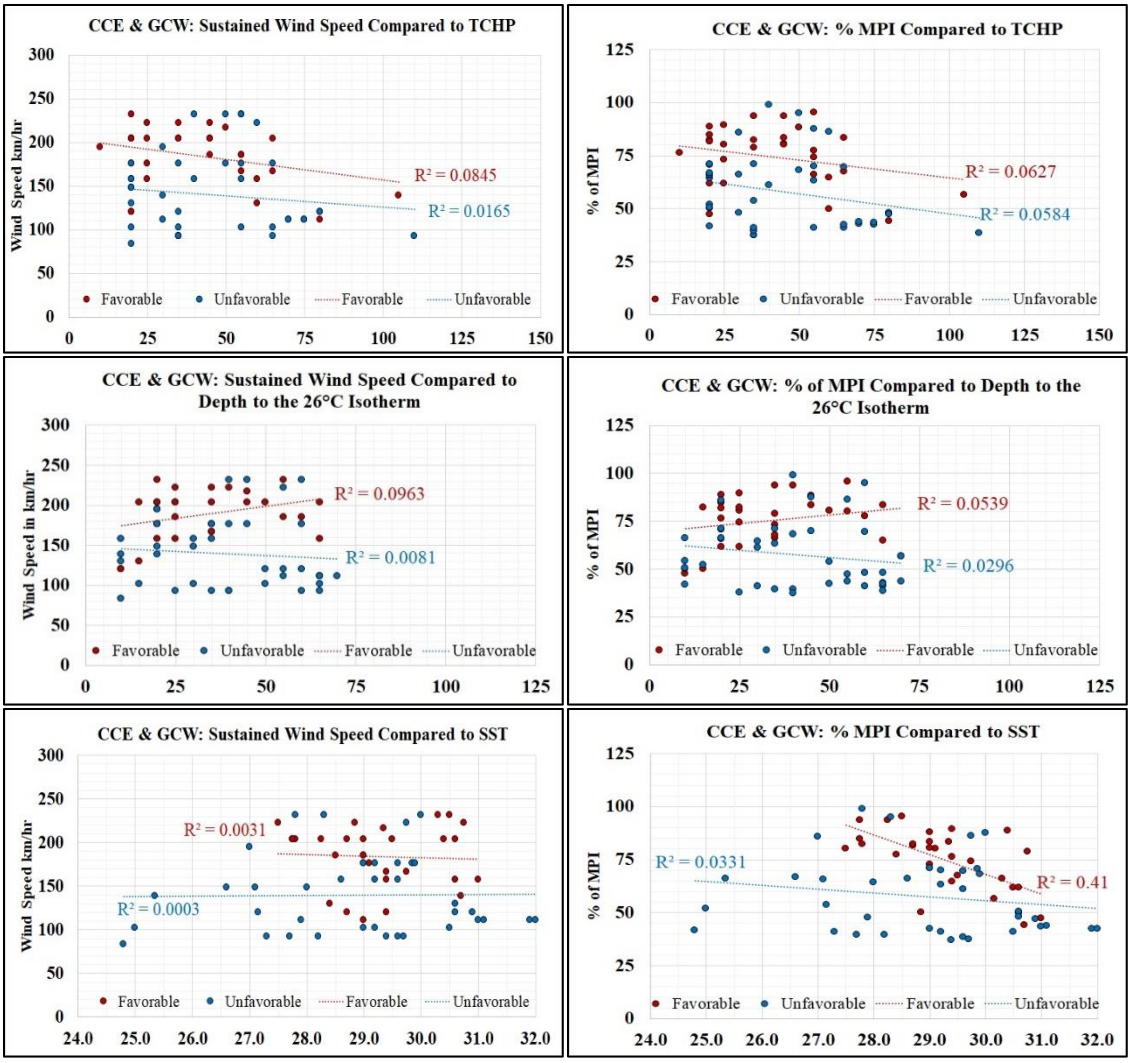

Figure 5-28 All storms CCE & GCW favorable & unfavorable Conditions.

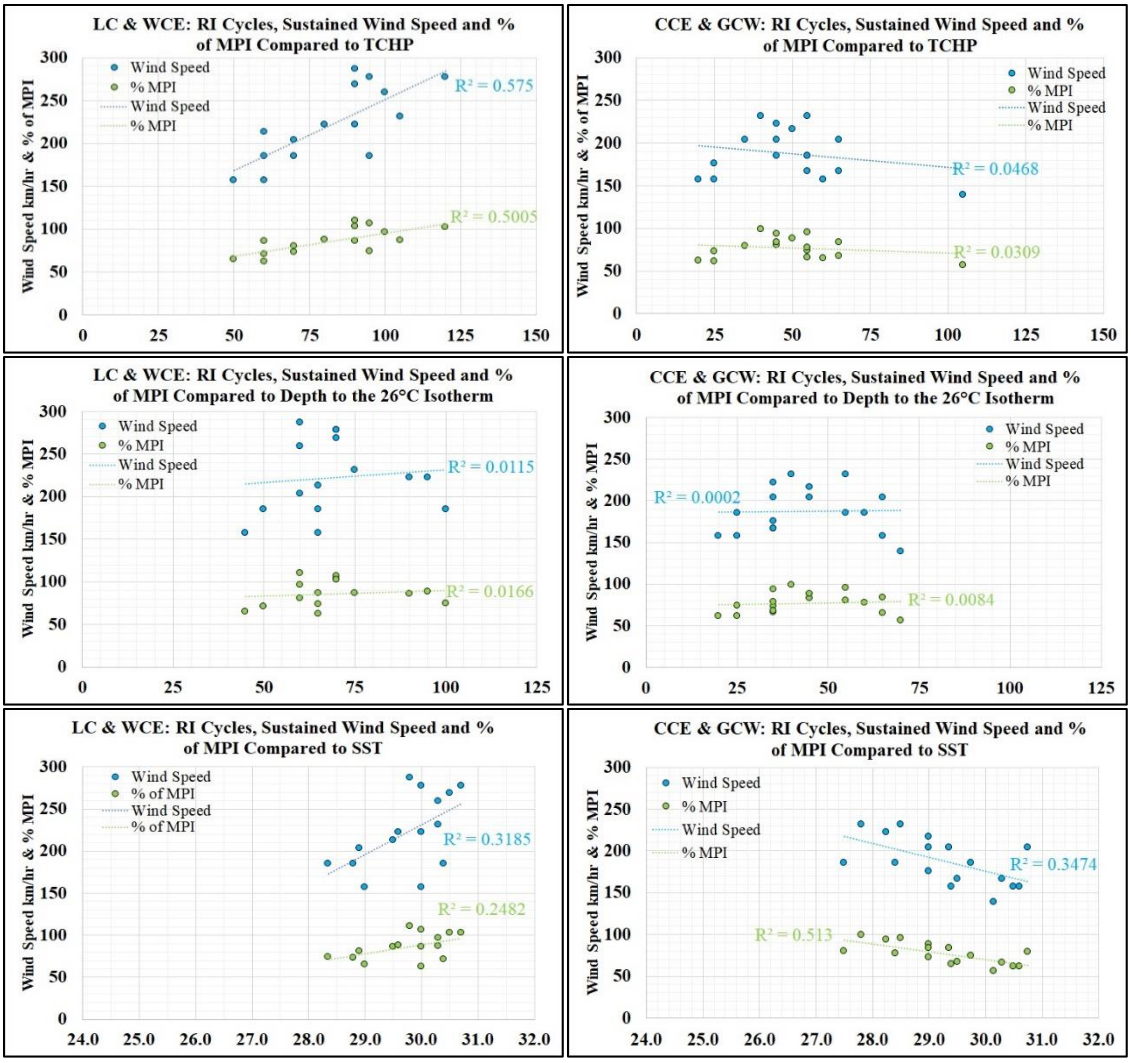

Figure 5-29 RI cycles: all locations

As figure 5-30 shows, correlation was more significant between data points during RI cycles over the LC and WCEs than over GCW and CCEs. Data points that occurred over the LC and WCE had the most significant correlations of .575 and .50 between TCHP and sustained wind speed and % of MPI respectively. SST and sustained wind speed and % of MPI had correlations of ~.318 and .248; the difference between the

R^2 for TCHP and SST suggests that the SST profile at depth is more important than SST alone for RI. Depth to the 26°C isotherm has no correlation between increased intensity with increased depth; however, the maximum wind speeds of 250 km/hr or more and 100% of MPI occurred when depths were between 60-70 m. RI occurred in the LC when TCHP was at or above 50 kJ/cm^2 with the maximum intensities occurring between 90-120 kJ/cm^2, maximum intensities peaked when SST was between 29.75°C-30.75°C.

No correlation was significant for data points over the GCW and CCEs for TCHP and depth to the 26°C isotherm compared to sustained wind speed or % of MPI. SST appears to have a negative correlation with sustained wind speed and % of MPI, one explanation for this is that 7 of the data points belong to Katrina and Rita when they were developing lower category hurricanes over the continental shelf or the Florida Straits where the SST was very high but their sustained winds were still low. The other factor for the negative correlation is that 5 of the data points belonged to Lili which underwent RI and increased from a category 3 to a category 4 hurricane while over low SST of 27°C-28°C which skewed the data upwards at the lower SST end. Dennis accounted for 5 remaining data points; this was during the RI cycle when Dennis's eye was over a CCE with high SST but its convective bands were over the LC and WCE. The main observation to note from the GCW and CCE graphs is that the maximums of intensity for these points all occurred when TCHP levels were between 40 and 55 kJ/cm^2 and the depths were between 35-55 m. Next, hurricanes that completed at least one RI cycle were

graphed to see how the variables affect RI in figure 5-31. Detailed information in Table 8-6 for RI cycles.

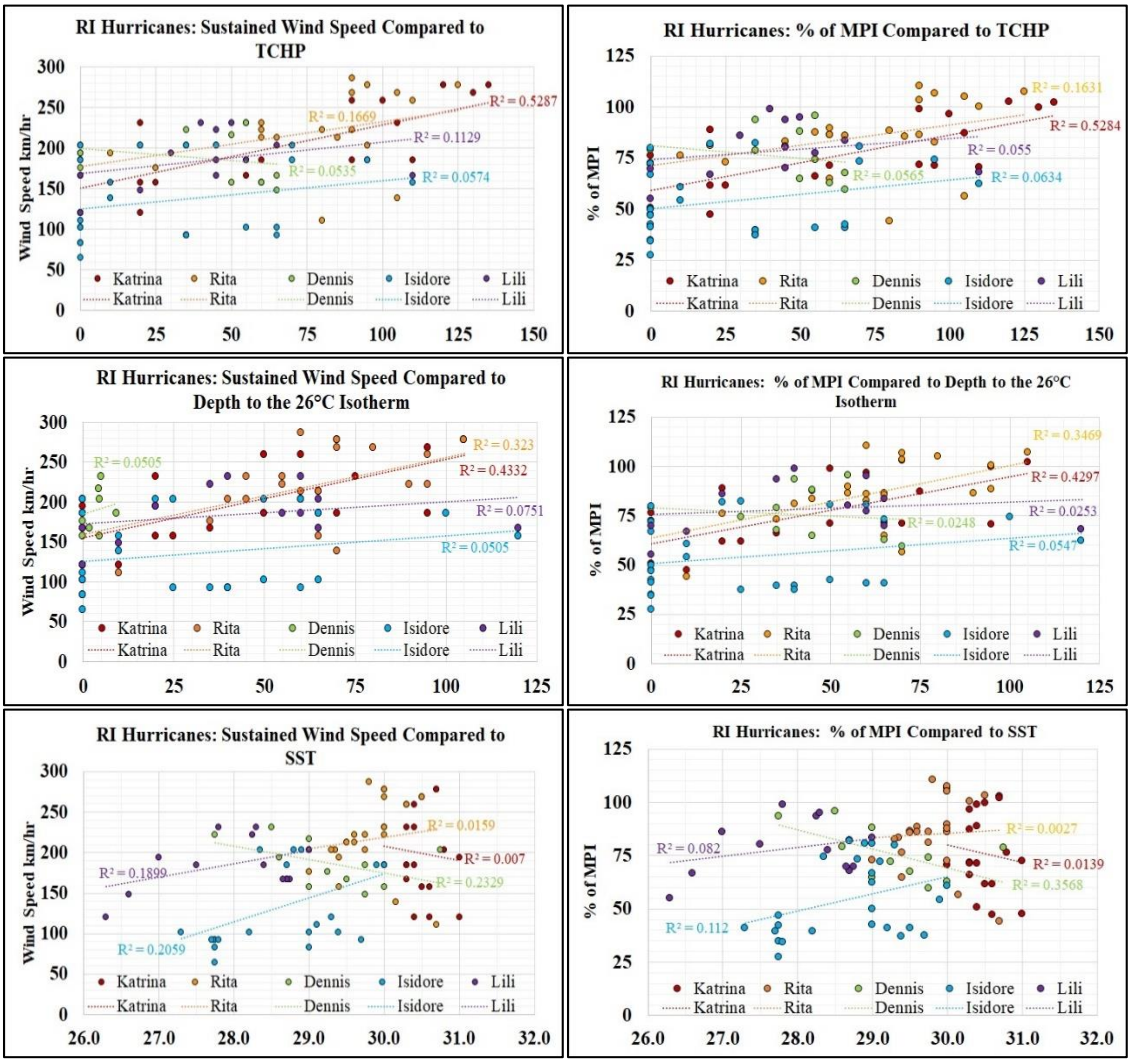

Figure 5-30 RI hurricanes

Data points graphed in Figure 5-31 include all data points for each hurricane that completed at least one RI cycle. Observations occurred during favorable and unfavorable conditions and for all locations; including points while the eye was on land. As shown above, the largest correlations were for Katrina's sustained wind speed and % of MPI to TCHP with R^2 of ~.53. The second largest correlations were for sustained wind speed and % of MPI to depth to the 26 °C isotherm for both Rita and Katrina. Katrina and Rita both intensified over areas with greater TCHP and depth to the 26 °C isotherm. The storms where SST had the largest correlations were Isidore, Lili and Dennis. Next the data points under only favorable conditions were graphed.

Figure 5-32 shows data points for the hurricanes that had complete RI cycles during only favorable conditions. Again, Katrina and Rita had the best correlations with TCHP and depth to the 26°C isotherm. Katrina's best correlations were for TCHP with an R^2 of .724 for sustained wind speed to TCHP and .695 for % of MPI to TCHP; while Rita had better correlations with depth to sustained wind speed and % of MPI. This data set contains points during RI episodes and not during RI. This affected Rita's R^2 values to TCHP because it lost intensity when it traveled over the second WCE and had lower intensity when it traveled over the Florida Current; TCHP and depth were high during both of these periods. Dennis has a strongly negative correlation for sustained wind speed to TCHP because it rapidly intensified while over the CCE and remained mostly stable while over the LC; SST was also highest in the CCE. Factors outside of TCHP, depth to the 26°C isotherm, and SST affected R^2 in all storms other than Katrina in this dataset.

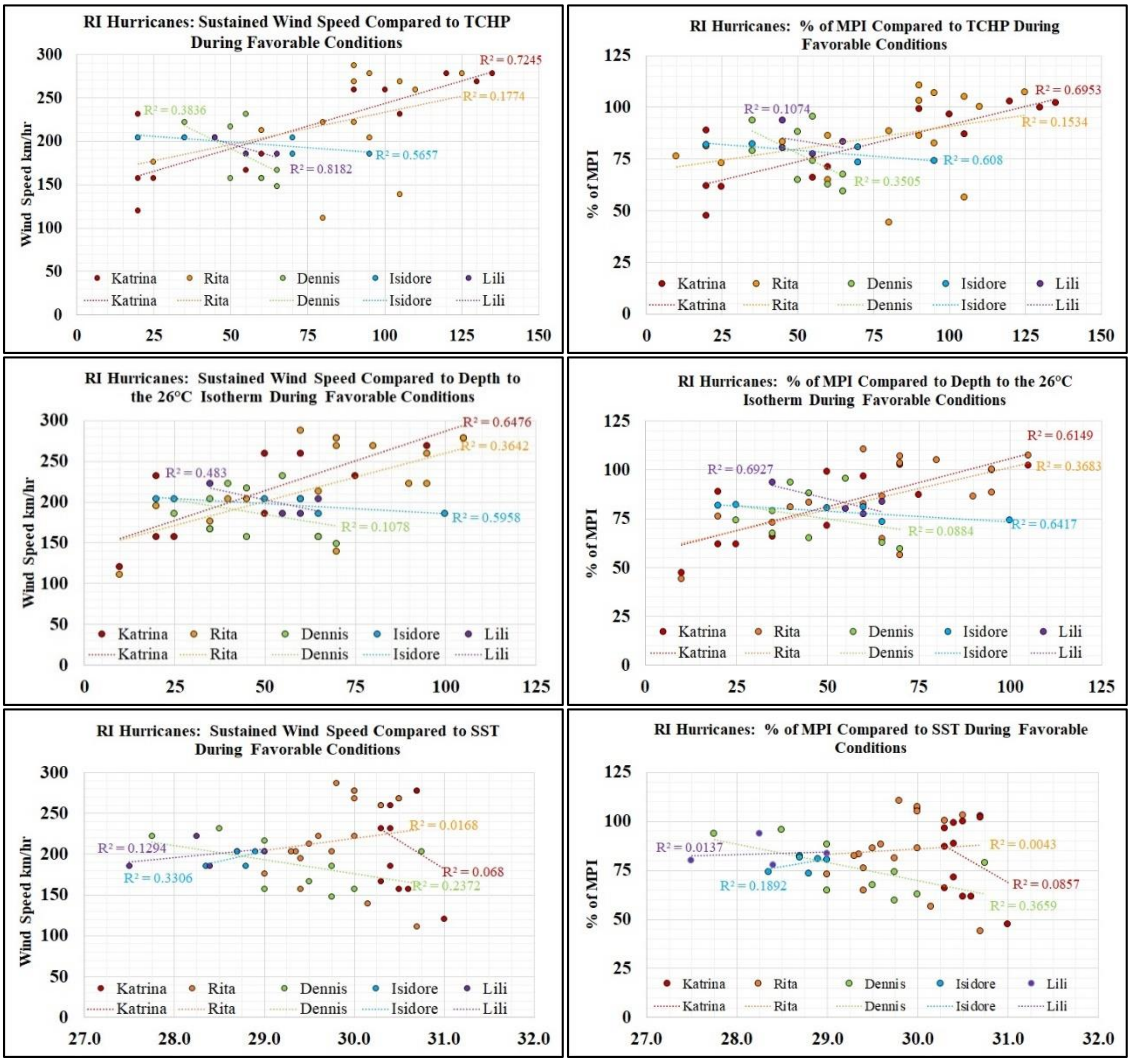

Figure 5-31 RI hurricanes favorable conditions.

In an attempt to isolate some of these factors, data points only during complete RI cycles were graphed in Figure 5-33. Only one point occurred during unfavorable conditions, the rest occurred during favorable conditions. Sustained wind speed compared

to TCHP had a R^2 of .322 and % of MPI to TCHP had a R^2 of ~.23. Data points with the highest sustained wind speeds and 100% or more of MPI occurred when TCHP was 90 kJ/cm^2 or more. Even though spread exists in the data because of other factors, the positive correlation is apparent. Depth to the 26°C isotherm and SST do not have significant R^2 values; however, the highest sustained wind speeds and % of MPI occurred when depth was between 60-70 m and SST was 29.75°C or more.

In the last set of graphs in Figure 5-34, data points during complete RI cycles were analyzed by hurricane. This removed some of the outside factors and improved some of the R^2 values. Sustained wind speed compared to TCHP for Katrina had an R^2 of .91, while % of MPI had a R^2 of .92. Compared to depth, sustained wind speed had a R^2 of .786 and % of MPI had a R^2 of .787. No correlation exists between SST and sustained wind and % of MPI for Katrina because SST did not vary more than 1°C along its track. Correlation for Rita improved to .616 for sustained wind to TCHP and .557 for % of MPI to TCHP; little correlation exists for depth to the 26°C isotherm for either factor. Correlation for SST to sustained wind speed for Rita improved to .573 and .519 for % of MPI. Isidore and Lili had strongly negative R^2 values, this is because they went over the LC early in their lifecycle as weaker storms after leaving Cuba. Dennis had really no correlation, the points were more widely spaced.

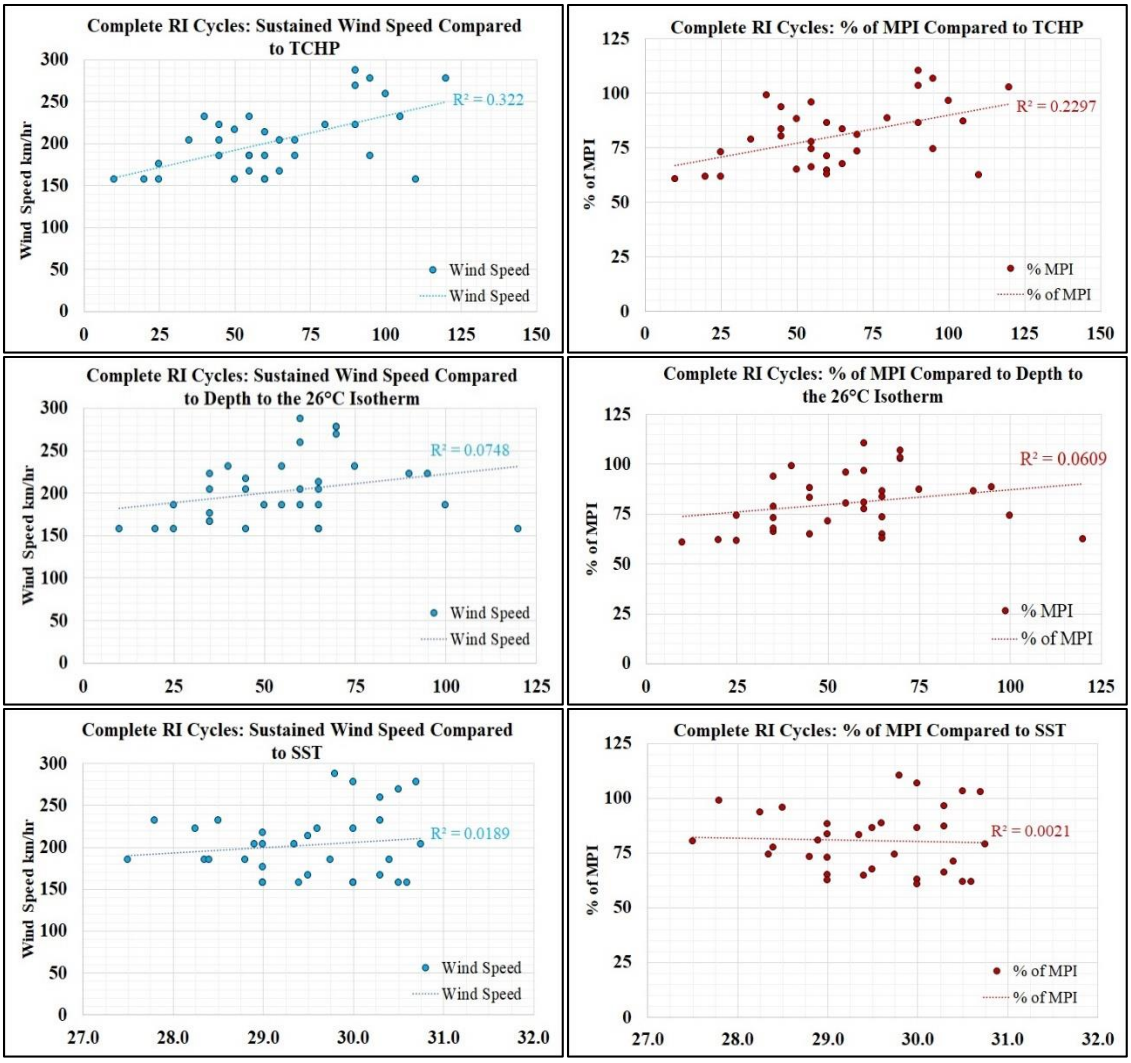

Figure 5-32 Complete RI cycles

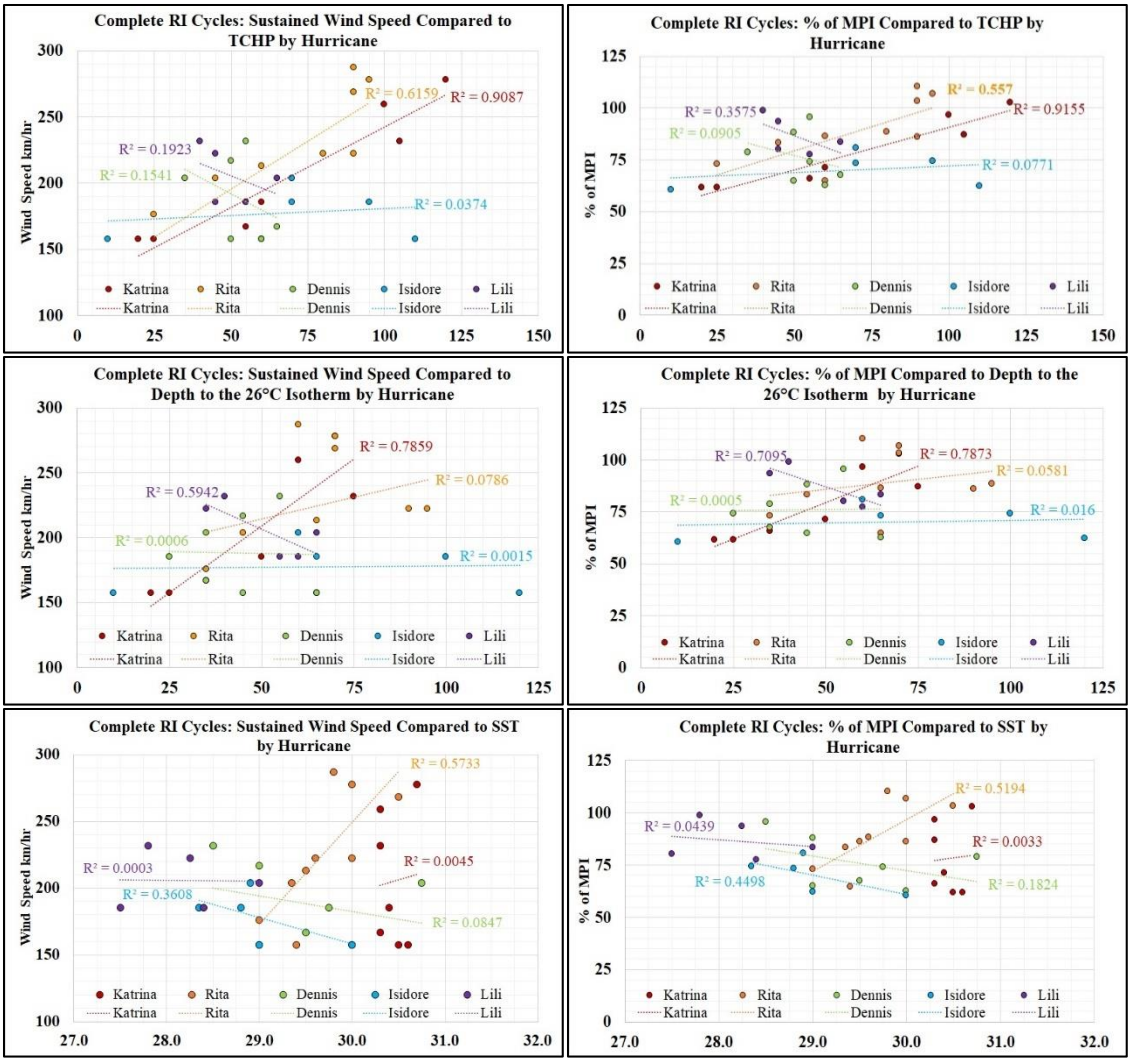

Figure 5-33 Complete RI by hurricane

6. DISCUSSION

6.1. Issues with Study

One of the largest challenges in this study was isolating the effects that SST, TCHP and depth to the 26°C isotherm had on changes in intensity, especially over time. NWS NHC raw text files are collected at specific time intervals; however, the changes occurred between the previous observation period and the time of the new observation. These intervals of time ranged from 1 hour to 8 hours. This discrepancy was less of a problem when the data were mapped in ArcMap and analyzed visually; it became a larger problem when calculating the probabilities and correlation statistics.

SST, TCHP, and depth to the 26°C isotherm at the time of the recorded intensity change was sometimes very different than what the values were over the previous several hours when the change actually occurred. For instance, Wilma at hour 30 reached the center of the LC where TCHP was high at 100 kJ/cm^2 and depth was 110 m. Wilma increased in intensity by 9.3 km/hr since the last observation at hour 24; the data used for the statistics at hour 30 were recorded as a slight increase of 9.3 km/hr for a point that had TCHP of 100 kJ/cm^2 with a depth of 110 m. The increase in intensity occurred because of the SST, TCHP and depth of the water Wilma had traveled over during the previous 6 hours, not at that exact location. Five hours later, Wilma increased by another 18.5 km/hr, but by this time had come off the LC and was over shallow GCW with TCHP of 45 kJ/cm^2 and a depth of only 55 m. Because the change was observed at this location,

the increase of 18.5 km/hr was assigned to shallow lower TCHP GCW instead of the LC water where the increase actually occurred sometime between hours 30-35.

To keep consistency, the observation data was always applied to the point where it was observed, which was always following the time period when it actually occurred. Sometimes the SST, TCHP and depth values were similar in magnitude during that entire period but sometimes were not. This mismatch of intensity changes and ocean surface attributes did result in error and spread in the statistical results. This is often what happens in statistical analysis of bulk hurricane data resulting in low correlation values.

In order to remove this discrepancy, a much greater sample size with a much shorter time interval would be required with continuous data being recorded over the entire life of the storm. A method that could capture properties of the ocean surface and temperature profile in real time with changes in the storm would be ideal. Miles et al. (2017) used autonomous underwater gliders during Hurricane Sandy (2012) to observe changes in the water column. They found that the winds from Sandy caused downwelling and Ekman transport of the bottom cold pool offshore which limited surface cooling preserving Sandy's intensity on the shelf. The use of autonomous underwater gliders such as those used by Miles et al. (2017) could greatly advance understanding of intensity and improve real-time forecasting.

Other factors that contributed to error in the results was a lack of detailed observations and precise data. NHC raw text data was not always detailed enough for all observation periods, often eyewall issues and wind shear were not reported or updated in all observations or not enough detail was given, sometimes new observations were not recorded for several hours causing gaps in the data. TCHP and depth to the 26°C isotherm were estimated from RMAS graphics based on the color and color coded legends; the shades of the colors were difficult to determine exactly at each location causing some error. Furthermore, data along the shores up to 200 meters in depth had no data. TCHP in these areas were estimated to be between 10 and 20 kJ based on distance from shore and depth and were compared to the NOAA climatological OHC graphics. Gridded satellite data or in-situ measurements would have been more precise but were unavailable.

Satellite collected SST data also introduced some error. SST data was averaged over a period of 8 days, sometimes this required getting data for over a week before or after the storm in order to limit effects from the storm on SST. In some cases, it was impossible to avoid using data that was partially affected by the storm or a previous storm such as in the case of hurricanes Isidore and Lili that occurred back to back. Error was also introduced into the calculated change in SST rasters because of some recovery of the SST over the 8-day period in which it was collected and averaged. Some SST data had small areas of "no data", often slightly earlier or later data was used to avoid "no data" pixels in the immediate vicinity of the storm's path. Also, SST data often varied

slightly by pixel usually up to +/- .2°C; neighborhood focal statistics was used to smooth the data by a circular 3 pixel mean to get an average SST within a 12 km radius under the eye.

There were several issues with the methods of analysis that introduced error and spread in the results as well. Hurricanes were analyzed directly under the eye for SST, TCHP, and depth to the 26°C isotherm. It became apparent during analysis that these parameters are important under the entire region of the convective bands. This was most obvious when analyzing Dennis. Dennis rapidly intensified over a CCE but the strong convection was occurring over the LC and WCE under Dennis's convective bands. Attribute values for Dennis were those of the CCE not the LC and WCE; this positively skewed the data for the CCE and negatively for the WCE and LC. A better method would have been to analyze the SST, TCHP and depth in areas showing the largest upward latent heat flux.

Several factors that affect intensification were not considered during binning, one of these factors was the translation speed. Translation speed was considered during analysis of the individual hurricanes during the mapping phase but not during the statistical analysis. Percentage of MPI already achieved also was not defined as a variable for binning because it was unknown if the hurricanes could intensity past 100%; both Rita and Katrina intensified beyond 100% of their MPI. Hurricanes with their convective bands over land but the eye over water were not considered as having occurred during

unfavorable conditions. This situation occurred when the storms were approaching landfall or while close to Florida and Cuba. Interaction with land, especially the mountainous region of Cuba, could have restricted or reduced intensity because the momentum coefficient would have increased, but how much of an effect this could have was unknown. For data points with the eye still over water, MPI was calculated based on SST and TCHP under the eye. If the eye was fully over land, the conditions were considered unfavorable. When the eye was not over water, such as when Isidore was over the Yucatán Peninsula, TCHP was assigned 0 and the SST closest to land where the bands were over water was used.

Some data points occurred during the hurricane's development stage and some while the hurricane was approaching land and degrading post max intensity. This had an effect on its ability to intensify. Holland (1997) stated that two distinct families of hurricanes exist, those decaying and those developing. Separating the data points into these two types could have reduced scatter. Furthermore, changes in intensity take various lengths of time between the trigger and response; it is unlikely that a storm coming off of Cuba over the LC would be able to immediately intensify from a weak storm with a low percentage of its MPI to 100% of its MPI even if the TCHP and depth could support that intensity. The data points represented snapshots of tropical cyclones at various stages of their lifecycles at a particular moment in time, this was also responsible for some scatter in the graphs and statistics.

7. CONCLUSIONS

Results suggest that the Loop Current and warm core eddies boost intensification during favorable conditions because of increased tropical cyclone heat potential and depth to the 26°C isotherm. Hurricane winds normally induce ocean surface cooling caused by mixing, upwelling, and advection known as the cold wake. Cooling of the surface to or below 26.5°C limits intensification of hurricanes by reducing the enthalpy flux to the storm because of a reduction in the moisture and thermodynamic disequilibrium between the ocean surface and the hurricane boundary layer. It is proposed that regions of high tropical cyclone heat potential with depths of 50 m or more to the 26°C isotherm such as the Loop Current and its warm core eddies, sustain or increase a hurricane's intensity by limiting hurricane induced ocean surface cooling and maintaining a sufficient enthalpy flux to the storm.

Hurricanes are more likely to reach 100% of maximum potential intensity or greater and have maximum sustained wind speeds of 250 km/hr or more when over water with sea surface temperature of 29.75°C or greater, tropical cyclone heat potential of 90 kJ/cm^2 or more, and with a depth to the 26°C isotherm of 50 m or more. Stronger hurricanes will affect the ocean to greater depths; very strong hurricanes may affect up to 100 m which would require an even greater depth to the 26°C isotherm to sustain intensity. Smaller, faster and weaker hurricanes may be able to rapidly intensify with

lower amounts of tropical cyclone heat potential and a shallower depth to the 26°C isotherm.

Hurricanes over the Loop Current had a greater probability of intensifying at 39% and undergoing rapid intensification at 26.5%, compared to those over Gulf common water where ~25% intensified and ~17% rapidly intensified, and had less of a probability of de-intensifying during both favorable and unfavorable conditions. During favorable conditions, hurricanes over the Loop Current intensified ~62% and rapidly intensified ~57% of the time while those over Gulf common water intensified ~48% and rapidly intensified ~40% of the time. Hurricanes over the Loop Current had a greater probability of rapidly intensifying at 57% than remaining stable or changing intensity by small amounts at 38%; while hurricanes over Gulf common water had a greater probability of remaining stable or changing intensity by small amounts at 56% than rapidly intensifying at 40%.

Hurricanes Katrina and Rita both rapidly intensified over the Loop Current; Katrina reached 103% of its maximum potential intensity while Rita reached 110%. Katrina had the best correlation between sustained wind speed and % of maximum potential intensity during its rapid intensification cycles and tropical cyclone heat potential at 91% and 91.5% respectively; followed by Rita with sustained wind speed to tropical cyclone heat potential at 61.6% and % of maximum potential intensity to tropical cyclone heat potential at 55.7%.

Factors affecting hurricane intensity are numerous and complex, the resulting maximum intensity is determined by a combination of all factors and their magnitudes. Even with this complexity and the deficiencies of the methods and data used, the results suggest that tropical cyclone heat potential and depth to the 26 °C isotherm have a larger effect on hurricane intensity than sea surface temperature alone. Further research should be done with in-situ real time ocean depth temperature profile data. It is also recommended that future studies explore if ocean warming due to climate change could increase tropical cyclone heat potential and depth to the 26°C isotherm in Gulf common water and what effects this may have on hurricane intensity in the future. Current research using autonomous underwater gliders and advancements in remote sensing and modeling will contribute to our understanding of hurricane intensity and rapid intensification and eventually lead to improved forecasting of intensity.

Summary of the most significant results found in this study:

- During favorable and unfavorable conditions (Table 5-6):
  - Loop Current: 38.8% intensified, 14.3% de-intensified, and 46.9% remained stable
  - Warm core eddy: 17.6% intensified, 47.1% de-intensified, and 35.3% remained stable, these results were skewed by Katrina and Rita which had already met 100% of maximum potential intensity

- Cold core eddy: 33.3% intensified, 20.0% de-intensified, and 46.7% remained stable, these results were skewed by Dennis who was over the cold core eddy while the enthalpy flux was from the warm core eddy and Loop Current
- Gulf common water: 25.3% intensified, 31.3% de-intensified, while 43.4% remained stable.
- Based on these results, a slightly larger probability exists of intensification over the Loop Current than Gulf common water while de-intensification is more probable over the Gulf common water

❖ During favorable conditions (Table 5-7):

- Loop Current: 61.9% intensified, 4.8% de-intensified, and 33.3% remained stable; for a total probability of 95.2% of remaining stable or intensifying
- Warm core eddy: 16.7% intensified, 50% de-intensified, and 33.3% remained stable, again these were skewed by Katrina and Rita
- Cold core eddy: 80.0% intensified (these were all Dennis), 0% de-intensified, and 20.0% remained stable
- Gulf common water: 48% intensified, 20.0% de-intensified, and 32% remained stable; for a total probability of 80% of remaining stable or intensifying

- There was a higher probability of hurricanes intensifying 61.9% to 48% over the Loop Current than the Gulf common water, and a higher probability of hurricanes de-intensifying 20% to 4.8% over the Gulf common water than the Loop Current during favorable conditions.

❖ Probability of rapid intensification and rapid de-intensification during favorable and unfavorable conditions (Table 5-9):

- Loop Current: 26.5% qualified as rapid intensification, 12.3% qualified as rapid de-intensification, and 61.2% qualified as stable or small changes in intensity
- Warm core eddy: 11.8% qualified as rapid intensification, 23.5% qualified as rapid de-intensification, and 64.7% qualified as stable or small changes in intensity, again these were skewed by Katrina and Rita
- Cold core eddy: 20.0% qualified as rapid intensification, 13.3% qualified as rapid de-intensification, and 66.7% qualified as stable or small changes in intensity, Dennis skewed this data.
- Gulf common water: 16.9% qualified as rapid intensification, 22.9% qualified as rapid de-intensification, and 60.2% remained stable or had small changes in intensity
- There was a higher probability of hurricanes rapidly intensifying 26.5% in the Loop Current than the Gulf common water at 16.9% during both favorable and unfavorable conditions.

- Probability of rapid intensification and rapid de-intensification during favorable conditions (Table 5-10)
    - Loop Current: 57.1% qualified as rapid intensification, 4.8% qualified as rapid de-intensification, and 38.1% remained stable or had small changes in intensity
    - Warm core eddy: 16.7% qualified as rapid intensification, 50% qualified as rapid de-intensification, and 33.3% remained stable or had small changes in intensity, this data was skewed by Katrina and Rita which had already met 100% of maximum potential intensity
    - Cold core eddy: 60% qualified as rapid intensification, 0% qualified as rapid de-intensification, and 40% remained stable or had small changes in intensity, this data was skewed by Dennis whose eye was over a cold core eddy while the enthalpy flux was from the warm core eddy and Loop Current
    - Gulf common water: 40% underwent rapid intensification, 4.0% underwent rapid de-intensification, and 56% remained stable or had small changes in intensity
    - Storms over the Loop Current had a greater probability of undergoing rapid intensification (57.1%) than remaining stable or changing intensity by small amounts (38.1%); storms over Gulf common water had a greater probability of remaining stable or changing intensity by small amounts (56%) than undergoing rapid intensification (40%).

- It appears that rapid de-intensification is not significantly probable at ~4-4.8% during favorable conditions over the Loop Current or Gulf common water
- Warm core eddy and cold core eddy data is skewed by Katrina, Rita, and Dennis, and includes little data from other storms; therefore, data is not sufficient to determine rapid intensification or rapid de-intensification probability in these locations.

❖ De-intensification was more probable over Gulf common water (36.2%) than the Loop Current (21.4%) and rapid de-intensification was more probable in Gulf common water at 31% than over the Loop Current at 17.8% during unfavorable conditions (Tables 5-8 & 5-11)

❖ Little correlation exists between maximum sustained wind speed and % of maximum potential intensity to tropical cyclone heat potential, SST, and depth to the 26°C isotherm, when all data points are compared because of other factors that affect intensity such as eyewall conditions and wind shear; however, weak positive correlations are apparent (Figure 5-24).

- ❖ When only favorable conditions are graphed by location:
    - Loop Current and warm core eddy: sustained wind speed to tropical cyclone heat potential = .39 & % of maximum potential intensity to tropical cyclone heat potential = .33
    - Cold core eddy and Gulf common water: sustained wind speed to tropical cyclone heat potential = -.08 % of maximum potential intensity to tropical cyclone heat potential = -.06
    - All data points that reached 100% or more of their maximum potential intensity or had a sustained wind speed of 250 km/hr or more, occurred over the Loop Current or warm core eddy when tropical cyclone heat potential was 90 kJ/cm^2 or more (Figure 5-27).

- ❖ During favorable conditions, correlation between sustained wind speed and % of maximum potential intensity to depth to the 26°C isotherm was not significant = .05-.09 for all locations.
    - Suggesting that intensity doesn't continue to increase with increasing depth
    - Threshold depth for the achieving maximum intensity
    - All datapoints that achieved 250 km/hr or more and 100% or more of their maximum potential intensity: depth to the 26°C isotherm = 50 m or more. Points only occurred in the Loop Current and warm core eddy (Figure 5-27).

- During favorable conditions: correlation between sustained wind speed and % of maximum potential intensity to SST:
    - Loop Current and warm core eddy: sustained wind speed = .44 % of maximum potential intensity = .35
    - Maximum potential intensity has a positive relationship with SST; maximum sustained wind speed would increase with SST
    - Datapoints that had sustained winds over 250 km/hr and achieved 100% or more of their maximum potential intensity, all occurred in the Loop Current or warm core eddy with SSTs at or above 29.75°C (Figure 5-27).

- Datapoints over the Loop Current and warm core eddy: favorable and unfavorable conditions
    - Unfavorable conditions: sustained wind speed and % of maximum potential intensity to tropical cyclone heat potential, depth to the 26 °C isotherm, and SST= <.01
    - Unfavorable conditions: sustained wind speed did not reach 250 km/hr or more even when tropical cyclone heat potential was above 90 kJ/cm^2, depth to the 26°C isotherm was more than 50 m, and SST was more than 29.75°C
    - Conditions must be favorable with low wind shear and a strong central core and eyewall with deep convection in order for the hurricane to make full use of the available energy in the ocean surface layer (Figure 5-28).

- ❖ Datapoints over the Gulf common water and cold core eddy: favorable and unfavorable conditions
    - No significant correlation existed between tropical cyclone heat potential, depth to the 26°C isotherm, or SST and the sustained wind speed or % of maximum potential intensity (Figure 5-29). These datapoints appeared to be capped at 240 km/hr.

- ❖ Rapid intensification cycle datapoints:
    - Loop Current and warm core eddy had more significant correlations than those over the Gulf common water and cold core eddy
    - Loop Current and warm core eddy: sustained wind speed and tropical cyclone heat potential = .575 and % of maximum potential intensity and tropical cyclone heat potential = .50
    - Loop Current and warm core eddy: sustained wind speed and SST = .318 % of maximum potential intensity and SST = .248
    - Loop Current and warm core eddy: depth to the 26°C isotherm had no correlation between increased intensity with increased depth
    - Maximum wind speeds of 250 km/hr or more and 100% of maximum potential intensity occurred when depths were between 60-70 m
    - Gulf common water and cold core eddy: sustained wind speed and % of maximum potential intensity to tropical cyclone heat potential and depth to the 26°C isotherm = no significant correlation= .0-.04

- SST appears to have a negative correlation with sustained wind speed and % of maximum potential intensity: believed to be due to developing or decaying storms on the continental shelves were SST is very warm (Figure 5-30)

❖ Rapid intensification cycles by hurricane

- Katrina had the best correlation, sustained wind speed compared to tropical cyclone heat potential = .91, % of maximum potential intensity to tropical cyclone heat potential = .92, depth to the 26 °C isotherm to sustained wind speed = .786 and to % of maximum potential intensity = .787. No correlation for SST to sustained wind and % of maximum potential intensity because SST did not vary more than 1°C along its track
- Rita: sustained wind speed compared to tropical cyclone heat potential = .616 % of maximum potential intensity to tropical cyclone heat potential = .557, little correlation existed for depth to the 26°C isotherm for either factor, SST to sustained wind speed = .573, SST to % of maximum potential intensity = .519, SST varied along Rita's track and intensity did increase with increases in SST and tropical cyclone heat potential
- Isidore and Lili had strongly negative R^2 values, this is because they went over the Loop Current early in their lifecycle as weaker storms after leaving Cuba

- Dennis had really no correlation, the points were more widely spaced, this is because the eye was over a cold core eddy but the enthalpy flux was from the Loop Current and warm core eddy (Figure 5-34)

APPENDIX

Data Charts & Tables

Table 8-1 Detailed results over Loop Current

Over the Loop Current	Intensified		Stable		De-Intensified		Total		
Met RI or RDI	#	%	#	%	#	%	#	%	
	13	68.4	0	0	6	85.7	19	38.8	
Didn't Meet RI or RDI	#	%	#	%	#	%	#	%	
	6	31.6	23	100	1	14.3	30	61.2	
Total	#	%	#	%	#	%	#	%	
	19	38.8	23	46.9	7	14.3	49	100	
Eyewall Factors Met RI or RDI	5		12		5		22		
	Yes	No	Yes	No	Yes	No	RI%	RDI%	No%
	1	4	0	12	4	1	4.5	18.2	77.3
Wind Shear Met RI or RDI	1		6		5		12		
	Yes	No	Yes	No	Yes	No	RI%	RDI%	No%
	0	1	0	6	4	1	0	33.3	66.7
Over Land Met RI or RDI	1		1		0		2		
	Yes	No	Yes	No	Yes	No	RI%	RDI%	No%
	1	0	0	1	0	0	50.0	0	50.0
100% of MPI Met RI or RDI	3		1		0		4		
	Yes	No	Yes	No	Yes	No	RI%	RDI%	No%
	3	0	0	1	0	0	75.0	0	25.0
Favorable Conditions Met RI or RDI	13		7		1		21		
	Yes	No	Yes	No	Yes	No	RI%	RDI%	No%
	12	1	0	7	1	0	57.1	4.8	38.1
Other Factors Unfavorable Conditions Met RI or RDI	6		16		6		28		
	Yes	No	Yes	No	Yes	No	RI%	RDI%	No%
	1	5	0	16	5	1	3.6	17.9	78.6
Chance of not meeting RI or RDI if all other factors favorable	Ratio	%	#	%	Ratio	%	Ratio	%	
	1/13	7.7	7/7	100	0/1	0	8/21	38.1	
Chance of meeting RI or RDI if all other factors favorable	Ratio	%	Ratio	%	Ratio	%	Ratio	%	
	12/13	92.3	0/7	0	1/1	100	13/21	61.9	
Total that Underwent RI or RDI or Stable	Ratio	%	Ratio	%	Ratio	%	Change < |2.3| > 0	%	
	13/49	26.5	23/49	47.0	6/49	12.2	7/49	14.3	

Table 8-2 Detailed results over warm core eddies

Over Warm Core Eddy	Intensified		Stable		De-Intensified		Total		
Met RI or RDI	#	%	#	%	#	%	#	%	
	2	66.7	0	0	4	50.0	6	35.3	
Didn't Meet RI or RDI	#	%	#	%	#	%	#	%	
	1	33.3	6	100	4	50.0	11	64.7	
Total	#	%	#	%	#	%	#	%	
	3	17.6	6	35.3	8	47.1	17	100	
Eyewall Factors Met RI or RDI	1		2		2		5		
	Yes	No	Yes	No	Yes	No	RI%	RDI%	No%
	0	1	0	2	1	1	0	20.0	80.0
Wind Shear Met RI or RDI	0		0		0		0		
	Yes	No	Yes	No	Yes	No	RI%	RDI%	No%
	0	0	0	0	0	0	0	0	0
Over Land Met RI or RDI	0		0		0		0		
	Yes	No	Yes	No	Yes	No	RI%	RDI%	No%
	0	0	0	0	0	0	0	0	0
100% of MPI Met RI or RDI	2		1		3		6		
	Yes	No	Yes	No	Yes	No	RI%	RDI%	No%
	2	0	0	1	2	1	33.33	33.33	33.33
Favorable Conditions Met RI or RDI	2		4		6		12		
	Yes	No	Yes	No	Yes	No	RI%	RDI%	No%
	2	0	0	4	3	3	16.7	25.0	58.3
Other Factors Unfavorable Conditions Met RI or RDI	1		2		2		5		
	Yes	No	Yes	No	Yes	No	RI%	RDI%	No%
	0	1	0	2	1	1	0	20.0	80.0
Chance of not meeting RI or RDI if all other factors favorable	Ratio	%	#	%	Ratio	%	Ratio	%	
	0/2	0	4/4	100	3/6	50.0	7/12	58.3	
Chance of meeting RI or RDI if all other factors favorable	Ratio	%	Ratio	%	Ratio	%	Ratio	%	
	2/2	100	0/4	0	3/6	50.0	5/12	41.7	
Total that Underwent RI or RDI or Stable	Ratio	%	Ratio	%	Ratio	%	Change < |2.3| >0	%	
	2/17	11.8	6/17	35.3	4/17	23.5	5/17	29.4	

Table 8-3 Detailed results over cold core eddies

Over Cold Core Eddy	Intensified		Stable		De-Intensified		Total		
Met RI or RDI	#	%	#	%	#	%	#	%	
	3	60.0	0	0	2	66.7	5	33.3	
Didn't Meet RI or RDI	#	%	#	%	#	%	#	%	
	2	40.0	7	100	1	33.3	10	66.7	
Total	#	%	#	%	#	%	#	%	
	5	33.3	7	46.7	3	20.0	15	100	
Eyewall Factors Met RI or RDI	1		6		2		9		
	Yes	No	Yes	No	Yes	No	RI%	RDI%	No%
	0	1	0	6	1	1	0	11.1	88.9
Wind Shear Met RI or RDI	0		1		2		3		
	Yes	No	Yes	No	Yes	No	RI%	RDI%	No%
	0	0	0	1	2	0	0	66.7	33.3
Over Land Met RI or RDI	0		0		0		0		
	Yes	No	Yes	No	Yes	No	RI%	RDI%	No%
	0	0	0	0	0	0	0	0	0
100% of MPI Met RI or RDI	0		0		0		0		
	Yes	No	Yes	No	Yes	No	RI%	RDI%	No%
	0	0	0	0	0	0	0	0	0
Favorable Conditions Met RI or RDI	4		1		0		5		
	Yes	No	Yes	No	Yes	No	RI%	RDI%	No%
	3	1	0	1	0	0	60.0	0	40.0
Other Factors Unfavorable Conditions Met RI or RDI	1		6		3		10		
	Yes	No	Yes	No	Yes	No	RI%	RDI%	No%
	0	1	0	6	2	1	0	20.0	80.0
Chance of not meeting RI or RDI if all other factors favorable	Ratio	%	#	%	Ratio	%	Ratio	%	
	1/4	25.0	1/1	100	0/0	0	2/5	40.0	
Chance of meeting RI or RDI if all other factors favorable	Ratio	%	Ratio	%	Ratio	%	Ratio	%	
	3/4	75.0	0/1	0	0/0	0	3/5	60.0	
Total that Underwent RI or RDI or Stable	Ratio	%	Ratio	%	Ratio	%	Change < |2.3| >0	%	
	3/15	20.0	7/15	46.7	2/15	13.3	3/15	20.0	

Table 8-4 Detailed results over Gulf common water

Over Gulf Common Water	Intensified		Stable		De-Intensified		Total		
Met RI or RDI	#	%	#	%	#	%	#	%	
	14	66.7	0	0	19	73.1	33	39.8	
Didn't Meet RI or RDI	#	%	#	%	#	%	#	%	
	7	33.3	36	100	7	26.9	50	60.2	
Total	#	%	#	%	#	%	#	%	
	21	25.3	36	43.4	26	31.3	83	100	
Eyewall Factors Met RI or RDI	9		18		11		38		
	Yes	No	Yes	No	Yes	No	RI%	RDI%	No%
	4	5	0	18	10	1	10.5	26.3	63.2
Wind Shear Met RI or RDI	4		5		5		14		
	Yes	No	Yes	No	Yes	No	RI%	RDI%	No%
	2	2	0	5	5	0	14.3	35.7	50.0
Over Land Met RI or RDI	1		13		18		32/24		
	Yes	No	Yes	No	Yes	No	RI%	RDI%	No%
	1	0	0	13	15	3	3.1	46.9	50.0
Over Land-Starts (8)	1	0	0	5	15	3	4.2	62.5	33.3
100% of MPI Met RI or RDI	0		0		0		0		
	Yes	No	Yes	No	Yes	No	RI%	RDI%	No%
	0	0	0	0	0	0	0	0	0
Favorable Conditions Met RI or RDI	12		8		5		25		
	Yes	No	Yes	No	Yes	No	RI%	RDI%	No%
	10	2	0	8	1	4	40.0	4.0	56.0
Other Factors Unfavorable Conditions Met RI or RDI	9		28		21		58		
	Yes	No	Yes	No	Yes	No	RI%	RDI%	No%
	4	5	0	28	18	3	6.9	31.0	62.1
Chance of not meeting RI or RDI if all other factors favorable	Ratio	%	#	%	Ratio	%	Ratio	%	
	2/12	16.7	8/8	100	4/5	80.0	14/25	56.0	
Chance of meeting RI or RDI if all other factors favorable	Ratio	%	Ratio	%	Ratio	%	Ratio	%	
	10/12	83.3	0/8	0	1/5	20.0	11/25	44.0	
Total that Underwent RI or RDI or Stable	Ratio	%	Ratio	%	Ratio	%	Change < |2.3| >0	%	
	14/83	16.9	36/83	43.4	19/83	22.9	14/83	16.9	

Table 8-5 Detailed results for all points

All Areas Combined	Intensified		Stable		De-Intensified		Total		
Met RI or RDI	#	%	#	%	#	%	#	%	
	32	66.7	0	0	31	70.5	63	38.4	
Didn't Meet RI or RDI	#	%	#	%	#	%	#	%	
	16	33.3	72	100	13	29.5	101	61.6	
Total	#	%	#	%	#	%	#	%	
	48	29.3	72	43.9	44	26.8	164	100	
Eyewall Factors Met RI or RDI	16		38		20		74		
	Yes	No	Yes	No	Yes	No	RI%	RDI%	No%
	5	11	0	38	16	4	6.8	21.6	71.6
Wind Shear Met RI or RDI	5		12		12		29		
	Yes	No	Yes	No	Yes	No	RI%	RDI%	No%
	2	3	0	12	11	1	6.9	37.9	55.2
Over Land Met RI or RDI	2		14		18		34/26		
	Yes	No	Yes	No	Yes	No	RI%	RDI%	No%
	2	0	0	14	15	3	5.9	44.1	50.0
Over Land-Starts (8)	2	0	0	6	15	3	7.7	57.7	34.6
100% of MPI Met RI or RDI	5		2		3		10		
	Yes	No	Yes	No	Yes	No	RI%	RDI%	No%
	5	0	0	2	2	1	50.0	20.0	30.0
Favorable Conditions Met RI or RDI	31		20		12		63		
	Yes	No	Yes	No	Yes	No	RI%	RDI%	No%
	27	4	0	20	5	7	42.9	7.9	49.2
Other Factors Unfavorable Conditions Met RI or RDI	17		52		32		101		
	Yes	No	Yes	No	Yes	No	RI%	RDI%	No%
	5	12	0	52	26	6	5.0	25.7	69.3
Chance of not meeting RI or RDI if all other factors favorable	Ratio	%	#	%	Ratio	%	Ratio	%	
	4/31	12.9	20/20	100	7/12	58.3	31/63	49.2	
Chance of meeting RI or RDI if all other factors favorable	Ratio	%	Ratio	%	Ratio	%	Ratio	%	
	27/31	87.1	0/20	0	5/12	41.7	32/63	50.8	
Total that Underwent RI or RDI or Stable	Ratio	%	Ratio	%	Ratio	%	Change < |2.3| >0	%	
	32/164	19.5	72/164	43.9	31/164	18.9	29/164	17.7	

Table 8-6 Change in wind speed rapid intensification cycles

Storm Name	Avg. Change Wind km/hr per Hour	TCHP kJ/cm^2	Storm Name	Avg. Change Wind km/hr per Hour	TCHP kJ/cm^2
Dennis	4.6	60	Katrina	9.3	20
Dennis	0.0	50	Katrina	0.0	25
Dennis	1.9	65	Katrina	1.5	55
Dennis	9.3	55	Katrina	3.1	60
Dennis	4.6	35	Katrina	7.7	105
Dennis	4.3	50	Katrina	27.8	100
Dennis	4.9	55	Katrina	3.7	120
Isidore	3.7	0	Rita	4.6	105
Isidore	0.0	110	Rita	3.1	60
Isidore	6.9	95	Rita	3.1	25
Isidore	0.0	70	Rita	9.3	45
Isidore	3.1	70	Rita	3.1	60
Lili	4.6	45	Rita	3.1	80
Lili	0.0	55	Rita	0.0	90
Lili	3.7	65	Rita	7.7	90
Lili	4.6	45	Rita	3.1	95
Lili	4.6	40	Rita	4.6	90

REFERENCES

Balaguru, K. Judi. D.R., Leung, L.R. 2016. Future hurricane storm surge risk for the U.S. gulf and Florida coasts based on projections of thermodynamic potential intensity. Climatic Change (2016) 138 pp: 99–110

Bell, M. M., Montgomery, M. T., Emanuel, K.A. 2012. Air–Sea Enthalpy and Momentum Exchange at Major Hurricane Wind Speeds Observed during CBLAST. Journal of Atmospheric Science. Vol. 69 pp: 3197-3221.

Blake, E.S., Landsea, C.W., and Gibney, E.J. 2011. The deadliest, costliest, and most intense United States tropical cyclones from 1851 to 2010 (and other frequently requested facts). NOAA Technical Memorandum NWS NHC-6, Updated: 2017. National Weather Service National Hurricane Center. https://www.nhc.noaa.gov/pdf/nws-nhc-6.pdf and https://www.ncdc.noaa.gov/billions/

Bosart, L.F., Velden, C.S., Bracken, W.E., Molinari, J., Black, P.G. 1999. Environmental influences on the rapid intensification of hurricane Opal (1995) over the Gulf of Mexico. Monthly Weather Review Vol. 128 pp: 322-352.

Boyer, T.P., Biddle, M., Hamilton, M., Mishonov, A.V., Paver, C. R., Seidov, D., Zweng, M., 2011. Gulf of Mexico Regional Climatology, NOAA/NODC, dataset doi 10.7289/V5C53HSW Last updated: Fri, 14-Aug-2015 18:46 UTC Accessed Sat, 17-Aug-2019 6:00 UTC https://www.nodc.noaa.gov/OC5/regional_climate/GOMclimatology/

Bright, R.J., Xie, L., Pietrafesa, L.J. 2002. Evidence of the Gulf Stream's influence on tropical cyclone intensity. Geophysical Research Letters. Vol. 29 No. 16 pp: 48.1-48.4

Ducet, N., Le Traon, P., Reverdin, G., 2000. Global high resolution mapping of ocean circulation from TOPEX/Poseidon and ERS-1 and -2. Journal of Geophysical Research. Vol. 105, pp: 19477-19498. NOAA Coast Watch, and AVISO dataset. https://coastwatch.pfeg.noaa.gov/erddap/griddap/erdTAssh1day.html Accessed 03/2017-03/2019.

Elliott, B. 1982. Anticyclonic rings in the Gulf of Mexico. Journal of Physical Oceanography. Vol. 12 pp: 1292-1309.

Emanuel, K. A. 1986. An air-sea interaction theory for tropical cyclones. Part1: steady state maintenance. Journal of Atmospheric Sciences. Vol. 43 No.6 pp: 585-604.

Emanuel, K. A. 1988. The maximum intensity of hurricanes. Journal of Atmospheric Sciences. Vol. 45 No. 7 pp: 1143-1155.

Emanuel, K.A. "Physics of Mature Tropical Cyclones, I." Lecture 4: Physics of Mature Tropical Cyclones, I, 13 Apr. 1998, 10:50, accessed 02/25/2017 wind.mit.edu/~emanuel/geosys/node4.html.

Emanuel, K. A. 1999. Thermodynamic control of hurricane intensity. Nature Vol 401. pp: 665-669.

Emanuel, K. 2003. Tropical Cyclones. Annual Review of Earth and Planetary Sciences 2003. Vol. 31 pp: 75-104.

Emanuel, K. A., Sundararajan, R. Williams, J. 2008: Hurricanes and global warming: Results from downscaling IPCC AR4 simulations. Bulletin of American Meteorology Society 89, pp: 347–367, doi:10.1175/BAMS-89-3-347.

Emanuel, K. A., Solomon, S., Folini, D., Davis, S. Cagnazzo, C. 2013: Influence of tropical tropopause layer cooling on Atlantic hurricane activity. Journal of Climate Vol. 26, pp: 2288–2301, doi:10.1175/JCLI-D-12-00242.1

Ezer, T. 2018. On the interaction between a hurricane, the Gulf Stream and coastal sea level. Ocean Dynamics v. 68 (10) pp:1259–1272.

Gelaroa, R., McCartya, W., Suáreza, M.J., Todlinga, R., Moloda, A., Takacs, L., and others… 2017. The Modern-Era Retrospective Analysis for Research and Applications, Version 2 (MERRA-2). Journal of Climate. Vol. 30 pp: 5419-5454. MERRA-2 data https://giovanni.gsfc.nasa.gov/giovanni https://gmao.gsfc.nasa.gov/reanalysis/MERRA-2/ accessed online from 08/2017-03/2017.

Holland, G.J., 1997. The maximum potential intensity of tropical cyclones. Journal of the Atmospheric Sciences. Vol. 54 pp: 2519-2541.

Irish, J.L., Resio, D.T., Ratcliff, J.J. 2008. The influence of storm size on hurricane surge. Journal of Physical Oceanography. Vol. 38 (9), pp: 2003-2013

Ho, C.R., Huang, S.J. 2011. Estimation of Tropical Cyclone Heat Potential from Oceanic Measurements. ASME pp:1-7.

Hong, X., Chang, S.W., Raman, S., Shay, L.K, Hodur, R. 2000. The Interaction between Hurricane Opal (1995) and a Warm Core Ring in the Gulf of Mexico. Monthly Weather Review Vol. 128 pp: 1347-1365

Huffman, G., Bolvin, D., Braithwaite, D., Hsu, K., Joyce, R., Xie, P., 2014: Integrated Multi-satellite Retrievals for GPM (IMERG), version 4.4. NASA's Precipitation Processing Center, accessed 31 March, 2015, ftp://arthurhou.pps.eosdis.nasa.gov/gpmdata/ TRMM data https://pmm.nasa.gov/trm https://giovanni.gsfc.nasa.gov/giovanni accessed 08/2017-03/2019

Iowa State University Iowa Environmental Mesonet (IEM) Archive NWS Text Products by Issuing Center by Date. https://mesonet.agron.iastate.edu/wx/afos/list.phtml Accessed 08/2017 to 03/2019.

Jaimes, B., Shay, L.K., Brewster, J.K. 2016. Observed air-sea interactions in tropical cyclone Isaac over Loop Current mesoscale eddy features. Dynamics of Atmospheres and Oceans Vol.76 pp: 306–324

Jeong, D., Haus, B.K., Donelan, M.A., 2012. Enthalpy Transfer across the Air–Water Interface in High Winds Including Spray. Journal of Atmospheric Sciences. Vol. 69 pp: 2733-2748.

Kaplan, J., DeMaria, M. 2003. Large-scale characteristics of rapidly intensifying tropical cyclones in the North Atlantic basin. Weather Forecasting, Vol. 18 issue: 6 pp:1093–1108

Kieper, M.E., Landsea, C. W., Beven, J. L. II. 2016. A reanalysis of hurricane Camille. Bulletin of the American Meteorological Society Boston Vol. 97 (3) pp: 367-384

Kaplan, J., DeMaria, M., and Knaff, J. A. 2010. A revised tropical cyclone rapid intensification index for the Atlantic and eastern North Pacific Basins. Weather Forecasting Vol. 25 Iss. 1 pp: 220–241

Knapp, K. R., M. C. Kruk, D. H. Levinson, H. J. Diamond, and C. J. Neumann, 2010. The International Best Track Archive for Climate Stewardship (IBTrACS): Unifying tropical cyclone best track data. Bulletin of the American Meteorological Society, Vol. 91 pp: 363-376. https://coast.noaa.gov/hurricanes/

Knutson, T.R., Sirutis, J.R., Zhao, M., Tuleya, R.E., Bender, M., Vecchi, G.A., Villarini, G., Chavas, D., 2015. Global projections of intense tropical cyclone activity for the late twenty-first century from dynamical downscaling of CMIP5/RCP4.5 Scenarios. American Meteorological Society. Journal of Climate Vol. 28 pp:7203-7224

Kotal, S.D., Kundu, P.K., Bhowmik, S.K.R. 2008. An analysis of sea surface temperature and maximum potential intensity of tropical cyclones over the Bay of Bengal between 1981 and 2000. Royal Meteorological Society. Vol. 16 pp: 169-177.

Kowaleski, A.M., Evans, J.L. 2015. Thermodynamic Observations and Flux Calculations of the Tropical Cyclone Surface Layer within the Context of Potential Intensity. Weather and Forecasting. Vol. 30 pp: 1303 – 1320.

Landsea, C. W., Franklin, J.L. 2013: Atlantic Hurricane Database Uncertainty and Presentation of a New Database Format. Monthly Weather Review Vol.141 pp: 3576-3592.

Latif, M., Keenlyside, N., Bader, J. 2007. Tropical sea surface temperature, vertical wind shear, and hurricane development. Geophysical Research Letters An AGU Journal. Vol. 34 Issue 1 January 2007. DOI: 10.1029/2006GL027969

LeHénaff, M., Kourafalou, V.H., Morel, Y., Srinivasan, A. 2012. Simulating the dynamics and intensification of cyclonic Loop Current Frontal Eddies in the Gulf of Mexico. Journal of Geophysical Research. Vol. 117 pp:1-20.

Leipper, D.F. and Volgenau, D. 1972. Hurricane Heat Potential of the Gulf of Mexico. Journal of physical oceanography. Vol. 2: pp: 218-224

Lin, I., Black, P., Price, J.F., Yang, Y. Chen, S., Lien, C., Harr, P., Chi, N. H., Wu, C.C., and D'Asaro, E.A., 2013 (a). An ocean coupling potential intensity index for tropical cyclones. Geophysical Research Letters, Vol. 40 pp: 1878–1882

Lin, I.I, Goni, G.J, Knaff, J.A., Forbes, C., Ali, M.M. 2013 (b). Ocean heat content for tropical cyclone intensity forecasting and its impact on storm surge. Natural Hazards. Vol. 66 pp: 1481-1500.

Mainelli, M., DeMaria, M., Shay, L.K., Goni, G. 2008. Application of Oceanic Heat Content Estimation to Operational Forecasting of Recent Atlantic Category 5 Hurricanes. Weather and Forecasting. Vol. 23. pp: 3-16.

Masters, J. 2014. The Gulf of Mexico Loop Current: A Primer. Weather Underground. Accessed 01/23/2018. https://www.wunderground.com/hurricane/loopcurrent.asp

Meehl, G.A., Stocker, T.F., Collins, W.D., Friedlingstein, P., Gaye, A.T., Gregory, J.M., Kitoh, A., Knutti, R., Murphy, J.M., Noda, A., Raper, S.C.B., Watterson, I.G., Weaver A.J., Zhao, J.C. 2007: Global Climate Projections. In: Climate Change 2007: The Physical Science Basis. Contribution of Working Group I to the Fourth Assessment Report of the Intergovernmental Panel on Climate Change [Solomon, S., D. Qin, M. Manning, Z. Chen, M. Marquis, K.B. Averyt, M. Tignor and H.L. Miller (eds.)]. Cambridge University Press, Cambridge, United Kingdom and New York, NY, USA

MERRA-2 Overview: The Modern-Era Retrospective Analysis for Research and Applications, Version 2 (MERRA-2), Ronald Gelaro, et al., 2017, Journal of Climate doi: 10.1175/JCLI-D-16-0758.1

McTaggart-Cowan, R., Bosart, L.F., Gyakum, J.R., Atallah, E.H. 2007. Hurricane Katrina (2005). Part I: Complex Life Cycle of an Intense Tropical Cyclone. Monthly Weather Review Vol.135 pp: 3905-3926

Miles, T., Seroka, G., Glenn, S. 2017. Coastal ocean circulation during Hurricane Sandy. Journal of Geophysical Research: Oceans Vol. 122 pp: 7095–7114,

National, Academies of Sciences, Engineering, and Medicine, et al. Understanding and Predicting the Gulf of Mexico Loop Current: Critical Gaps and Recommendations, National Academies Press, 2018. ProQuest Ebook Central, https://ebookcentral-proquest-com.mutex.gmu.edu/lib/gmu/detail.action?docID=5359335.

Needham, H.F., and Keim, B.D., 2013. Correlating storm surge heights with tropical cyclone winds at and before landfall. 2013. Earth Interactions. Vol.18 (2014) Paper no. 7. pp: 1-26.

NOAA AOML TCHP Gulf of Mexico Fields Tropical Cyclone Heat Potential Loop graphics by date http://www.aoml.noaa.gov/phod/cyclone/data/go.html Last updated 2018 Sep 01 11:04

NOAA Gulf of Mexico Data Atlas. Bathymetry Gulf Wide. National Geophysical Data Center, NESDIS, NOAA, U.S. Department of Commerce. Accessed 03/23/2019 https://www.ncddc.noaa.gov/website/DataAtlas/atlas.htm?plate=Bathymetry%20-%20Gulf

Oouchi, K. Yoshimura, J., Yoshimura, H., Mizuta, R., Kusunoki, S., and Noda, A., 2006. Tropical cyclone climatology in a global-warming climate as simulated in a 20km-mesh global atmospheric model: frequency and wind intensity analysis. Journal of Meteorology Society of Japan: Vol. 84 pp: 259–276.

OBPG. 2015. MODIS Terra Level 3 SST Thermal IR 8 Day 4km Daytime v2014.0. Ver. 2014.0. PO. DAAC, CA, USA. Dataset accessed [2017-08-01- 2019-03-23] at http://dx.doi.org/10.5067/MODST-8D4D4.

Rapport, E. N., Franklin, J. L., Schumacher, A.B., DeMaria, M., Shay, L.K., Gibney, E. J. 2010. Tropical Cyclone Intensity Change before U.S. Gulf Coast Landfall. Weather and Forecasting Vol. 25 pp: 1380-1396.

Resio, D. T., and Westerink, J.J., 2008. Modeling the physics of storm surges. Physics today. 09/01/2008 Vol. 61 (9) pp: 33

Riehl, H. 1948. Aerology of tropical storms. *Compendium of Meteorology* American Meteorological Society pp: 902-913

Richter, D.H., Bohac, R., Stern, D.P. 2016. An assessment of the flux profile method for determining air-sea momentum and enthalpy fluxes from dropsonde data in tropical cyclones. Journal of Atmospheric Sciences. Vol. 73 pp: 2665-2682.

Seo, H. and Xie, S.P., 2013. Impact of ocean warm layer thickness on the intensity of hurricane Katrina in a regional coupled model. Meteorology Atmospheric Physics (2013) Vol. 122 pp:19–32

Schott, T., Landsea, C., Hafele, G., Lorens, J., Taylor, A., Thurm, H., Ward, B., Willis, M., Zaleski, W. The Saffir-Simpson Team. 2012. The Saffir-Simpson Hurricane Wind Scale. Accessed 08/06/2018 at 4:00 pm https://www.nhc.noaa.gov/pdf/sshws.pdf.

Shay, L.K, Goni, G.J., Black, P. G. 2000: Effects of a warm oceanic feature on Hurricane Opal. Monthly Weather Review Vol.128, pp: 1366–1383.

Shay, L.K., Uhlhorn, E.W., 2008. Loop Current Response to Hurricanes Isidore and Lili. Monthly Weather Review. Vol.136. pp: 3248-3274.

Shay, L. K. 2019. TCHP and depth to the 26 °C Isotherm figures. RSMAS Ocean Heat Content North Atlantic, The University of Miami's Upper Ocean Dynamics Laboratory (UODL). These data were provided by the Upper Ocean Dynamics Laboratory at the University of Miami- Rosenstiel School of Marine and Atmospheric Sciences (https://upper-ocean-dynamics.rsmas.miami.edu)". Accessed 08/2017-03/2019.

Sheinbaum, J., Candela, J. Badan, A., Ochoa, J. 2002. Flow structure and transport in the Yucatán Channel. Geophysical Research Letters, Vol. 29(3)

Sobel, A.H., Camargo, S.J., Hall, T.M., Lee, C.Y., Tippett, M.K., Wing, A.A. 2016. Human influence on tropical cyclone intensity. Natural Hazards. Vol. 353 Issue 6296.

Uhlhorn, E.W., Shay, L.K., 2011. Loop Current Mixed Layer Energy Response to Hurricane Lili (2002). Part I: Observations. Journal of Physical Oceanography. Vol. 42. pp: 400-419.

U.S. Census Bureau, Population Division. U.S. Coastline Counties: 2016. Internet release Internet Release Date: August 2018.

Walker, N., Leben, R., Anderson, S., Haag, A., Pilley, C., Korobkin, M. 2009. Exploration of real-time satellite measurements to advance hurricane intensity prediction in the northern Gulf of Mexico. Oceans pg. 1-9.

Walsh, K.J.E., McBride, J.L., Klotzbach, P.J., Balachandran, S., Camargo, S.J., Holland, G., Knutson, T.R., Kossin, J.P., Lee, T. Sobel, A., Sugi, M. 2015. Tropical cyclones and climate change. WIREs Climate Change 2015. doi: 10.1002/wcc.371 wires.wiley.com/climatechange

Willoughby, H. E., Clos, J.A., Shoreibah, M.G. 1982. Concentric eyewalls, secondary wind maxima, and the evolution of the hurricane vortex. Journal of Atmospheric Science. Vol. 39 pp: 395-411

Wilson, S.G. and Fischetti, T.R. 2010. Coastline population trends in the United States: 1960 to 2008. U.S. Department of Commerce Economics and Statistics Administration U.S. Census Bureau. https://www.census.gov/prod/2010pubs/p25-1139.pdf Accessed on 01/15/2018

Wu, L., Su, H., Fovell, R.G., Wang, B., Shen, J.T., Kahn, B.H., Hristova-Veleva, S.M., Lambrigtsen, B.H., Fetzer, E.J., Jiang, J.H. 2012. Relationship of environmental relative humidity with North Atlantic tropical cyclone intensity and intensification rate. Geophysical Research Letters. Vol. 39 pp: 1-8

Wu, C.C., Lee, C.Y., Lin, I.I. 2007. The Effect of the Ocean Eddy on Tropical Cyclone Intensity. Journal of Atmospheric Science. Vol. 64 pp: 3562-3578.

BIOGRAPHY

Sherry L. Young received her Bachelor of Science; majoring in Geology and Geography, from The University of Mary Washington, Fredericksburg, Virginia, in 2015. She was employed as a lab instructor at George Mason University in Fairfax County for three years and received her Master of Science, Earth Systems Science from George Mason University in 2019. She is currently pursuing her Doctorate of Philosophy Earth Systems and Geoinformation Sciences from George Mason University.